On the fixed points and invariants of Dykhne transformations and the stability of the solutions of the problem of the effective conductivity of randomly inhomogeneous two-phase media

V. E. Arkhincheev
Buryat Science Center, Siberian Branch of the Russian Academy of Sciences, 670047 Ulan-Udé, Russia

(Submitted 30 April 1998)
Pis'ma Zh. Éksp. Teor. Fiz. **67**, No. 11, 951–958 (10 June 1998)

The fixed points and invariants of Dykhne transformations are determined. It is established that they correspond to the exact solutions and duality relations for the effective characteristics of an inhomogeneous medium. The stability of the exact solutions for the effective conductivity, which are fixed points of the Dykhne transformations, is studied by bifurcation-theory methods, and a classification of these fixed points by stability type is given. It is shown that the effective conductivity tensor of a two-phase medium in magnetic and ac electric fields for certain parameters of the medium can be an unstable point of the ''saddle'' type. © *1998 American Institute of Physics.*
[S0021-3640(98)02111-2]

PACS numbers: 72.80.Ng

INTRODUCTION

A general approach for studying the properties of two-dimensional two-phase media was developed in works by Dykhne.[1,2] The approach is based on the invariance of the constant-current equations

$$\nabla \cdot \mathbf{j} = 0, \quad \nabla \times \mathbf{e} = 0 \tag{1}$$

and Ohm's law

$$\mathbf{j} = \tilde{\sigma}\mathbf{e} \tag{2}$$

under linear rotational transformations:

$$\mathbf{j} = aj' + ib\mathbf{e}', \quad \mathbf{e} = c\mathbf{e}' + id\mathbf{j}'. \tag{3}$$

Here the vectors $\mathbf{j}$ and $\mathbf{e}$ are the electric current and the electric field, $\tilde{\sigma} = \sigma/(1 - i\beta)$ is the conductivity tensor of the medium in a magnetic field, σ is the conductivity, $\beta = \mu B$ is the Hall factor, μ is the particle mobility, and the coefficients a, b, c, and d are real. The magnetic field is directed perpendicular to the plane. After the transformations (3) Ohm's law likewise holds in the new (primed) system, and the following expression is obtained for the conductivity tensor of the primed system:

$$\tilde{\sigma}' = (b + ic\tilde{\sigma})/(d\tilde{\sigma} + ia). \quad (4)$$

A similar expression is also obtained for the effective conductivity tensor of the primed system.

The effective characteristics of randomly inhomogeneous two-phase media with equal phase concentrations were established by the use of these transformations. The method was further elaborated in Refs. 3 and 4. The duality relations and the one-to-one correspondence (isomorphism) between the problems of the conductivity of a two-phase medium with and without a magnetic field were established. In Ref. 5 this approach was used to study the quantum Hall effect in inhomogeneous media. For a random mixture of Hall ($\sigma_{xx}=0$, $\sigma_{xy}=$ const) and metallic phases the effective characteristics of the system were found in a wide interval of concentrations. In the entire interval of concentrations, so long as percolation via the Hall phase is present, the effective characteristics are constant and equal to the values in the Hall phase.

The objective of the present letter is to study the properties of the Dykhne transformations as linear-fractional transformations and to examine the stability of the solutions of the conductivity problem. The point is that formula (4) can be regarded as a linear-fractional transformation of the plane of a variable Z into an image region W:

$$W = L(z) = (b + icZ)/(dZ + ia). \quad (5)$$

In the first part of this work the fixed points of this transformation are found and it is established that they correspond to the exact solutions of the conductivity problem with and without a magnetic field. The invariants of the linear-fractional transformation (5) are also found and it is shown that they are equivalent to the exact duality relations. The second part is devoted to the question of the stability of the exact solutions of the conductivity problems near the fixed points, and a classification of the solutions is constructed according to the stability type with respect to variations of the parameters of the two-phase medium. The stability of the solutions of the conductivity problem in magnetic and ac electric fields is studied as an example.

2. FIXED POINTS OF THE DYKHNE TRANSFORMATIONS AND THEIR EQUIVALENCE TO THE EXACT SOLUTIONS OF THE CONDUCTIVITY PROBLEMS

Let us find the possible fixed points of the transformation (5). They are determined from the equation

$$dZ^2 + i(a-c)Z - b = 0. \quad (6)$$

Here $Z = X + iY$ is a complex quantity.

Let us investigate the simplest case $a = c = 0$. Then a fixed point has only a real part and is degenerate:

$$X = \pm (b/d)^{1/2}, \quad Y = 0. \quad (7)$$

Choosing as the variable Z the effective conductivity without a magnetic field and determining the coefficients b and d in an appropriate manner, we obtain an expression for the effective conductivity of a two-phase medium at the percolation threshold (for equal phase concentrations):

$$\sigma_e=(\sigma_1\sigma_2)^{1/2}. \tag{8}$$

Therefore the fixed point (7) corresponds to the well-known solution of Ref. 1.

Let us now consider a two-phase medium in a magnetic field. In this case the complete transformations must be used; all coefficients are nonzero. However, in the case when the coefficients a and c are equal, $a=c$, we obtain once again a fixed point of the form (7). But in this case it corresponds to a different solution. Let us take as the variable Z the effective conductivity tensor in a magnetic field: $Z=\sigma_{xx}+\sigma_{xy}$. Then according to Eq. (7) we have

$$\sigma^e_{xx}=(b/d)^{1/2}, \quad \sigma^e_{xy}=0. \tag{9}$$

It follows from Eq. (9) that the effective conductivity tensor of a system in a magnetic field should nonetheless have a diagonal form. In other words, the problem of the conductivity of a two-phase two-dimensional medium in a magnetic field reduces to the problem of the conductivity of the same system without a magnetic field at the percolation threshold (when the effective characteristics are constant). Isomorphism for arbitrary concentrations was established by a different method in Ref. 4.

Let the variable Z have only an imaginary part: $Z=iY$. In this case the fixed points of the transformations (5) are determined by the relations (the determinant of Eq. (6) is assumed to be negative)

$$X=0, \quad Y=-(a-c)\pm[4bd+(a-c)2]^{1/2}/2d. \tag{10}$$

In this case the variable Z will correspond to the effective conductivity tensor with an off-diagonal component only:

$$\sigma^e_{xx}=0, \quad \sigma^e_{xy}=\text{const}. \tag{11}$$

The two solutions for σ_{xy} reflect two possibilities for current flow along phase 1 or 2 depending on the concentration of the phase. The solution (11) with a fixed point of the type (10) is obtained in two physical situations. One was obtained by the present author and É. G. Batyev for a random mixture of a Hall phase ($\sigma_{xx}=0$, $\sigma_{xy}=\text{const}$) and a metallic phase in a wide interval of phase concentrations, so long as flow along the Hall phase is present.[5] The second solution, similar to Eq. (11), is obtained for a mixture of two Hall phases with arbitrary concentrations.[6]

In the general case there exist two fixed points:

$$Z=i(a-c)\pm[4bd-(a-c)2]^{1/2}/2d. \tag{12}$$

Here the determinant is positive-definite.

Taking as the variable Z the effective conductivity tensor, we obtain in a magnetic field the solutions corresponding to the fixed point (12)

$$\sigma^e_{xx}=[4bd-(a-c)2]^{1/2}/2d, \quad \sigma^e_{xy}=(c-a)/2d. \tag{13}$$

It is easy to see that constant solutions for the components of the effective conductivity tensor correspond to the solutions at the percolation threshold:

$$\sigma^2_e=\sigma_1\sigma_2/(1+(\sigma_1\beta_2-\sigma_2\beta_1)^2, \quad \beta^2_e=\sigma^2_e(\beta_1+\beta_2)/(\sigma_1+\sigma_2), \tag{14}$$

(see, for example, Refs. 2 and 6).

However, there is one other physical solution corresponding to the fixed point (12) — a uniform medium:

$$\sigma^e_{xx}=\sigma_{xx}, \quad \sigma^e_{xy}=\sigma_{xy}. \tag{15}$$

It occurs in the entire interval of concentrations. It can be shown that a randomly inhomogeneous two-phase medium in a magnetic field is isomorphic to a uniform medium with equal Hall concentrations:

$$\sigma_1/\beta_1=\sigma_2/\beta_2. \tag{16}$$

Specifically, this follows from the results of Ref. 6.

Let us examine the three-dimensional case. In this case the transformations (3) are used in a truncated form with coefficient $d=0$. We obtain for the transformation W

$$iaW=b+icZ. \tag{17}$$

It is easy to see that in the three-dimensional case there is only one fixed point of the transformations:

$$Z=ib/2c(c=-a) \tag{18}$$

with a solution corresponding to the formation of an infinite cluster consisting of a nondissipative Hall phase:

$$\sigma^e_{xx}=\sigma^e_{yy}=\sigma^e_{zz}=0, \quad \sigma^e_{xy}=b/2c. \tag{19}$$

Thus we have considered all fixed points of Dykhne transformations in the two- and three-dimensional cases. It has been shown that each of the fixed points established corresponds to an exact solution of the problem of the effective conductivity with the effective conductivity or the conductivity tensor in a magnetic field taken as the variable of the transformations. Let us list these solutions. The first two solutions — conductivity without a magnetic field and conductivity tensor in a magnetic field — were obtained by Dykhne.[1,2] The third solution — isomorphism between the problems of the galvanomagnetic properties and the conductivity problem — was found by Balagurov.[5] The fourth solution — the effective conductivity of a mixture of Hall and metallic phases in the entire interval of concentrations so long as flow along the Hall phase is present — was obtained by the present author and Batyev.[5] A particular case of this problem is a mixture of two Hall phases.[6] The fifth solution — equivalence of a two-phase medium in a magnetic field with equal Hall concentrations (15) to a uniform medium — and the sixth solution for mixtures of Hall phases in the three-dimensional case (19) have apparently been obtained for the first time. Therefore the exact solutions of the conductivity problem can be classified according to their correspondence to the fixed points of the Dykhne transformations.

3. INVARIANTS OF LINEAR-FRACTIONAL DYKHNE TRANSFORMATIONS

As is well known, linear-fractional transformations, which the Dykhne transformations for conductivity are, are determined by prescribing three points Z_i and their images W_i $(i=1,2,3)$. According to the general theory of linear-fractional transformations, they are also characterized by the invariance of the double ratio of four points:[7]

$$(Z-Z_1)/(Z-Z_2):(Z_3-Z_1)/(Z_3-Z_2)=(W-W_1)/(W-W_2):(W_3-W_1)/(W_3-W_2). \tag{20}$$

Let us clarify the physical meaning of these invariants. Let us consider the case of an inhomogeneous two-phase medium. Let the variable Z equal the effective conductivity $\sigma_e(\epsilon)$ (where $\epsilon=X-1/2$ — is the deviation from the percolation threshold), and let the points equal: $Z_1=\sigma_1$, $Z_2=\sigma_2$, $Z_3=(\sigma_1\sigma_2)^{1/2}$. As an example let us take a system differing from the initial system by interchange of the phases: $W=\sigma_e'(\epsilon)=\sigma_e(-\epsilon)$, $W_i=\sigma_1\sigma_2/\sigma_i$ $(i=1,2)$, $W_3=(\sigma_1\sigma_2)^{1/2}$. Then, after simple calculations, we obtain that the invariant (20) for this transformation corresponds to the well-known duality relation

$$\sigma_e(\epsilon)\sigma_e(-\epsilon)=\sigma_1\sigma_2. \tag{21}$$

Let us now study the invariants for a two-phase system in a magnetic field. In this case the conductivity must be replaced by the corresponding conductivity tensors. As was noted earlier,[6] there exist at least three transformations for the primed system.

1. The transformed system is distinguished by an initial interchange of the phases:

$$W=\tilde{\sigma}'(\epsilon)=\tilde{\sigma}(-\epsilon), \quad W_i=\tilde{\sigma}_1\tilde{\sigma}_2/\tilde{\sigma}_i, \quad \sigma_i'=\sigma_1\sigma_2/\sigma_i,$$

$\beta_i'=\beta_1\beta_2/\beta_i$, $i=1,2$, and the image $W_3=\sigma_e(0)$ equals the effective conductivity tensor at the percolation threshold. In this case the invariant (20) is equivalent to the following duality relation between the effective conductivity and the Hall factor:

$$(\sigma_e(\epsilon)+\sigma_e(-\epsilon))/(\sigma_1+\sigma_2)=(\beta_e(\epsilon)+\beta_e(-\epsilon))/(\beta_1+\beta_2). \tag{22}$$

2. For a transformation with interchange of the phases and a change in the direction of the magnetic field

$$W_i=\tilde{\sigma}_1^*\tilde{\sigma}_2^*/\tilde{\sigma}_i^*, \quad \sigma_i'=\sigma_1\sigma_2/\sigma_i,$$

$$\beta_i'=-\beta_1\beta_2/\beta_i, \quad i=1,2, \quad W_3=\tilde{\sigma}_e(0)$$

we obtain from the invariant (20) one other duality relation for the effective characteristics:

$$(\sigma_e(\epsilon)-\sigma_e(-\epsilon))/(\sigma_1-\sigma_2)=(\beta_e(\epsilon)-\beta_e(-\epsilon))/(\beta_1-\beta_2). \tag{23}$$

Here $\tilde{\sigma}^*$ is the complex conjugate conductivity tensor.

3. In the case of the third transformation, in which only the direction of the magnetic field changes and $W_i=\tilde{\sigma}_i^*$ $(\sigma_i'=\sigma_i,\ \beta_i'=-\beta_i)$, $i=1,2$, $W_3=\tilde{\sigma}_e(0)$, a relation between the components of the effective conductivity tensor is obtained from the invariant of the double ratio of four points:

$$(\sigma_{xx}^e)^2+(\sigma_{xy}^e)^2+2c\sigma_{xy}-b=0. \tag{24}$$

Therefore the invariants of the double ratio with an appropriate choice of the variable Z and the points Z_i $(i=1,2,3)$ and their images W and W_i correspond to the relations (22), (23), and (24).

Let us briefly discuss the results obtained. The properties of the Dykhne transformations as linear-fractional conformal transformations were studied on the basis of a general approach. The fixed points and invariants of these transformations were found.

Their correspondence to the exact solutions of the effective conductivity problem was established on the basis of an analysis of the fixed points, and two more exact solutions were found.

4. ON THE STABILITY OF THE SOLUTIONS OF CONDUCTIVITY PROBLEMS IN A MAGNETIC FIELD

Let us consider the question of the stability of the established exact solutions with respect to changes in the parameters of the phases: the conductivities and the Hall factors. In other words, we shall study the stability of the fixed points and classify them by stability type.

To study the stability we represent the transformation (6) in the form of a finite-difference equation

$$Z_{n+1}-Z_n=(b+icZ_n)/(dZn+ia)-Z_n, \tag{25}$$

i.e., the value after $n+1$ transformations is chosen as the image W. Correspondingly, we obtain a nonlinear system of equations for the real X and imaginary Y parts:

$$X_{n+1}=X_n[(ac+bd)/(X_n^2d^2+(Y_nd+a)^2)],$$

$$Y_{n+1}=[(X_n^2+Y_n^2)cd+Y_n(ac-bd)-ab]/(X_n^2d^2+(Y_nd+a)^2). \tag{26}$$

This system will be investigated using the methods of bifurcation theory.[8] Let us represent the left-side in the form of a time derivative — a derivative with respect to the number of the transformations, and let us linearize the right-hand side near the fixed points:

$$X_n=X_0+\eta, \quad Y_n=Y_0+\xi.$$

As a result we obtain the following system of equations:

$$\begin{pmatrix} S\eta \\ S\xi \end{pmatrix}=\begin{pmatrix} A_{11} & A_{12} \\ A_{21} & A_{22} \end{pmatrix}\begin{pmatrix} \eta \\ \xi \end{pmatrix}, \tag{27}$$

where the matrix elements equal

$$A_{11}=-1+(ac+bd)K-2X_0d^2K^2,$$

$$A_{12}=-2(ac+bd)(Y_0d+a)K,$$

$$A_{21}=2X_0cd-2X_0d^2[(X_0^2+Y_0^2)cd+Y_0(ac-bd)-ab]K^2,$$

$$A_{22}=(2Y_0cd+ac-bd)K-2(Y_0d+a)[(X_0^2+Y_0^2)cd+Y_0(ac-bd)-ab]K^2-1,$$

$$K^{-1}=X_0^2d^2+(X_0d+a)^2.$$

The values of X_0 and Y_0 for each fixed point are unique.

Let us study first the stability of a fixed point of the type (7) ($a=c$). In this case the matrix elements simplify substantially:

$$A_{11}=2b^{1/2}d^{3/2}K, \quad A_{12}=-2aK,$$

$$A_{21}=-2cb^{3/2}d^{1/2}K, \quad A_{22}=2bdK.$$

Let us find the eigenvalues S. As is well known, the stability of a solution is determined by the sign of $\mathrm{Re}(S)$. In our case they equal

$$2S_{1,2}=-(A_{11}+A_{22})\pm[(A_{11}+A_{22})^2-A_{12}A_{21}]^{1/2}. \tag{28}$$

A ''node'' type point, according to the classification of bifurcation theory,[8] corresponds to both negative values. As follows from Eq. (23), the exact solution (8) for the effective conductivity of a two-phase medium without a magnetic field is such a node-type point.

Let us now analyze the behavior near the fixed point (11), which corresponds to the effective conductivity of an inhomogeneous medium under QHE conditions. In this case $b^*d=1$ and correspondingly the eigenvalues equal

$$S_1=-2/(1+a^2), \quad S_2=-1-i(2ab-a^2-1)/(1+a^2)^{3/2}. \tag{29}$$

For $a=1$ the solution for the effective conductivity under QHE conditions possesses stability of the node type: $S_1=S_2=-1$, as expected.

In the general case, when the effective conductivity tensor has two components, in a magnetic field we obtain for the elements for the matrix A at the fixed points (12) the values

$$A_{11}=-2(a^2+d(db-a^2K^{-1/2})K, \quad A_{12}=0, \quad A_{21}=\mathrm{const}, \quad A_{22}=-2dbK.$$

Therefore the eigenvalues of the parameter S are determined by the diagonal elements of the matrix A. Depending on the parameters of the medium, the following types of behavior for the fixed points are possible: ''node'' and ''saddle''. An unstable point of the saddle type can be obtained by changing the numerical values of the coefficients a, b, and d, i.e., changing the values of the parameters σ and β of the two-phase medium in a magnetic field.

Let us discuss the results obtained. As follows from the solutions presented above, the exact solutions for the effective conductivity of two-phase media without a magnetic field and media under QHE conditions (nondissipative Hall phases) are found to be absolutely stable for any parameters of the phases — they are fixed points of the node type. At the same time the effective conductivity tensor of two-phase media in a magnetic field at the percolation threshold and the problem of the isomorphism of media with and without a magnetic field can be fixed points of the saddle type for certain parameters of the media, i.e., they will be unstable. This result about the instability of the effective conductivity tensor is in accord with recent results obtained in Refs. 9 and 10, where it was indicated that the linear approximation is limited in problems of the conductivity in inhomogeneous media. An assertion that the linear approach is limited is also contained in Ref. 11.

5. ON THE STABILITY OF THE EFFECTIVE CONDUCTIVITY IN AN AC ELECTRIC FIELD

In this section we shall consider the question of the stability of an effective medium with equal phase concentrations in an ac electric field.

Let the first phase consist of a resistance and an inductance, while the second phase consists of a resistance and a capacitance, i.e., the conductivities of the phases are assumed to equal

$$\hat{\sigma}_1=\sigma_1+i\omega L; \quad \hat{\sigma}_2=\sigma_2+1/i\omega C.$$

Using the transformations for such a medium, we obtain for the effective conductivity of the transformed system at frequency ω

$$\sigma_e'=[(\sigma_1+i\omega L)(\sigma_2+1/i\omega C)]/\sigma_e, \tag{30}$$

i.e., we obtain a linear-fractional transformation in the form

$$W=\hat{\sigma}_1\hat{\sigma}_2/Z. \tag{31}$$

It possesses a fixed point of the type (7):

$$Z_0=(\hat{\sigma}_1\hat{\sigma}_2)^{1/2}. \tag{32}$$

We obtain the following expressions for the quantities X_0 and Y_0:

$$(X_0)^2+(Y_0)^2=C, \quad A^2+B^2=C^2, \quad Y_0/X_0=\tan(\varphi). \tag{33}$$

Here $A=\mathrm{Re}(\sigma_e^2)$ and $B=\mathrm{Im}(\sigma_e^2)$ from Eq. (27).

Next, let us investigate the stability of the fixed point (28) by the method described above. Calculations similar to those performed above yield

$$S_{1,2}=-1+(A\pm iB)\exp(\pm 2i\varphi)/C. \tag{34}$$

Therefore, depending on the quantities A,B, and $\tan(\varphi)$, three types of stability are possible for the exact solution for the effective conductivity at a frequency: ''node'', ''saddle'', and ''focus'', according to Eq. (34). The form of the stability depends on both the parameters of the medium and the frequency of the ac electric field.

Let us consider low frequencies, lower than any characteristic frequencies of the problem. In this case $B<0$ (the capacitive current makes the main contribution to the conductivity of the second phase) and $B\approx C$. After the corresponding calculations, it can be shown that the fixed point (33), corresponding to the effective conductivity of the medium at a frequency, possesses stability of the node type at low frequencies. This solves the question of the existence of an effective conductivity at low frequencies (at long times). At long times self-averaging of macroscopic quantities occurs in an inhomogeneous medium. The time, the reciprocal of $\mathrm{Re}(\sigma_e)$, enters as a characteristic time.

The results of the qualitative analysis of the stability of the solutions agree with the results of a numerical solution of equations of the type (22) for the transformation (32) with different numerical values of A and B. The results of a numerical solution of the equations for the effective characteristics in a magnetic field and at a frequency will be presented in a detailed paper.

In closing, I wish to thank Yu. B. Bashkuev and A. P. Semenov for their support of the present investigations.

[1] A. M. Dykhne, Zh. Éksp. Teor. Fiz. **59**, 110 (1970) [Sov. Phys. JETP **32**, 63 (1971)].
[2] A. M. Dykhne, Zh. Éksp. Teor. Fiz. **59**, 641 (1970) [Sov. Phys. JETP **32**, 348 (1971)].
[3] B. Ya. Balagurov, Zh. Éksp. Teor. Fiz. **108**, 2202 (1995) [JETP **81**, 1200 (1995)].
[4] B. Ya. Balagurov, Zh. Éksp. Teor. Fiz. **82**, 1333 (1982) [Sov. Phys. JETP **55**, 774 (1982)].
[5] V. E. Arkhincheev and É. G. Batyev, Solid State Commun. **72**, 1059 (1989).
[6] V. E. Arkhincheev, Phys. Status Solidi **161**, 815 (1990).
[7] A. I. Markyshevich, *Short Course in the Theory of Analytic Functions* [in Russian], Nauka, Moscow, 1978.

[8] F. Moon, *Chaotic Vibrations*, Wiley, New York, 1987 [Russian transl., Mir, Moscow, 1990].
[9] A. M. Dykhne, V. V. Zosimov, and S. A. Rybak, Dokl. Akad. Nauk **345**, 467 (1995) [Phys. Dokl. **40**, 613 (1995)].
[10] A. M. Satanin and V. V. Skuzovatkin, JETP Lett. **66**, 126 (1997).
[11] V. E. Arkhincheev, JETP Lett. **67**, 545 (1998).

Translated by M. E. Alferieff

Search for inelastic interactions of WIMPs with excitation of ^{73}Ge nuclei

A. A. Klimenko, S. B. Osetrov, A. A. Smol'nikov, and S. I. Vasil'ev
Institute of Nuclear Studies, Russian Academy of Sciences, 117312 Moscow, Russia

(Submitted 16 April 1998)
Pis'ma Zh. Éksp. Teor. Fiz. **67**, No. 11, 835–840 (10 June 1998)

A method is proposed for conducting an experimental search for inelastic interactions of weakly interacting massive particles (WIMPs) involving the excitation of long-lived levels of ^{73}Ge nuclei. Analysis of the first experimental results has made it possible to obtain the background level for these reactions as 0.0013 events/(keV·kg (^{73}Ge)·day). Experimental limits are obtained as to the cross section for spin-dependent inelastic interactions of WIMPs with ^{73}Ge nuclei. © *1998 American Institute of Physics.* [S0021-3640(98)00111-X]

PACS numbers: 27.50.+e, 95.35.+d, 23.70.+j

Analysis of diverse observational data makes it possible today to give preference to theoretical models in which the dark matter of the universe can consist of ~10% baryonic, ~60% nonbaryonic cold (nonrelativistic), and ~30% nonbaryonic hot (relativistic) dark matter.[1]

The results of the few experiments to date (see, for example, the reviews[2,3]) on the direct detection of particles of cold dark matter, specifically, particles of the weakly interacting massive particle (WIMP) class, which can comprise a large fraction of the invisible dark halo of our galaxy, can so far give only the boundaries of exclusion for the cross sections of interaction between WIMPs and detector nuclei at the corresponding values of the particle masses.

The energy spectrum of the recoil nuclei resulting from the elastic interaction of WIMPs with a target–detector is a continuous, exponentially decaying spectrum, a large portion of which lies in the region of several keV. The relative ionization efficiency factor, for example, for Ge recoil nuclei, at 10 keV equals 0.25. For such a response function it is virtually impossible to distinguish the desired WIMP spectrum from the spectrum of background events by means of only the shape of the spectrum. In order to make an unequivocal claim that WIMPs have been detected it is necessary to use a method that makes it possible to distinguish, with a high probability, the true interaction of WIMPs from the background interaction, according to structure.

In the present letter it is proposed that a unique scheme of long-lived excited levels of ^{73}Ge nucleus in the case of inelastic scattering of WIMPs by a target–detector be used. This nucleus possesses two low-lying levels with energies 13.26 and 66.73 keV (metastable) with half-lives of 2.95 μs and 0.50 s, respectively.[4] The level scheme of ^{73}Ge is displayed in Fig. 1.

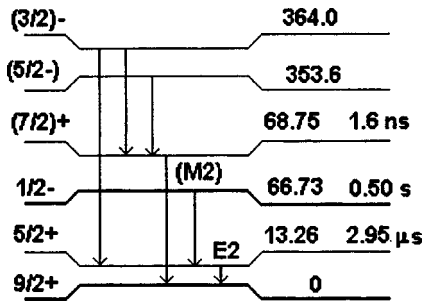

FIG. 1. Scheme of low-energy levels of ^{73}Ge (the level energies are given in keV).

The method employs simultaneously amplitude analysis and temporal analysis of events together with the trace of the pulse shape. A true event should consist of a sequence of several signals: first a signal from the recoil nucleus as a result of inelastic scattering of WIMPs (continuous spectrum) and then, over a period of several half-lives, a complicated signal due to deexcitation. In the case of the excitation of the metastable level, the second signal will be due to internal conversion (Auger electrons and x rays or a single γ ray, $e_c/\gamma=7.2$) with fixed energy (66.73$-$13.26 keV), and after a shorter time interval there will be an analogous signal with fixed energy from the 13.26 keV level. In the case of excitation of a lower level the second signal will be due to internal conversion or a γ ray ($e_c/\gamma=325$) with a fixed energy of 13.26 keV. Essentially the only possible background in such an experiment is the interaction of neutrons with excitation of the above-indicated levels. However, computational and experimental estimates show that the contribution from neutrons can be made negligibly small by performing the experiment in a deep underground laboratory with sufficiently thick neutron shielding.

In the present work a low-background germanium detector is employed, consisting of material having the natural isotopic composition of Ge (Ref. 5), with an active mass of 0.952 kg and thus containing 74 grams of ^{73}Ge.

In order to have sufficient kinetic energy to excite the first level of ^{73}Ge the WIMPs must have mass $m>9$ GeV, and in order to excite the second level the particles must have mass $m>24$ GeV. Such excitations can produce particles of the photino or higgsino type, with spin-dependent interactions. The shape of the pulse for inelastic scattering of WIMPs with excitation of the 13.26 keV level is a superposition of the energy releases of the recoil nucleus and electrons and (or) γ rays (see Fig. 2a) and differs substantially from the shape of the background γ-ray or electron pulses (see Fig. 2b). In Fig. 2a the first component (E_1) of the ionization pulse belongs to the recoil nucleus, while the second component (E_2) belongs to conversion electrons or γ rays with detected energy 13.26 keV with an accuracy to within the resolution of the detector. The time interval T between the two maxima lies in the range from 0 to several lifetimes of the excited level. In the case when the 66.73 keV level is excited, two successive events with a time interval from 0 to several seconds should be detected, and on account of the 53.47 and 13.26 keV cascade transitions the shape of the pulse of the second composite event (just as in the case when the 13.26 keV level is excited) differs substantially from that of the pulse due to background events.

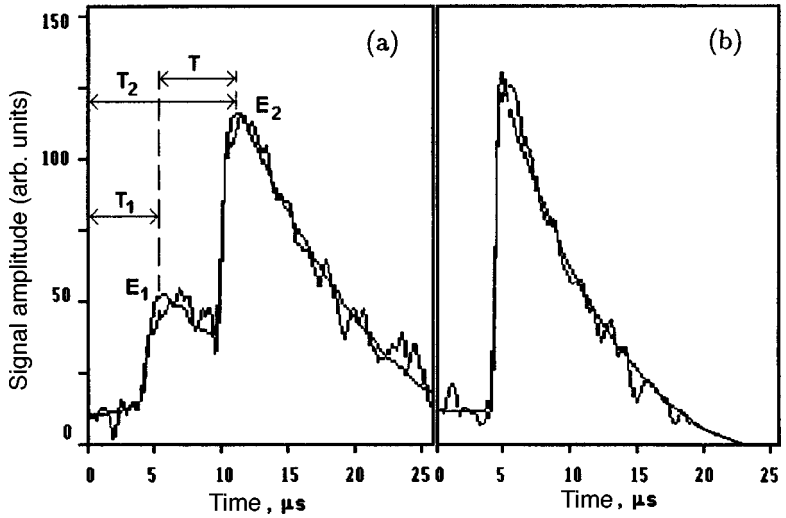

FIG. 2. a) Example of the shape of a double-event pulse. The first component of the pulse (E_1) can be produced by the recoil nucleus and the second component (E_2) can be produced by conversion electrons or γ rays with energy 13.26 keV. b) Example of the standard shape of a pulse produced by a γ ray or electron. The smooth solid curve shows the results of a fit.

To search for events with the above-described signature of the signal data collected over 637 days of useful time (47.1 kg·days in terms of the ^{73}Ge) in an underground low-background laboratory at a depth of 660 meters of water equivalent (mwe) were used.

To select double events a superposition of two standard pulses (see Fig. 2a) with the positions (T_1, T_2) of the maxima and the amplitudes (E_1, E_2) as free parameters was fit to the shape of the detector pulses. Double events with low values of the amplitude of the first component (E_1) and of the time interval (T) can be mimicked by an instability of the slope of the leading edge of the pulse and by noise, i.e., it is necessary to determine the time resolution and the energy threshold for the first component.

Information about the energy releases in each component of double events can only be obtained from the pulse shape on a digital oscilloscope, and the energy resolution in this case is worse than when spectrometric analog-to-digital converters (ADCs) are used. Using a ^{60}Co calibration source and comparing the amplitudes of the signals obtained from a spectrometric ADC and computed from the shape of the pulse, the energy resolution on the digital oscilloscope was determined to be 2 keV near 13.26 keV. The temporal resolution for double events (in the case of excitation of the 13.26 keV level), equal to 2 μs, and the energy threshold for the first component, equal to 2.5 keV, were determined by analyzing for a ^{60}Co source the distribution of the time intervals in the events that had been selected as double events (see Fig. 3) for which the energy of the second component lay in the interval $9.3 < E_2 < 17.3$ keV. Double events can be imitated with a ^{60}Co source can be imitated on account of the spread in the rise times (0.75 ± 0.22 μs for the 9–35 keV range), superposition of detector and amplifier noise on the real signal, and the random pile-up of pulses. A total of 17116 events with a ^{60}Co source were analyzed. With a counting rate of 20 events/s the probability of random pile-up of

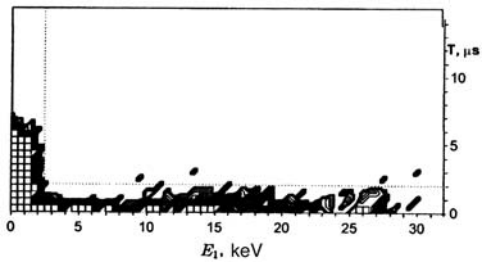

FIG. 3. Distribution in the (E_1, T) plane of events selected as double events in the case of a ^{60}Co source (E_1 is the energy of the first component, and T is the interval between maxima).

pulses in a 15 μs window equals 3×10^{-4}, which for our case comprises five of the 17116 events. In the measurements with the ^{60}Co source seven events were detected above the time-resolution threshold of 2 μs (horizontal dotted line in Fig. 3) and above the energy threshold for detection of the first component (to the right of the vertical dotted line); this agrees with the number of random pile-ups. Therefore we can confidently detect double events with a time interval $2\leqslant T\leqslant 15$ μs between the maxima E_1 and E_2. The upper limit is due to the pulse tracking time 25 μs of the digital oscilloscope, with allowance for 5 μs in front of the leading edge and 5 μs on the trailing edge of the pulse. The detection efficiency for the desired events, equal to 0.62, was determined by comparing this time interval with the decay curve for $t_{1/2}=2.95$ μs.

Figure 4 shows a similar distribution obtained by analyzing background events accumulated over a period of 637 days (32128 events in all). Twenty-nine events fall into the range above the thresholds (dotted lines). Twenty seven events (of the 29) are in coincidence with the active shielding, i.e., they are due to the cosmic-ray background. Only two events in Fig. 4 (the energies of the first components are indicated by the arrows) do not coincide with the active shielding and can be considered as candidates for inelastic scattering of WIMPs with excitation of the 13.26 keV level. However, for these two events the time interval between the maxima equals 2.1 and 2.2 μs, i.e., close to the limit of uncertainty of the time resolution. Taking into account that fact that the probability of high-energy events with the desired exponential distribution is low and the inefficiency factor of the active shielding is $\sim$7%, these two events can also be attributed to the background with a high degree of confidence. But, even taking account of these

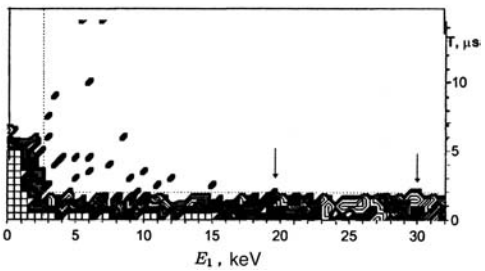

FIG. 4. Distribution in the (E_1, T) plane of background double events collected in a period of 637 days (E_1 is the energy of the first component, and T is the interval between maxima).

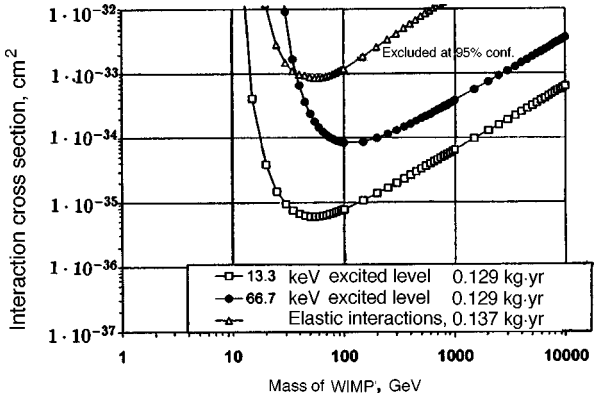

FIG. 5. Regions of excluded WIMP masses and interaction cross sections obtained by analyzing inelastic scattering with excitation of the 13.26 keV and 66.73 keV levels of ^{73}Ge on 74 g of the isotope ^{73}Ge in a collection time of 637 days.

events, the background level is 0.0013 events/(keV·kg (^{73}Ge)·day). The background level of the same detector for elastic scattering in the energy range 2.5–35 keV equals 0.51 events/(keV·kg·day), i.e., the relative reduction of the background is by a factor of greater than 300. Comparing the number of double events in coincidence (27) and in anticoincidence (2) with the active shielding shows that the main source of background for the detector at the depth at which the apparatus is now located is from cosmic rays, generating neutrons in the vicinity of the detector. A much greater decrease of the background can be achieved by performing experiments of this type at a greater depth using enriched ^{73}Ge detectors and using a better digital oscilloscope. To check the correctness of the operation of the program selecting the double events and to estimate the probability of random generations of events of this type, a search was made for double events with the same selection criteria but with the energy of the second component $17.3 \leqslant E_2 \leqslant 25.3$ keV. Not one double event satisfying these selection criteria was found.

In searching for events which occurred during a 3-second time interval prior to the event with an energy of about 66.73 keV, five events in the energy 2.5–35 keV were detected. This corresponds to a background level of 0.0032 events/(keV·kg(^{73}Ge)·day). The possibility of selection by shape of the second event (cascade 53.4 and 13.26 keV) was not used in selecting these events, since the dynamic range of the digital oscilloscope employed is inadequate.

The regions of excluded masses and interaction cross sections for inelastic scattering of WIMPs by ^{73}Ge nuclei with excitation of the 13.26 and 66.73 keV levels are presented in Fig. 5. The following initial assumptions were used to calculate the limits: The dark halo of the galaxy with density 0.3 GeV/cm^3 in the region of the Earth consists completely of WIMPs with the mass under consideration and a Maxwell–Boltzmann velocity distribution with average velocity $v_{\rm rms}=270$ km/s and maximum velocity $v_{\rm esc}=580$ km/s. The Earth's velocity relative to the halo is $v_{\rm Earth}=245$ km/s. The same figure also shows the limits obtained on the spin-dependent elastic interactions in this experiment from the difference of the spectra obtained with the detector described above and a detector not containing ^{73}Ge. It is evident from a comparison of the limits that the use of

the special signature of events in the case of inelastic scattering of WIMPs with excitation of long-lived levels of ^{73}Ge makes it possible to improve the limits on the mass and cross sections of spin-dependent interactions of WIMPs by at least two orders of magnitude compared with elastic interactions. However, the question of the probability of such processes remains open, since the probabilities of such interactions have been calculated in only a few works (see, for example, Refs. 6 and 7), where only M_1 transitions are considered. The γ transitions in ^{73}Ge which were studied here are E_2 and M_2.

This work was supported by the Russian Fund for Fundamental Research (Project 98-02-17973).

[1] J. R. Primack, in *Proceedings of the International Workshop on Dark Matter in Astro- and Particle Physics*, World Scientific, Singapore, 1997, p. 127.
[2] F. T. Avignone, in *Proceedings of the International Workshop on Dark Matter in Astro- and Particle Physics*, World Scientific, Singapore, 1997, p. 427.
[3] R. Bernabei, Riv. Nuovo Cimento **18**(5), 1 (1995).
[4] C. M. Lederer and V. S. Shirley (eds.), *Table of Isotopes*, Wiley, New York, 1987.
[5] A. A. Klimenko, S. B. Osetrov, A. A. Smolnikov *et al.*, Preprint INR-0948/97/, August 1997.
[6] J. Ellis and R. A. Flores, Phys. Lett. B **212**, 375 (1989).
[7] M. W. Goodman and E. Witten, Phys. Rev. D **31**, 3059 (1985).

Translated by M. E. Alferieff

Vortex versus spinning string: Iordanskii force and gravitational Aharonov–Bohm effect

G. E. Volovik

Low Temperature Laboratory, Helsinki University of Technology, P. O. Box 2200, FIN-02015 HUT, Finland; L. D. Landau Institute of Theoretical Physics, 117334 Moscow, Russia

(Submitted 29 April 1998)
Pis'ma Zh. Éksp. Teor. Fiz. **67**, No. 11, 841–846 (10 June 1998)

We discuss the transverse force acting on a spinning cosmic string, moving in the background matter. It comes from the gravitational Aharonov–Bohm effect and corresponds to the Iordanskii force acting on the vortex in superfluids, when the vortex moves with respect to the normal component of the liquid. © *1998 American Institute of Physics.* [S0021-3640(98)00211-4]

PACS numbers: 11.27.+d, 04.20.Gz

INTRODUCTION

In superfluids, with their two-fluid hydrodynamics (for the superfluid and normal components of the liquid) there are 3 different topological contributions to the force acting on the quantized vortex.[1] The more familiar Magnus force arises when the vortex moves with respect to the superfluid vacuum. For a relativistic cosmic string such force is absent since the corresponding superfluid density of the quantum physical vacuum is zero. However the analog of this force appears if the cosmic string moves in a uniform background charge density.[2,3] The other two forces of topological origin also have analogs for the cosmic strings: one of them comes from the analog of the axial anomaly in the core of an electroweak string (see reviews[4]), and another one — the Iordanskii force — is now under active discussion in the condensed-matter community.[5–7]

As distinct from the Magnus force, the Iordanskii force[8,9] arises when the vortex moves with respect to the heat bath represented by the normal component of the liquid, which consists of the quasiparticle excitations. The latter corresponds to matter in particle physics. The interaction of quasiparticles with the velocity field of the vortex resembles the interaction of the matter with the gravitational field induced by such a cosmic string having an angular momentum — a so-called spinning cosmic string.[10] The spinning string induces a peculiar space–time metric that leads to a time delay for any particle orbiting around the string with the same speed but in opposite directions.[11] This gives rise to the quantum gravitational Aharonov–Bohm (AB) effect.[10,12,13] We discuss here how the same effect leads to the asymmetry in the scattering of particles on the spinning string and finally to the Iordanskii lifting force acting on the spinning string.

VORTEX VERSUS SPINNING COSMIC STRING

To clarify the analogy between the Iordanskii force and AB effect, let us consider the simplest case of phonons propagating in the velocity field of the quantized vortex in the Bose superfluid ^{4}He. According to the Landau theory of superfluidity, the energy of a quasiparticle moving in the superfluid velocity field $\mathbf{v}_s(\mathbf{r})$ is Doppler shifted: $E(\mathbf{p}) = \epsilon(\mathbf{p}) + \mathbf{p}\cdot\mathbf{v}_s(\mathbf{r})$. In the case of the phonons with the spectrum $\epsilon(\mathbf{p}) = cp$, where c is the sound velocity, the energy–momentum relation is thus

$$(E - \mathbf{p}\cdot\mathbf{v}_s(\mathbf{r}))^2 = c^2 p^2. \tag{1}$$

Equation (1) can be written in the general Lorentzian form with $p_\mu = (E, \mathbf{p})$:

$$g^{\mu\nu} p_\mu p_\nu = 0, \quad g^{00} = 1, \quad g^{0i} = -v_s^i, \quad g^{ik} = -c^2\delta^{ik} + v_s^i v_s^k. \tag{2}$$

Thus the dynamics of phonons in the presence of the velocity field is the same as the dynamics of photons in the gravity field:[14] both are described by the light-cone equation $ds = 0$, where the interval ds is given by the inverse metric $g_{\mu\nu}$:

$$ds^2 = g_{\mu\nu} dx^\mu dx^\nu. \tag{3}$$

Here we are interested in the velocity field circulating around a quantized vortex, $\mathbf{v}_s = N\kappa\hat{\phi}/2\pi r$, where κ is the quantum of circulation and N is the circulation quantum number. This flow induces an effective space in which the phonon propagates along geodesic curves, with the interval

$$ds^2 = \left(1 - \frac{v_s^2}{c^2}\right)\left(dt + \frac{N\kappa d\phi}{2\pi(c^2 - v_s^2)}\right)^2 - \frac{dr^2}{c^2} - \frac{dz^2}{c^2} - \frac{r^2 d\phi^2}{c^2 - v_s^2}. \tag{4}$$

Far from the vortex, where v_s^2/c^2 is small and can be neglected, one has

$$ds^2 = \left(dt + \frac{d\phi}{\omega}\right)^2 - \frac{1}{c^2}(dz^2 + dr^2 + r^2 d\phi^2), \quad \omega = \frac{2\pi c^2}{N\kappa}. \tag{5}$$

The connection between the time and the azimuthal angle ϕ in the interval suggests that there is a characteristic angular velocity ω. For the vortex in superfluid ^{4}He, where $\kappa = 2\pi\hbar/m_4$ and m_4 is the mass of ^{4}He atom, it is $\omega = m_4 c^2/N\hbar$. A similar metric with rotation was obtained for the so-called spinning cosmic string in $3+1$ space–time, which has the rotational angular momentum J concentrated in the string core, and for a spinning particle in $2+1$ gravity:[10,13,15,16]

$$ds^2 = \left(dt + \frac{d\phi}{\omega}\right)^2 - \frac{1}{c^2}(dz^2 + dr^2 + r^2 d\phi^2), \quad \omega = \frac{1}{4JG}, \tag{6}$$

where G is the gravitational constant. This gives the following correspondence between the circulation $N\kappa$ around the vortex and the angular momentum J of the spinning string

$$\kappa N = 8\pi JG. \tag{7}$$

Although we are considering the analogy between a spinning string and vortices in superfluid ^{4}He, there is a general statement that vortices in any superfluids have the properties of spinning cosmic strings.[2] In particular, a spinning string generates an angular momentum density in the vacuum outside the string.[17] The angular momentum density

in the superfluid vacuum outside the vortex is also nonzero and equal to $\hbar Nn$, where n is the number density of elementary bosons in the superfluid vacuum: the density of ^{4}He atoms in superfluid ^{4}He or of Cooper pairs in superfluid ^{3}He.

GRAVITATIONAL AB EFFECT

An effect peculiar to a spinning string, which can be modeled in condensed matter, is the gravitational AB topological effect.[10] On the classical level the propagation of phonons is described by the equation $ds^2=0$. Outside the string the metric, which enters the interval ds, is locally flat. But there is a time difference for the particles propagating around the spinning string in the opposite directions. For the vortex (at large distances from the core) this time delay approaches[11]

$$2\tau=\frac{4\pi}{\omega}. \tag{8}$$

This asymmetry between the particles moving on different sides of the vortex is the origin of the Iordanskii force acting on the vortex in the presence of a net momentum of the quasiparticles. On the quantum level, the connection between the time variable t and the angle variable ϕ in the metric (6) implies that the cross section for scattering of phonons (photons) on the vortex should be a periodic function of the energy, with a period equal to $\hbar\omega$. The asymmetric part of this cross section gives rise to the Iordanskii force.

There was an extreme interpretation of the gravitational AB effect put forward by Mazur.[10] He argued that for the infinitely thin spinning cosmic string there is a region in which causality is violated. To avoid causality violation the string should be transparent to the excitations, and this is possible only if in the presence of the spinning cosmic string the energy of the elementary particles is strictly quantized: $E=n\hbar\omega$. In other words the gravitational AB effect leads to the energy quantization in the same manner as the quantization of the electric charge should take place in the presence of the Dirac magnetic monopole. On the other hand there are solutions for cosmic strings which do not contain closed timelike curves.[18] In this case the severe energy quantization is not necessary (see, however, the discussion in Refs. 12,13,19,20). In any case the periodicity with period $\Delta E=\hbar\omega$ is retained, and the symmetric part of the scattering cross section of a particle with energy E in the background of a spinning string with zero mass is:[12,13]

$$\frac{d\sigma}{d\theta}=\frac{\hbar c}{2\pi E\sin^2(\theta/2)}\sin^2\frac{\pi E}{\hbar\omega}. \tag{9}$$

We argue that in addition to this symmetric part there is a topological asymmetric contribution, which gives rise to a transverse cross section

$$\sigma_\perp=\int_0^{2\pi}d\theta\,\sin\,\theta|a(\theta)|^2. \tag{10}$$

The asymmetry in the scattering of the quasiparticles on the velocity field of the vortex has been calculated by Sonin[5] for phonons and rotons in ^{4}He and by Cleary[21] for the Bogoliubov–Nambu quasiparticles in conventional superconductors. In the case of

phonons the propagation is described by the Lorentzian equation for the scalar field, $g^{\mu\nu}\partial_\mu\partial_\nu\Phi=0$. In the asymptotic region the quadratic terms $\mathbf{v}_s^2/c^2$ can be neglected, and this equation can be rewritten as[5]

$$E^2\Phi - c^2\left(-i\nabla + \frac{E}{c}\mathbf{v}_s(\mathbf{r})\right)^2\Phi = 0. \tag{11}$$

This equation maps the problem under discussion to the Aharonov–Bohm problem for a magnetic flux tube[22] with the vector potential $\mathbf{A}=\mathbf{v}_s$, where the electric charge e is replaced by the mass E/c^2 of the particle.[12,17,23] Because of the mapping between the electric charge and the mass of the particle, the Lorentz force, which acts on the flux tube in the presence of electric current, has its counterpart — the Iordanskii force, which acts on the vortex in the presence of the mass current carried by the normal component.[7]

If one directly follows the mapping of the phonon scattering on vortices described by Eq. (11) to the AB scattering, one obtains the AB result[22] for the symmetric part of the differential cross section, now written in the form of Eq. (9). There is a not very important difference, which comes from the definition of the quasiparticle current: as distinct from the charged particles in the AB effect, the current in our case is not gauge invariant. As a result, the scattering of a phonon with momentum p and energy E by the vortex is somewhat different:[5]

$$\frac{d\sigma}{d\theta} = \frac{\hbar c}{2\pi E}\cot^2\frac{\theta}{2}\sin^2\frac{\pi E}{\hbar\omega}. \tag{12}$$

The difference between Eq. (12) and the AB result in Eq. (9) is $(c/2\pi E)\sin^2(\pi E/\omega)$, which is independent of the scattering angle θ and thus is not important for the singularity at small scattering angles. For small E the result in Eq. (12) was obtained by Fetter.[24] The generalization of the Fetter result for the quasiparticles with arbitrary spectrum $\epsilon(\mathbf{p})$ (rotons in ^{4}He and the Bogoliubov–Nambu fermions in superconductors) was recently suggested in Ref. 25. In our notations it is $(N\kappa^2 p/8\pi v_G^2)\cot^2(\theta/2)$, where $v_G = d\epsilon/dp$ is the group velocity of quasiparticle.

ASYMMETRIC CROSS SECTION

The Lorentz-type Iordanskii force comes from the asymmetric singularity in the cross section.[7] This additional topological term is determined by the same asymptotic behavior of the flow velocity, which causes singularity at small angles in the symmetric cross section. The asymmetric part of the differential cross section gives the following transverse cross section:[5]

$$\sigma_\perp = \frac{\hbar}{p}\sin\frac{2\pi E}{\hbar\omega}. \tag{13}$$

At low E this result was generalized for arbitrary excitations with the spectrum $E(\mathbf{p}) = \epsilon(\mathbf{p}) + \mathbf{p}\cdot\mathbf{v}_s$ moving in the background of the velocity field $\mathbf{v}_s$ around the vortex, using a simple classical theory of scattering.[5] Far from the vortex, where the circulating velocity is small, the trajectory of the quasiparticle is almost a straight line parallel to, say, the y axis, with the distance from the vortex line being the impact parameter x. It moves along this line with an almost constant momentum $p_y \approx p$ and an almost constant group velocity $v_G = d\epsilon/dp$. The change in the transverse momentum during this motion is

determined by the Hamilton's equation $dp_x/dt = -\partial E/\partial x = -p_y \partial v_{sy}/\partial x$, or $dp_x/dy = -(p/v_G)\partial v_{sy}/\partial x$. The transverse cross section is obtained by integration of $\Delta p_x/p$ over the impact parameter x:

$$\sigma_\perp = \int_{-\infty}^{+\infty} \frac{dx}{v_G} \int_{-\infty}^{+\infty} dy \frac{\partial v_{sy}}{\partial x} = \frac{N\kappa}{v_G}. \tag{14}$$

Note that this result is purely classical: Planck's constant $\hbar$ drops out.

IORDANSKII FORCE ON SPINNING STRING

This asymmetric part of the scattering, which describes the momentum transfer in the transverse direction, after integration over the distribution of excitations gives rise to a transverse force acting on the vortex if the vortex moves with respect to the normal component. This is the Iordanskii force:

$$\mathbf{f}_{\text{Iordanskii}} = \int \frac{d^3p}{(2\pi)^3} \sigma_\perp(p) v_G n(\mathbf{p}) \mathbf{p} \times \hat{\mathbf{z}} = -N\kappa \hat{\mathbf{z}} \times \int \frac{d^3p}{(2\pi)^3} n(\mathbf{p}) \mathbf{p} = N\kappa \mathbf{P}_n \times \hat{\mathbf{z}}. \tag{15}$$

It depends only on the mass current density $\mathbf{P}_n$ carried by excitations (matter) and on the circulation $N\kappa$ around the vortex. This confirms the topological origin of this force. In the case of an equilibrium distribution of quasiparticles one has $\mathbf{P}_n = \rho_n \mathbf{v}_n$, where ρ_n and $\mathbf{v}_n$ are the density and velocity of the normal component of the liquid (to avoid the conventional Magnus force, we assume that the asymptotic velocity of the superfluid component of the liquid is zero in the vortex frame).

Since Eq. (15) was obtained using the asymptotic behavior of the flow field $\mathbf{v}_s$, which induces the same effective metric as the metric around the spinning string, one can apply this result directly to the spinning string. The asymmetric cross section for the scattering of relativistic particles on the spinning string is given by Eq. (13). This means that in the presence of the momentum of matter the spinning cosmic string experiences a kind of lifting force, which corresponds to the Iordanskii force in superfluids. This force can be obtained by relativistic generalization of Eq. (15). The momentum density $\mathbf{P}_n$ of quasiparticles should be replaced by the component T_0^i of the energy–momentum tensor. As a result, for $2+1$ space–time and for small energy E, which corresponds to a low temperature T of the matter, the Iordanskii force on spinning string moving with respect to the matter is

$$f^\alpha_{\text{Iordanskii}} = 8\pi J G e^{\alpha\beta\gamma} u_\beta u_\mu T^\mu_\gamma. \tag{16}$$

Here u_α is the 3-velocity of the string and T^μ_γ is the asymptotic value of the energy–momentum tensor of the matter at the location of the string. Using the Einstein equations one can rewrite this as

$$f^\alpha_{\text{Iordanskii}} = J e^{\alpha\beta\gamma} u_\beta u_\mu R^\mu_\gamma, \tag{17}$$

where R^μ_γ is the Riemannian curvature, which is induced by external sources, at the location of the string. This corresponds to the force acting on a particle with spin J from the gravitational field due to interaction of the spin with the Riemann tensor.[26]

CONCLUSION

There is an analogy between the asymptotic velocity field far from the vortex core in superfluids and the gravitational field induced by a spinning cosmic string. As a result, both systems experience the gravitational Aharonov–Bohm effect, which in particular leads to the Iordanskii force acting on the vortex (the spinning string) when it moves with respect to the heat bath of quasiparticles (the matter).

The Iordanskii force has been experimentally identified in rotating superfluid ^{3}He–B. According to the theory for the transport of vortices in ^{3}He–B, the Iordanskii force completely determines the mutual friction parameter $d_\perp \approx -\rho_n/\rho$ at low T Ref. 27, where ρ is the total density of the liquid. This is in accordance with the experimental data, which show that $d_\perp$ does approach its negative asymptote at low T (Ref. 28). At higher T another topological force, which comes from the spectral flow of the fermion zero modes in the vortex core,[29,4] becomes dominating and leads to reversal of the sign of $d_\perp$. The observed negative sign of $d_\perp$ at low T provides experimental verification of the condensed-matter analog of the gravitational Aharonov–Bohm effect on a spinning cosmic string.

I thank Pawel Mazur and Edouard Sonin for illuminating discussions and Bjorn Jensen for sending copies of his papers. This work was supported by the Russian Fund for Fundamental Research under Grant 96-02-16072, by the Russian Academy of Sciences program ''Statistical Physics'' and by European Science Foundation network on ''Topological Defects in Cosmology and Condensed Matter Physics.''

[1] G. E. Volovik, JETP Lett. **62**, 65 (1995).
[2] R. L. Davis and E. P. S Shellard, Phys. Rev. Lett. **63**, 2021 (1989).
[3] K.-M. Lee, Phys. Rev. D **49**, 4265 (1994).
[4] G. E. Volovik and T. Vachaspati, Int. J. Mod. Phys. B **10**, 471 (1996); G. E. Volovik, http://xxx.lanl.gov/abs/cond-mat/9802091.
[5] E. B. Sonin, Phys. Rev. B **55**, 485 (1997).
[6] C. Wexler, Phys. Rev. Lett. **79**, 1321 (1997).
[7] A. Shelankov, http://xxx.lanl.gov/abs/cond-mat/9802158.
[8] S. V. Iordanskii, Ann. Phys. **29**, 335 (1964); Zh. Éksp. Teor. Fiz. **49**, 225 (1965) [Sov. Phys. JETP **22**, 160 (1966)].
[9] E. B. Sonin, Zh. Éksp. Teor. Fiz. **69**, 921 (1975) [Sov. Phys. JETP **42**, 469 (1976)].
[10] P. O. Mazur, Phys. Rev. Lett. **57**, 929 (1986).
[11] D. Harari and A. P. Polychronakos, Phys. Rev. D **38**, 3320 (1988).
[12] P. O. Mazur, Phys. Rev. Lett. **59**, 2380 (1987).
[13] P. O. Mazur, http://xxx.lanl.gov/abs/hep-th/9611206.
[14] W. G. Unruh, Phys. Rev. D **14**, 870 (1976); **51**, 2827 (1995).
[15] A. Staruszkievicz, Acta Phys. Pol. **24**, 734 (1963).
[16] S. Deser, R. Jackiw, and G. t'Hooft, Ann. Phys. **152**, 220 (1984).
[17] B. Jensen and J. Kučera, J. Math. Phys. **34**, 4975 (1993).
[18] B. Jensen and H. H. Soleng, Phys. Rev. D **45**, 3528 (1992).
[19] G. N. Glushchenko, Zh. Éksp. Teor. Fiz. **104**, 273 (1995) [JETP **80**, 145 (1995)].
[20] G. E. Volovik, Low Temp. Phys. (Kharkov) **24**, 127 (1998).
[21] R. M. Cleary, Phys. Rev. **175**, 587 (1968).
[22] Y. Aharonov and D. Bohm, Phys. Rev. **115**, 485 (1959).
[23] D. V. Gal'tsov and P. S. Letelier, Phys. Rev. D **47**, 4273 (1993).
[24] A. L. Fetter, Phys. Rev. A **136**, 1488 (1964).
[25] E. Demircan, P. Ao and Q. Niu, Phys. Rev. B **52**, 476 (1995).
[26] K. S. Thorne and J. B. Hartle, Phys. Rev. D **31**, 1815 (1985); Y. Mino, M. Sasaki, and T. Tanaka, http://xxx.lanl.gov/abs/gr-qc/9705073.

[27] N. B. Kopnin, G. E. Volovik, and Ü. Parts, Europhys. Lett. **32**, 651 (1995).
[28] T. D. C. Bevan, A. J. Manninen, J. B. Cook *et al.*, Phys. Rev. Lett. **74**, 750 (1995).
[29] T. D. C. Bevan, A. J. Manninen, J. B. Cook *et al.*, Nature **386**, 689 (1997).

Published in English in the original Russian journal. Edited by Steve Torstveit.

k-Symmetry and anomalous magnetic moment of superparticles

A. A. Zheltukhin[a)] and D. V. Uvarov
Kharkov Physicotechnical Institute National Science Center, 310108 Kharkov, Ukraine

(Submitted 10 April 1998)
Pis'ma Zh. Éksp. Teor. Fiz. **67**, No. 11, 847–853 (10 June 1998)

It is shown that *k*-symmetry breaking arising upon the minimal inclusion of an interaction of massive spin-1/2 particles with an $N=2$ extended Maxwell supermultiplet is restored by taking into account their anomalous magnetic moment (AMM). The *k*-invariant action of massive superparticles is constructed, and it is shown that *k*-symmetry uniquely fixes the value of their AMM. © *1998 American Institute of Physics.* [S0021-3640(98)00311-9]

PACS numbers: 11.25.Sq, 11.30.Pb

1. The requirement of *k*-symmetry[1–3] is the key principle for constructing theories of superstrings and super-*p*- (and *D*-) branes that are self-consistent at the quantum level.[4–6] For this reason it is of interest to determine whether *k*-symmetry is preserved on switching from free supersymmetric theories to theories with interaction. The model of charged superstrings in an external electromagnetic field[7] is one of the simplest supersymmetric schemes with interaction. In the case of $N=1$ massless superparticles the transition to a *k*-symmetric model with interaction is accomplished by using only the principle of minimal inclusion of electromagnetic interactions. An important consequence of the presence of *k*-symmetry in a model with interaction is that the correct constraints are obtained for the fields of the $N=1$ Maxwell supermultiplet.[8]

The compatibility of the principle of minimality and *k*-symmetry is destroyed, however, on switching to $N=2$ massive superparticles and this, as was pointed out in Ref. 9, requires modifications of the extended theories, similar to those studied in Ref. 10 and 11 for the case of particles with spin. These modifications, based on ''renormalizations'' of the mass parameters, turned out to be equivalent to taking into account the anomalous magnetic moment (AMM) of particles with spin in a superfield description.[12] In the process, no limitations on the value of the AMM appeared.

A similar picture also arises in the case of $N=2$ massive superparticles studied below, but here the requirement of *k*-symmetry will strictly fix the value of the AMM of the superparticles.

2. The minimally extended action of a massive superparticle in an external electromagnetic field has the form

$$S^{(e)}_{\min}=\int dr\left[\frac{1}{2}\left(\frac{\omega^\mu\omega_\mu}{g}-gm^2\right)+m(\theta^\alpha_i\dot\theta^i_\alpha+\bar\theta_{\dot\alpha i}\dot{\bar\theta}^{\dot\alpha i})\right]+ie\int dr(\omega^\mu A_\mu+\dot\theta^\alpha_i A^i_\alpha+\dot{\bar\theta}_{\dot\alpha i}\bar A^{\dot\alpha i}),\tag{1}$$

where $z^\mu(\tau)=(x^\mu(\tau),\theta^\alpha_i(\tau),\bar\theta_{\dot\alpha i}(\tau))$ are the coordinates of the superparticle, $\omega^\mu=\dot x^\mu+i\theta^\alpha_i\sigma^\mu_{\alpha\dot\alpha}\dot{\bar\theta}^{\dot\alpha i}-i\dot\theta^\alpha_i\sigma^\mu_{\alpha\dot\alpha}\bar\theta^{\dot\alpha i}$, $\dot\theta^\alpha_i$, and $\dot{\bar\theta}_{\dot\alpha i}$ are the $N=2$ supersymmetric Cartan forms, $A_M(x,\theta,\bar\theta)=(A_\mu,A^i_\alpha,\bar A_{\dot\alpha i})$ are the $U(1)$-gauge superfields. Here we adopt the notation of Ref. 8, and we shall also often make use of an abbreviated notation for the $SO(1,3)$ and $SU(2)$ spinor indices $\theta_\alpha\equiv\theta^i_\alpha$, $\bar\theta_{\dot\alpha}\equiv\bar\theta_{\dot\alpha i}$ and so on. We shall show that the action (1) does not possess k-symmetry. It is convenient to give the proof on the basis of the Dirac Hamiltonian formalism.[13] Introducing the canonical momenta

$$p_\mu=\frac{\partial L}{\partial\dot x^\mu}=\frac{\omega_\mu}{g}+ieA_\mu,\quad p_g=\frac{\partial L}{\partial\dot g}\ \text{and}\ \pi^i_\alpha=\frac{\partial L}{\partial\dot\theta^\alpha_i}=-\frac{i\omega_{\alpha\dot\alpha}\bar\theta^{\dot\alpha i}}{g}-m\theta^i_\alpha+eA_{\alpha\dot\alpha}\bar\theta^{\dot\alpha i}+ieA^i_\alpha,$$

$$\bar\pi_{\dot\alpha i}=\frac{\partial L}{\partial\dot{\bar\theta}^{\dot\alpha i}}=-\frac{i\theta^\alpha_i\omega_{\alpha\dot\alpha}}{g}-m\bar\theta_{\dot\alpha i}+e\theta^\alpha_i A_{\alpha\dot\alpha}+ie\bar A^i_{\dot\alpha i},\tag{2}$$

where π^i_α and $\bar\pi_{\dot\alpha i}$ are conjugate to the Grassmann spinors θ^α_i and $\bar\theta^{\dot\alpha i}$, we obtain for the Hamiltonian $H_0=\dot x^\mu p_\mu+\dot\theta^\alpha_i\pi^i_\alpha+\bar\theta_{\dot\alpha i}\bar\pi^{\dot\alpha i}-L$

$$H_0=\frac{g}{2}[(p^\mu-ieA^\mu)^2+m^2].\tag{3}$$

Since the definitions (2) imply the primary constraints $p_g\approx0$ and

$$V^i_\alpha=\pi^i_\alpha+ip_{\alpha\dot\alpha}\bar\theta^{\dot\alpha i}+m\theta^i_\alpha-ieA^i_\alpha\approx0,\quad V_{\dot\alpha i}=\bar\pi_{\dot\alpha i}+i\theta^\alpha_i p_{\alpha\dot\alpha}+m\bar\theta_{\dot\alpha i}-ie\bar A_{\dot\alpha i}\approx0,\tag{4}$$

the Hamiltonian H_0 must be extended to the full Hamiltonian H including all primary constraints

$$H=\frac{g}{2}[(p^\mu-ieA^\mu)^2+m^2]+\lambda\underline{}^\alpha V_{\underline{\alpha}}+\bar\lambda_{\underline{\dot\alpha}}\bar V\underline{}^{\dot\alpha}+\varphi p_g.\tag{5}$$

The requirement that the primary constraints be conserved in time leads to the secondary constraint $\chi=(p^\mu-ieA^\mu)^2+m^2\approx0$ and to a system of equations for the Lagrange multipliers $\lambda\underline{}^\alpha$ and $\bar\lambda_{\underline{\dot\alpha}}$:

$$Q_{\underline{\alpha}}+\lambda\underline{}^\beta M_{\underline{\beta\alpha}}+\bar\lambda\underline{}^{\dot\beta}N_{\underline{\alpha\dot\beta}}=0,\quad \bar Q_{\underline{\dot\alpha}}+\lambda\underline{}^\beta N_{\underline{\beta\dot\alpha}}+\bar\lambda\underline{}^{\dot\beta}\bar M_{\underline{\dot\beta\dot\alpha}}=0,\tag{6}$$

where for convenience we have introduced the notation

$$Q_{\underline{\alpha}}=\frac{eg}{2}P^{\dot\beta\beta}F_{\beta\dot\beta,\underline{\alpha}},\quad \bar Q_{\underline{\dot\alpha}}=\frac{eg}{2}P^{\dot\beta\beta}F_{\beta\dot\beta,\underline{\dot\alpha}},\quad M_{\underline{\beta\alpha}}=-2im\epsilon_{\underline{\beta\alpha}}-eF_{\underline{\beta\alpha}},$$

$$\bar M_{\underline{\dot\beta\dot\alpha}}=-2im\epsilon_{\underline{\dot\beta\dot\alpha}}-eF_{\underline{\dot\beta\dot\alpha}},\quad N_{\alpha\dot\alpha}=2P_{\underline{\alpha\dot\alpha}}-eF_{\underline{\alpha\dot\alpha}},\quad P_{\underline{\alpha\dot\alpha}}=p_{\underline{\alpha\dot\alpha}}-ieA_{\underline{\alpha\dot\alpha}}.\tag{7}$$

The superfield intensities are defined in Ref. 14. In order for k-symmetry to exist the rank of the system (6) must equal 4, just as in the free case. A necessary and sufficient condition for this is the presence of the following constraints:

$$\overline{Y}_{\underline{\dot\beta\dot\alpha}} \equiv \overline{M}_{\underline{\dot\beta\dot\alpha}} - N_{\underline{\alpha\dot\beta}} M^{-1\,\underline{\alpha\beta}} N_{\underline{\beta\dot\alpha}} \approx 0, \tag{8}$$

$$\overline{Q}_{\underline{\dot\alpha}} - N_{\underline{\beta\dot\alpha}} M^{-1\,\underline{\beta\alpha}} Q_{\underline{\alpha}} \approx 0. \tag{9}$$

Just as in the free case, we assumed that matrices inverse to M and N exist. Ultimately, only four independent equations remained in the system (6); the same number of Lagrange multipliers will remain arbitrary after the system is solved, indicating that there exist four first class spinor constraints. Substituting the solution (6) into the Hamiltonian (5), we find these constraints in explicit form:

$$V^{(1)}_{\underline{\alpha}} = V_{\alpha} - N_{\underline{\alpha\dot\beta}} \overline{M}^{-1\,\underline{\dot\beta\dot\alpha}} \overline{V}_{\underline{\dot\alpha}} \approx 0. \tag{10}$$

It can be shown that the Poisson bracket (PB) of the constraints (10) is a quadratic polynomial $Y_{\underline{\alpha\beta}}$ in powers of $P_{\underline{\alpha\dot\alpha}}$:

$$\{V^{(1)}_{\underline{\alpha}}, V^{(1)}_{\underline{\beta}}\} = Y_{\underline{\alpha\beta}} \equiv a_{\underline{\alpha\beta}} + b^{\dot\lambda}_{\underline{(\alpha}} P_{\underline{\beta)\dot\lambda}} + c^{\underline{\dot\lambda\dot p}} P_{\underline{\alpha\dot\lambda}} P_{\underline{\beta\dot p}} \tag{8'}$$

with structure functions a, b, and c which depend on the spinor components of the superfield intensities F_{MN}. Since the PB of the first class constraints $V^{(1)}_{\alpha}$ must close on the constraint, we find that the polynomial $Y_{\underline{\alpha\beta}}$ must be regarded as a new additional constraint $Y_{\underline{\alpha\beta}} = 0$. Calculation of the PB of the constraints $V^{(1)}_{\alpha}$ with the constraints $Y_{\underline{\beta\gamma}}$ leads to a cubic polynomial $Y_{\underline{\alpha\beta\gamma}}$ in powers of the momenta $\overline{P}_{\underline{\alpha\dot\alpha}}$

$$\{V^{(1)}_{\underline{\alpha}}, Y_{\underline{\beta\gamma}}\} = Y_{\underline{\alpha\beta\gamma}} \equiv a_{\underline{\alpha\beta\gamma}} + \sum_{(\underline{\alpha\beta\gamma})} (b^{\dot\lambda}_{\underline{\alpha\beta}} P_{\underline{\gamma\dot\lambda}} + c^{\underline{\dot\lambda\dot p}}_{\underline{\alpha}} P_{\underline{\beta\dot\lambda}} P_{\underline{\gamma\dot p}}) + d^{\underline{\dot\lambda\dot p\dot\delta}} P_{\underline{\alpha\dot\lambda}} P_{\underline{\beta\dot p}} P_{\underline{\gamma\dot\delta}}$$

with the structure functions a, b, c, and d depending on the superfield intensities and their derivatives. Analysis shows that the polynomial $Y_{\underline{\alpha\beta\gamma}}$ does not reduce to previously obtained constraints and must be declared a new additional constraint, satisfying the consistency conditions. Continuing this process of checking the obtained constraints for consistency, we arrive at an infinite sequence of new constraints which are polynomials of arbitrarily high degree in powers of $P_{\alpha\dot\alpha}$. This analysis does not make it possible to draw a conclusion about the reducibility of the infinite set of constraints obtained to some finite set of linearly independent constraints.

A possibility of avoiding uncontrollable multiplication of constraints is identical satisfaction of a constraint at any stage (for arbitrary P). Since the coefficients of the powers of $P_{\alpha\dot\alpha}$ are constructed from superfield intensities and their derivatives, this possibility actually signifies a limitation on the field configurations. Identical satisfaction of a constraint at the nth stage would lead to identical satisfaction of the constraints at all subsequent stages. However, we were not able to implement this program for arbitrary n because of the complexity of the expressions obtained. Analysis of the first two steps showed that identical satisfaction of the constraints $Y_{\underline{\beta\gamma}}$ and $Y_{\underline{\alpha\beta\gamma}}$ leads to much too strong limitations on the $N=2$ physical superfields W and $\overline{W}$:[14] $W=$ const, $\overline{W}=$ const. Apparently, this also happens at subsequent stages.

Our analysis shows the impossibility of the existence of first class spinor constraints and, in consequence, k-symmetry within a finite algebra of constraints. We arrive at the conclusion that the principle of minimality by itself is inadequate for constructing the k-invariant action of a $N=2$ superparticle.

3. Preservation of k-invariance upon inclusion of the electromagnetic field requires introducing nonminimal terms. For particles possessing an anomalous magnetic moment μ in addition to a charge e, there is a possibility of introducing such terms without destroying the minimal scheme of interactions due to the charge e. Taking into account the dimensions of the AMM $[\mu]=L$ (in the system $c=\hbar=1$), it is possible to construct dimensionless gauge-invariant scalars $\mu F\frac{\alpha}{\alpha}$ and $\mu F\frac{\dot\alpha}{\dot\alpha}$ which are linear in the intensities. Similar considerations were employed in Ref. 15 to introduce nonminimal terms by lengthening the connection. Then the action for a superparticle with charge e and AMM μ can be written in the form

$$S^{(e,\mu)}=-m\int dr\sqrt{-F\omega^\mu\omega_\mu}+m\int dr(\theta^\alpha\dot\theta_\alpha+\bar\theta_{\dot\alpha}\dot{\bar\theta}^{\dot\alpha})+ie\int dr(\omega^\mu A_\mu+\dot\theta^\alpha A_\alpha+\dot{\bar\theta}_{\dot\alpha}\bar A^{\dot\alpha}),$$

$$F=\left(1-\frac{i\mu}{4}F\frac{\alpha}{\alpha}\right)\left(1-\frac{i\mu}{4}F\frac{\dot\alpha}{\dot\alpha}\right). \tag{11}$$

The modification of the kinetic term of the superparticles achieved by replacing the mass parameter m in the first term by the field function $m^*\equiv(m^2F)^{1/2}$ is, by construction, a gauge-invariant and supersymmetric procedure. However, an analogous procedure with the parameter m in the second term would have led to breaking of global supersymmetry. Introducing the einbein g on the world line, the Lagrangian of a superparticle in Eq. (11) can be represented in the form

$$L^{(e,\mu)}=\frac{1}{2}\left(\frac{F\omega^2}{g}-gm^2\right)+m(\theta^\alpha\dot\theta_\alpha+\bar\theta_{\dot\alpha}\dot{\bar\theta}^{\dot\alpha})+ie(\omega^\mu A_\mu+\dot\theta^\alpha A_\alpha+\dot{\bar\theta}_{\dot\alpha}\bar A^{\dot\alpha}). \tag{12}$$

Defining, as in Sec. 2, the momenta

$$p_\mu=\frac{\partial L}{\partial\dot x^\mu}=\frac{F\pi_\mu}{g}=ieA_\mu,\quad p_g=\frac{\partial L}{\partial\dot g}=0\ \text{ and }\ \pi^i_\alpha=\frac{\partial L}{\partial\theta^\alpha_i}=-\frac{iF}{g}\omega_{\alpha\dot\alpha}\bar\theta^{\dot\alpha i}-m\theta^i_\alpha$$

$$+eA_{\alpha\dot\alpha}\bar\theta^{\dot\alpha i}+ieA^i_\alpha,\quad \bar\pi_{\dot\alpha i}=\frac{\partial L}{\partial\bar\theta^{\dot\alpha i}}=-\frac{iF}{g}\theta^\alpha_i\omega_{\alpha\dot\alpha}-m\bar\theta_{\dot\alpha i}+e\theta^\alpha_iA_{\alpha\dot\alpha}+ie\bar A_{\dot\alpha i} \tag{13}$$

for the Hamiltonian

$$H_0=\frac{g}{2F}[(p^\mu-ieA^\mu)^2+m^{*2}], \tag{14}$$

we obtain the primary constraints $p_g\approx0$ and

$$V^i_\alpha=\pi^i_\alpha+ip_{\alpha\dot\alpha}\bar\theta^{\dot\alpha i}+m\theta^i_\alpha-ieA^i_\alpha\approx0,\quad \bar V_{\dot\alpha i}=\bar\pi_{\dot\alpha i}+ip_{\alpha\dot\alpha}\theta^\alpha_i+m\bar\theta_{\dot\alpha i}-ie\bar A_{\dot\alpha i}\approx0. \tag{15}$$

The complete Hamiltonian equals

$$H=H_0+\lambda^{\underline{\alpha}}V_{\underline{\alpha}}+\overline{\lambda}_{\underline{\dot{\alpha}}}\overline{V^{\underline{\alpha}}}+\varphi p_g\,. \tag{16}$$

We note that the primary constraints, in contrast to the Hamiltonians H and H_0, have turned out to be ''insensitive'' to the nonminimal terms. Just as in Sec. 2, from the conservation of the primary constraints in time we obtain the secondary constraint $\chi=P^2+m^{*2}\approx 0$ as well as a system of equations for the Lagrange multipliers that is identical in form to the system (6), except that now

$$Q_{\underline{\alpha}}=\frac{eg}{2F}P^{\dot\beta\beta}F_{\beta\dot\beta,\underline{\alpha}}+\frac{igm^2}{2F}D_{\underline{\alpha}}F,\quad Q_{\underline{\dot\alpha}}=\frac{eg}{2F}P^{\beta\dot\beta}F_{\beta\dot\beta,\underline{\dot\alpha}}+\frac{igm^2}{2F}\overline{D}_{\underline{\dot\alpha}}F.$$

A necessary and sufficient condition for decreasing the rank by a factor of 2 is the presence of the constraints (8) and (9). The first class spinor constraints arising when the solutions of the system (6) are substituted into the Hamiltonian (16) have precisely the form (10). For this reason, repeating the arguments in Sec. 2, we can state that an infinite algebra of constraints can be avoided if $Y_{\underline{\alpha\beta}}=M_{\underline{\alpha\beta}}-N_{\underline{\alpha\dot\alpha}}\overline{M}^{-1\underline{\dot\alpha\dot\beta}}N_{\underline{\dot\beta\dot\beta}}\approx 0$. It will be convenient for us to expand the superfield intensities appearing in $\overline{Y}_{\underline{\alpha\beta}}$ in terms of the generators of $SU(2)$:

$$F_{\underline{\alpha\beta}}=-\epsilon_{\underline{\alpha\beta}}\overline{W}+\tau_a^{ij}\tilde{F}^a_{\alpha\beta},\quad F_{\underline{\dot\alpha\dot\beta}}=\epsilon_{\underline{\dot\alpha\dot\beta}}W+\tau_{aij}\tilde{F}^a_{\dot\alpha\dot\beta},\quad F_{\underline{\alpha\dot\alpha}}=v_{\underline{\alpha\dot\alpha}}+\tau^i_{aj}\tilde{F}^a_{\alpha\dot\alpha}. \tag{17}$$

Now it is easy to find $\overline{M}^{-1}$:

$$\overline{M}^{-1\underline{\dot\beta\dot\alpha}}=\frac{i}{2(m-ieW/2)}\left\{\epsilon^{\underline{\dot\beta\dot\alpha}}+\sum_{n=1}^{\infty}\left[\frac{ie}{2(m-ieW/2)}\right]^n\tilde{F}^{\underline{\dot\beta\dot\alpha}_1}\tilde{F}_{\underline{\dot\alpha}_1\underline{\dot\alpha}_2}\ldots\tilde{F}^{\underline{\dot\alpha}_{n-1}\underline{\dot\alpha}_n}\right\}. \tag{18}$$

Substituting expressions (17) and (18) into Eq. (8′) and equating the coefficients of the various powers of $p_{\alpha\dot\alpha}$ to zero, we find:

the quadratic term

$$\sum_{n=1}^{\infty}\left[\frac{ie}{2(m-ieW/2)}\right]^n\tilde{F}^{\underline{\dot\beta\dot\alpha}_1}\ldots\tilde{F}^{\underline{\dot\alpha}_{n-1}\underline{\dot\alpha}_n}=0\Rightarrow\tilde{F}^{\underline{\dot\beta\dot\alpha}}=0; \tag{19}$$

the linear term

$$F_{\underline{\alpha\dot\beta}}=0; \tag{20}$$

the free term

$$-2i(m+ie\overline{W}/2)\epsilon_{\underline{\alpha\beta}}+\frac{2im^2F\epsilon_{\underline{\alpha\beta}}}{m-ieW/2}-e\tilde{F}_{\underline{\alpha\beta}}=0.$$

Since the τ matrices are linearly independent, we have

$$\tilde{F}_{\underline{\alpha\beta}}=0,\quad (m+ie\overline{W}/2)(m-ieW/2)=(m+im\mu\overline{W})(m+im\mu W). \tag{21}$$

Substituting the constraints (19) and (20) and $\tilde{F}_{\underline{\alpha\beta}}=0$ into the Bianchi identities for the superfield intensities leads to the standard constraints on $N=2$ physical superfields $\tilde{D}_{\underline{\dot\alpha}}W=D_{\underline{\alpha}}\overline{W}=0$, $D^{ij}W-\overline{D}^{ij}\overline{W}=0$. Equation (21) can be written in the form ($m\mu$

$-e/2)[im(W-\overline{W})-(m\mu+e/2)W\overline{W}]=0$. Vanishing of the second bracket, with allowance for the chirality of $W(\overline{W})$, leads to vanishing of the physical degrees of freedom: $W=$ const, $\overline{W}=\overline{\text{const}}$. At the same time, fixing the value of the AMM $\mu=e/2m$ does not impose additional limitations on $W(\overline{W})$.

Thus, in contrast to the purely minimal case, it is possible for first class spinor constraints (and k-symmetry) to exist within the framework of a finite number of constraints, but for the field configurations (19)–(21). It is nontrivial that the constraints obtained are sufficient for selecting an $N=2$ Maxwell supermultiplet and that doing so fixes the AMM μ as well. On this basis the Lagrangian (12) and the spinor constraints (10) can be written in the form

$$L^{(e,\mu(e))}=\frac{1}{2}\left[\frac{(m-ieW/2)(m+ie\overline{W}/2)\omega^2}{g}-gm^2\right]$$
$$+m(\theta^{\alpha}\dot{\theta}_{\alpha}+\overline{\theta}_{\dot{\alpha}}\dot{\overline{\theta}}^{\dot{\alpha}})+ie(\omega^{\mu}A_{\mu}+\overleftarrow{\theta}_{\dot{\alpha}}\overline{A}^{\dot{\alpha}}+\dot{\theta}^{\alpha}A_{\alpha}), \tag{22}$$

$$V^{(1)}_{\alpha}=V_{\alpha}-\frac{iP_{\alpha\dot{\beta}}\overline{V}^{\dot{\beta}}}{(m-ieW/2)};\quad V^{(1)}_{\dot{\alpha}}=V_{\dot{\alpha}}-\frac{iP_{\beta\dot{\alpha}}V^{\beta}}{(m+ieW/2)}, \tag{23}$$

and only four constraints are independent, since $iP^{\dot{\alpha}\alpha}V^{(1)}_{\alpha}/(m+ieW/2)\approx\overline{V}^{\dot{\alpha}(1)}$. The complete Hamiltonian H is obtained by substituting the solutions of the system (6) into Eq. (16) and taking into account the constraints (19)–(21). The first class constraints appearing in H and corresponding to reparametrization and k-symmetries of the action (11) turn out to be $SU(2)$ invariant. It can be shown that $SU(2)$ invariance of the original reparametrization constraint T is restored by adding to it a combination of the spinor constraints and simultaneously redefining the Lagrange multipliers λ_1^{α} and $\overline{\lambda}_{\dot{\alpha}2}$. The new constraint T acquires zero PBs with all other constraints. With the modifications noted the desired complete Hamiltonian H becomes

$$H=\frac{g}{2F}\left[(P^2+m^{*2})-\frac{ie}{4}D^{\alpha}WV_{\alpha}+\frac{ie}{4}\overline{D}_{\dot{\alpha}}\overline{WV}^{\dot{\alpha}}\right]+\lambda_1^{\alpha}V^{(1)1}_{\alpha}+\overline{\lambda}_{\dot{\alpha}2}\overline{V}^{(1)\dot{\alpha}2}\approx 0. \tag{24}$$

The action (11), taking account of the conditions (19)–(21) and $\mu=e/2m$, turns out to be invariant with respect to the following k-symmetry transformations with a local parameter $(k^i_{\beta}(\tau),k^{\beta j}(\tau))$:

$$\begin{pmatrix}\delta\theta^i_{\alpha}\\ \delta\overline{\theta}^{\dot{\alpha}i}\end{pmatrix}=P_1\begin{pmatrix}k^j_{\beta}(\tau)\\ \overline{k}^{\dot{\beta}j}(\tau)\end{pmatrix}=\frac{1}{2}\begin{pmatrix}k^i_{\alpha}-\dfrac{im^*\omega_{\alpha\dot{\beta}}\overline{k}^{\dot{\beta}i}}{\sqrt{-\omega^2}(m+ie\overline{W}/2)}\\ k^{\dot{\alpha}i}+\dfrac{im^*\omega^{\dot{\alpha}\beta}k^i_{\beta}}{\sqrt{-\omega^2}(m-ie\overline{W}/2)}\end{pmatrix}, \tag{25}$$

$$\delta x^{\mu}=-i\theta_i\sigma^{\mu}\delta\overline{\theta}^i+i\delta\theta_i\sigma^{\mu}\overline{\theta}^i,$$

where

$$P_{\mathrm{I}}=\frac{1}{2}\,\delta^i_j\begin{pmatrix}\delta^\beta_\alpha & \dfrac{-im^*\omega_{\alpha\dot\beta}}{\sqrt{-\omega^2}(m+ie\overline{W}/2)}\\ \dfrac{im^*\omega^{\dot\alpha\beta}}{\sqrt{-\omega^2}(m-ieW/2)} & \delta^{\dot\alpha}_{\dot\beta}\end{pmatrix}. \tag{26}$$

The matrix P_{I} is a projector and can be used for covariant separation of the primary constraints by class:[16]

$$\begin{pmatrix}V^{(1)i}_\alpha\\ \overline{V}^{(1)\dot\alpha i}\end{pmatrix}=P_{\mathrm{I}}\begin{pmatrix}V^j_\beta\\ \overline{V}^{\dot\beta}{}_j\end{pmatrix},\quad \begin{pmatrix}V^{(2)i}_\alpha\\ \overline{V}^{(2)\dot\alpha i}\end{pmatrix}=P_{\mathrm{II}}\begin{pmatrix}V^j_\beta\\ \overline{V}^{\dot\beta j}\end{pmatrix}, \tag{27}$$

where

$$\begin{aligned}P_{\mathrm{I}}&=\frac{1}{2}\,\delta^i_j\begin{pmatrix}\delta^\beta_\alpha & \dfrac{-iP_{\alpha\dot\beta}}{m-ieW/2}\sqrt{\dfrac{m^{*2}}{-P^2}}\\ \dfrac{iP^{\dot\alpha\beta}}{m+ieW/2}\sqrt{\dfrac{m^{*2}}{-P^2}} & \delta^{\dot\alpha}_{\dot\beta}\end{pmatrix},\\ P_{\mathrm{II}}&=\frac{1}{2}\,\delta^i_j\begin{pmatrix}\delta^\beta_\alpha & \dfrac{iP_{\alpha\dot\beta}}{m-ieW/2}\sqrt{\dfrac{m^{*2}}{-P^2}}\\ \dfrac{-iP^{\dot\alpha\beta}}{m+ieW/2}\sqrt{\dfrac{m^{*2}}{-P^2}} & \delta^{\dot\alpha}_{\dot\beta}\end{pmatrix},\end{aligned} \tag{28}$$

satisfy the relations $P^2_{\mathrm{I,II}}=P_{\mathrm{I,II}}$ and $P_{\mathrm{I}}P_{\mathrm{II}}=P_{\mathrm{II}}P_{\mathrm{I}}$. The price for keeping covariance is linear dependence of the constraints (27):

$$V^{(1)i}_\alpha\frac{iP^{\dot\alpha\beta}}{m+ieW/2}\sqrt{\frac{m^{*2}}{-P^2}}=\overline{V}^{(1)\dot\beta i},\quad \frac{-iP^{\dot\beta\alpha}}{m+ieW/2}\sqrt{\frac{m^{*2}}{-P^2}}V^{(2)i}_\alpha=\overline{V}^{(2)\dot\beta i}.$$

The algebra of PBs of first class spinor constraints can be represented in the following form: $\{X^{(1)},Z\}=C(W,\overline{W},P_\mu)\chi$, $\{\chi,\chi\}=0$, where $X^{(1)}=(V^{(1)}_{\underline{\alpha}},\overline{V}^{(1)}_{\underline{\dot\alpha}})$, $Z=(V^{(1)}_{\underline{\alpha}},\overline{V}^{(1)}_{\underline{\dot\alpha}}),V_{\underline{\alpha}},\overline{V}_{\underline{\dot\alpha}},\chi)$. The indicated PBs are supplemented by the PBs of the reparametrization first class constraint T, which have the form $\{T,Z\}=0$. We point out that the algebra of first class spinor constraints closes on the second class bosonic constraint χ.

We now show that the interaction constant μ introduced in the Lagrangian (12) is indeed the AMM of a particle. For this, let us examine in Eq. (12) the term $(i\mu/2g)\omega^\mu\omega_\mu(\overline{W}-W)$. We separate in the component expansion of the chiral superfield W the photon term $W=\ldots-2i\theta_i\sigma^{\mu\nu}\theta^i_{\mu\nu}+\ldots$ and substitute it into Eq. (12). As a result, switching to the bispinors

$$\Psi^i=\begin{pmatrix}(-i\omega^2/g)^{1/2}\theta^i_\alpha\\ (i\omega^2/g)^{1/2}\overline{\theta}^{\dot\alpha i}\end{pmatrix}$$

and introducing the spin operator $\Sigma^{\mu\nu}=\frac{i}{4}[\gamma^{\mu},\gamma^{\mu}]$ (the γ matrices are taken in the Weyl basis), we obtain

$$\frac{i\mu}{2g}\omega^{\mu}\omega_{\mu}(\overline{W}-W)\Big|_{\text{photon}}=\mu\Psi_{i}\Sigma^{\mu\nu}\Psi^{i}\upsilon_{\mu\nu}(x)+\text{higher}-\text{order corrections.} \tag{29}$$

Formula (29) is the standard Pauli term. This makes it possible to interpret μ as the AMM of a particle. Therefore it has been shown that the k-symmetry breaking arising upon the minimal inclusion of electromagnetic interactions in the $N=2$ supersymmetric electrodynamics of charged superparticles is restored by taking into account the AMM of the particles.

This work was supported in part by INTAS Grant 93-127-ext and Ukrainian DFFD Grants F4/1751 for Basic Research and 2.5.1/54 for High-Energy Physics.

[a)]e-mail: zheltukhin@kipt.kharkov.ua

[1] J. A. de Azcárraga and J. Lukiersky, Phys. Lett. B **113**, 170 (1982); Phys. Rev. D **28**, 1337 (1983).
[2] W. Siegel, Phys. Lett. B **128**, 397 (1983).
[3] M. Green, J. H. Schwarz, and E. Witten, *Superstring Theory*, Vol. 1, Cambridge University Press, Cambridge, 1987 [Russian translation, Mir, Moscow, 1990].
[4] M. J. Duff, R. R. Khuri, and J. X. Lu, Phys. Rep. **259**, 213 (1995).
[5] E. Bergshoeff, E. Sezgin, and P. K. Townsend, Ann. Phys. **199**, 340 (1989).
[6] P. K. Townsend, ''Four lectures on M-theory,'' http://xxx.lanl.gov/abs/hep-th/9612121.
[7] J. A. Shapiro and C. C. Taylor, Phys. Rep. **191**, 221 (1990); G. V. Grigoryan and V. I. Tyutin, Teor. Mat. Fiz. **111**, 389 (1997).
[8] J. Wess and J. Bagger, *Supersymmetry and Supergravity*, Princeton University Press, Princeton, N. J., 1983 [Russian translation, Mir, Moscow, 1986].
[9] L. Lusanna and B. Milevski, Nucl. Phys. B **247**, 396 (1984).
[10] A. Barducci, Phys. Lett. B **118**, 112 (1982).
[11] A. Barducci, R. Casalbuoni, and L. Lusanna, Nuovo Cimento A **35**, 377 (1976).
[12] A. A. Zheltukhin, Teor. Mat. Fiz. **65**, 151 (1985).
[13] P. A. M. Dirac, *The Principles of Quantum Mechanics*, Clarendon Press, Oxford, 1958 [Russian translation, Nauka, Moscow, 1979].
[14] P. West, *Introduction to Supersymmetry and Supergravity*, World Scientific, Philadelphia, 1986 [Russian translation, Mir, Moscow, 1989].
[15] A. A. Zheltukhin and V. V. Tugaĭ, JETP Lett. **61**, 539 (1995); Yad. Fiz. **61**, 325 (1998) [Phys. At. Nucl. **61**, 274 (1998)]; http://xxx.lanl.gov/abs/hep-th/9706114.
[16] J. M. Evans, preprint OUTP-89-41P (1989).

Translated by M. E. Alferieff

Baryonic systems with charm and bottom in the bound-state soliton model

V. B. Kopeliovich
Institute for Nuclear Research, Russian Academy of Sciences, 117312 Moscow, Russia

(Submitted 22 April 1998)
Pis'ma Zh. Éksp. Teor. Fiz. **67**, No. 11, 854–859 (10 June 1998)

The binding energies of baryonic systems with baryon number $B=2$, 3, and 4 possessing heavy flavor, charm, bottom, or top, are estimated within the rigid oscillator version of the bound-state approach to chiral soliton models. Two tendencies are noted: the binding energy increases with increasing mass of the flavor and with increasing B. Therefore, the charmed or bottom baryonic systems have a better chance of being bound than do the strange baryonic systems discussed previously.

[S0021-3640(98)00411-3]

PACS numbers: 14.20.Mr, 14.20.Lq, 14.20.Pt

1. Many efforts have been made lately to investigate the properties of baryonic systems with nonzero strangeness, first of all, the possibility of existence of states stable with respect to strong decays.

Recently some of the predictions of theory have begun to find experimental confirmation. The near-threshold enhancement in the $\Lambda\Lambda$ system observed in Ref. 1 can be interpreted as a component of a 27-plet obtained from the bound $SU(2)$ torus-like configuration with $B=2$ by means of the collective coordinates method described in Refs. 2 and 3. Similar enhancement in the ΛN system was observed many years ago in the kaon production reaction on nucleons[4] and was confirmed in Λp scattering.[5] It can belong to a 27-plet or to an antidecuplet of dibaryons. The singlet NN scattering state with isospin $T=1$ belongs to a 27-plet (for a review of the theoretical predictions in the $B=2$ sector, see, e.g., Ref. 6). Analogous results are obtained in the more conventional potential approach as well.

The question of whether baryonic systems with a flavor different from u and d can exist is more general, of course. The charm, bottom, and top quantum numbers are also of interest. These can be considered in the framework of chiral soliton models, in particular, the bound-state approach to heavy flavors which was proposed in Ref. 7 and developed in Refs. 8–10. Although charmed and bottom baryonic systems have less chance to play an important role in astrophysics than do the strange baryonic systems (such a role is not ruled out, however!), their studies can be very useful for understanding the peculiarities of nuclear matter fragments with unusual properties. It might be similar to heavy quarkonia, the studies of which were very important for the development and checking of QCD itself.

Here the baryonic systems with heavy flavors are considered within the rigid oscillator version of the bound-state approach to strange baryons, which was proposed by Kaplan and Klebanov[9] and used later in Ref. 10. This model has definite advantages over the collective coordinates quantization method when heavy flavors are included in consideration, primarily because of its simplicity. However, there are also some obvious drawbacks.

2. The ansatz for the chiral fields used in Refs. 9 and 10 is:

$$U(r,t)=R(t)U_0(r)R^\dagger(t), \quad R(t)=A(t)S(t), \tag{1}$$

where U_0 is an $SU(2)$ soliton embedded into $SU(3)$ in the usual way (into the upper left corner), $A(t)\in SU(2)$ describes $SU(2)$ rotations, and $S(t)\in SU(3)$ describes rotations in the ''charm'' or ''bottom'' direction. For definiteness we shall consider the extension of the (u,d) $SU(2)$ Skyrme model in the charmed direction, when D is the field of D mesons (it is clear, however, that quite similar extensions can be made in the bottom and top directions),

$$S(t)=\exp(iD(t)), \quad D(t)=\sum_{a=4,\dots 7} D_a(t)\lambda_a, \tag{2}$$

where λ_a are Gell-Mann matrices of (u,d,c) or (u,d,b) $SU(3)$ groups. The (u,d,b) $SU(3)$ subgroup is quite analogous to the (u,d,s) one, and for the (u,d,c) subgroup a simple redefinition of the hypercharge should be made. $D_4=(D^0+\overline{D^0})/\sqrt{2}$, $D_5=i(D^0-\overline{D^0})/\sqrt{2}$, etc.

After some calculation the well-known Lagrangian of the Skyrme model in the lowest order in the field D takes the form[9,10]

$$L=-M_{cl,B}+4\Theta_{F,B}\dot{D}^\dagger\dot{D}-\Gamma_B(m_D^2-m_\pi^2)D^\dagger D+i\frac{N_cB}{2}(D^\dagger\dot{D}-\dot{D}^\dagger D). \tag{3}$$

Here D is a doublet formed by D^0 and D^- mesons, and we have kept our former notation for the moment of inertia for the rotation into the ''strange,'' ''charm,'' or ''bottom'' direction: $\Theta_c=\Theta_b=\Theta_s=\Theta_F$. This moment of inertia has a simple analytical form for arbitrary starting $SU(2)$ skyrmion, regardless its symmetry properties:

$$\Theta_{F,B}=\frac{1}{8}\int(1-c_f)\left[F_\pi^2+\frac{1}{e^2}((\mathbf{d}f)^2+s_f^2(\mathbf{d}\alpha)^2+s_f^2s_\alpha^2(\mathbf{d}\beta)^2)\right]d^3r, \tag{4a}$$

F_π and e are parameters of the model. The general parametrization of the $SU(2)$ skyrmions has been used here, $U=c_f+s_f\boldsymbol{\tau}\cdot\mathbf{n}$ with $n_z=c_\alpha$, $n_x=s_\alpha c_\beta$, $n_y=s_\alpha s_\beta$, $s_f=\sin f$, $c_f=\cos f$, etc. For the axially symmetric ansatz $\beta=n\phi$, where ϕ is the azimuthal angle, and $\Theta_{F,B}$ takes the form drawn in Ref. 11:

$$\Theta_{F,B}=\frac{\pi}{4}\int(1-c_f)\left[F_\pi^2+\frac{1}{e^2}\left((f,f)+s_f^2(\alpha,\alpha)+\frac{n^2}{r^2}s_f^2s_\alpha^2\right)\right]rdrdz, \tag{4b}$$

$(f,f)=(\partial f/\partial r)^2+(\partial f/\partial z)^2$, and r and z are cylindrical coordinates. The quantity Γ_B defines the contribution of the mass term in the Lagrangian:

$$\Gamma_B=\frac{F_\pi^2}{2}\int(1-c_f)d^3r. \tag{5}$$

TABLE I. The static characteristics of the $B=1$ hedgehog and toroidal solitons with $B=2,3,4$ (Ref. 14).

B	$M_{cl,B}$	$\Theta_{F,B}$	$\Theta_{T,B}$	$\Theta_{J,B}$	Γ_B	ω_s	ω_c	ω_b
1	0.865	1.86	5.14	5.14	3.98	0.200	1.18	3.66
2	1.656	3.79	10.55	16.45	7.80	0.196	1.15	3.62
3	2.523	6.16	16.85	37.85	12.85	0.205	1.17	3.63
4	3.446	8.84	23.65	72.5	18.80	0.215	1.19	3.68
4*	3.140	—	—	—	—	0.196	1.15	3.62
B	$\epsilon_{s=-2}$	$\epsilon_{c=1}$	$\epsilon_{c=2}$	$\epsilon_{b=-1}$	$\epsilon_{b=-2}$			
1	—	—	—	—	—			
2	0.096	0.16	0.15	0.17	0.19			
3	0.12	0.22	0.23	0.26	0.27			
4	0.18	0.23	0.21	0.25	0.25			
4*	0.52	0.58	0.61	0.60	0.65			

Note: $M_{cl,B}$ is in GeV, and the moments of inertia $\Theta_{F,B}=\Theta_c=\Theta_b$, Θ_T, Θ_J and Γ are in GeV^{-1}. The excitation frequencies $\omega_{s,c,b}$ are in GeV. The binding energies (in GeV) of baryonic systems with $B=2,3,4$, $S=-2$, charm $c=1,2$ ($\epsilon_{c=1,2}$) and bottom $b=-1,-2$ ($\epsilon_{b=-1,-2}$) are shown. The parameters of the model are $F_\pi=108$ MeV, $e=4.84$ (Ref. 3). The row $B=4^*$ shows the binding energies for the $B=4$ configuration found in Refs. 15 and 16 with extrapolation for $\omega_{B=4}=\omega_{B=2}$. The uncertainty of these estimates within our choice of the model and configurations is ~ 0.02 GeV.

Numerical values of $\Theta_{F,B}$, Γ_B and some other quantities are shown in Table I.

The term in (3) proportional to N_cB arises from the Wess–Zumino–Witten term in the action and is responsible, within this approach, for the splitting between the excitation energies of charm and anticharm (flavor and antiflavor in general case).[8–10] N_c is the number of colors in the underlying QCD; in all other cases here the index c means the charm quantum number. B is the baryon number of the configuration, which can be written in terms of the functions f,α and β as

$$B=-\frac{1}{2\pi^2}\int s_f^2 s_\alpha(\partial f\ \partial\alpha\ \partial\beta)d^3r. \tag{6}$$

In other words, it is the Wronskian of the system described by 3 profiles, f, α, and β (Ref. 2). For the axially symmetrical configuration possessing also symmetry $z\to -z$, $B=n(f(0)-f(\infty))/\pi=n$ for configurations of lowest energy.

The zero-modes quantum corrections due to rotation with the matrix $A(t)$ have order of magnitude N_c^{-1} and are not crucial, although they are also important (see also Sec. 4).

3. After the canonical quantization procedure the Hamiltonian of the system takes the form:

$$H_B=M_{cl,B}+\frac{1}{4\Theta_{F,B}}\Pi^\dagger\Pi+\left(\Gamma_B m'^2_D+\frac{N_c^2B^2}{16\Theta_{F,B}}\right)D^\dagger D-i\frac{N_cB}{8\Theta_{F,B}}(D^\dagger\Pi-\Pi^\dagger D), \tag{7}$$

$m_D^{2\prime}=m_D^2-m_\pi^2$. The momentum Π is canonically conjugate to the variable D. Equation (7) describes the oscillator-type motion of the field D in the background formed by the (u,d) $SU(2)$ soliton. After diagonalization, which can be done explicitly according to Refs. 9 and 10, the Hamiltonian can be written as

$$H_B = M_{cl,B} + \omega_{F,B} a^\dagger a + \bar{\omega}_{F,B} b^\dagger b + O(1/N_c), \tag{8}$$

where $a^\dagger$ and $b^\dagger$ are the creation operators for the charm and anticharm (bottom and antibottom) quantum numbers, $\omega_{F,B}$ and $\bar{\omega}_{F,B}$ being the frequencies of heavy flavor (antiflavor) excitation. D and Π are connected with a and b in the following way:[9,10]

$$D^i = \frac{1}{\sqrt{N_c B \mu_{F,B}}}(a^i + b^{\dagger i}), \quad \Pi^i = \frac{\sqrt{N_c B \mu_{F,B}}}{2i}(a^i - b^{\dagger i}) \tag{9}$$

with

$$\mu_{F,B} = (1 + 16 m_D'^2 \Gamma_B \Theta_{F,B}/(N_c B)^2)^{1/2}.$$

The flavor (antiflavor) excitation frequencies ω and $\bar{\omega}$ are:

$$\omega_{F,B} = \frac{N_c B}{8\Theta_{F,B}}(\mu_{F,B} - 1), \quad \bar{\omega}_{F,B} = \frac{N_c B}{8\Theta_{F,B}}(\mu_{F,B} + 1). \tag{10}$$

It should be noted that the difference $\bar{\omega}_{F,B} - \omega_{F,B} = N_c B/(4\Theta_{F,B})$ is the same to leading order in N_c as that obtained in the collective coordinates approach.[12,13] Indeed, in the collective coordinates approach the zero-modes energy of the soliton rotated in the $SU(3)$ configuration space and depending on the ''flavor'' inertia $\Theta_{F,B}$ can be written as:

$$E_{\rm rot}(\Theta_{F,B}) = \frac{1}{4\Theta_{F,B}}[N_c B + n_{q\bar{q}}(N_c B + 2n_{q\bar{q}} + 2 - 2T_r)], \tag{11}$$

where $n_{q\bar{q}}$ is the number of additional quark–antiquark pairs present in the quantized state, $N_c B + 3n_{q\bar{q}} = p + 2q$, p, q are the numbers of indices in the spinor describing the $SU(3)$ irrep, $T_r = (p + n_{q\bar{q}})/2$ is the so-called right isospin characterizing the irrep (see Ref. 13, where the $B = 1$, $n_{q\bar{q}} = 0$ case was considered, and Ref. 12, where (11) was obtained for $N_c = 3$). The term proportional to $n_{q\bar{q}} N_c B$ in (11) coincides with the difference of $\bar{\omega}_{F,B}$ and $\omega_{F,B}$ in (10).

For the difference of the frequencies of excitation in the cases of $B \geqslant 2$ and $B = 1$ systems we obtain:

$$\Delta\omega \simeq \frac{m_F'}{2}\left[\left(\frac{\Gamma_1}{\Theta_{F,1}}\right)^{1/2} - \left(\frac{\Gamma_B}{\Theta_{F,B}}\right)^{1/2}\right]. \tag{12}$$

It is proportional to the heavy quark mass m_F and is positive if $\Gamma_1/\Theta_{F,1} \geqslant \Gamma_B/\Theta_{F,B}$. For $B = 2, 3$ this is in fact the case. The characteristics of $SU(2)$ toroidal solitons with baryon numbers $B = 2, 3, 4$ have been calculated previously.[14] For $B = 2$ they agree to good accuracy with those given later in Ref. 10. For greater baryon numbers some configurations of lower energy have been found,[15,16] but necessary quantities like $\Theta_{F,B}$ and Γ_B are still lacking.

As a result, the binding energy of heavy flavored dibaryons, tribaryons, etc. increases in comparison with strange flavor case, as can be seen from the results of numerical estimates shown in Table I.

4. The $\sim 1/N_c$ zero-modes quantum correction to the energies of baryonic systems can be estimated according to the expression[9,10]

$$\Delta E_{1/N_c}=\frac{1}{2\Theta_{T,B}}[c_{F,B}T_r(T_r+1)+(1-c_{F,B})I(I+1)+(\overline{c}_{F,B}-c_{F,B})T(T+1)], \quad (13)$$

where I is the isospin of the baryonic systems, T_r is a quantity analogous to the ''right'' isospin T_r in the collective coordinates approach,[3,11,6] and $\mathbf{T}_r=\mathbf{I}^{bf}+\mathbf{T}$;

$$c_{F,B}=1-\frac{\Theta_{T,B}}{2\Theta_{F,B}\mu_{F,B}}(\mu_{F,B}-1), \quad \overline{c}_{F,B}=1-\frac{\Theta_{T,B}}{\Theta_{F,B}(\mu_{F,B})^2}(\mu_{F,B}-1). \quad (14)$$

In the rigid-oscillator model the states predicted are not identified with definite $SU(3)$ or $SU(4)$ representations. However, that can be done, as was shown in Ref. 10. The quantization condition $(p+2q)/3=B$ (Ref. 3) for arbitrary N_c is changed to $(p+2q)=N_cB+3n_{q\bar{q}}$. For example, the state with $c=2$, $I=0$, and $n_{q\bar{q}}=0$ should belong to the 27-plet of the (u,d,c) $SU(3)$ group, if $N_c=3$ (see also Ref. 10). For a 27-plet of dibaryons $T_r=1$, and for an antidecuplet $T_r=0$. For a $\overline{35}$-plet of tribaryons $T_r=1/2$, and for an arbitrary (p,q) irrep to which the baryonic system belongs one has $T_r=p/2$ if $n_{q\bar{q}}=0$. I and T take the lowest possible values, 0 or 1/2 in our case. If $\Theta_F\to\infty$, Eq. (13) goes over to the expression obtained for axially symmetric baryonic systems in the collective coordinates approach,[11] while in the realistic case with $\Theta_T/\Theta_F\simeq 2.7$ the structure of (13) is more complicated.

The quantum correction due to usual spatial rotations, also of the order of $1/N_c$, is of exactly the same form as obtained in Ref. 11 (see Refs. 9 and 10). The binding energies shown in Table I are defined relative to the decay into B baryons, nucleons or flavored hyperons. The binding energy of the $B=4$ state relative to 2 dibaryons, for example, will be smaller or negative. Since we are interested in the lowest energy states, we discuss here the baryonic systems with the lowest allowed angular momentum, $J=0$ for $B=2$, 4, and $J=3/2$ for $B=3$. The latter value is due to the constraint imposed by the symmetry properties of the configuration. The value $J=1/2$ is allowed for the configuration found in Ref. 15.

For $B=3$ and 4 the toroidal configurations we have used here do not correspond to the minimum of the static energy, but it is only for such configurations that the necessary quantities $\Theta_{F,B}$ and Γ_B are known. For $B=3$ the toroidal configuration does not differ much in energy from the tetrahedral one, which is known to be the configuration of minimum energy.[15,16] (The masses of stranglets obtained from bound skyrmions with B up to 17 (Ref. 16) have been estimated recently[17] in the bound-state soliton model.) For $B=4$ the difference is large, $\sim$300 MeV in energy. However, it would be incorrect to decrease all the $B=4$ energies by 300 MeV and increase the binding energies, because the other soliton characteristics and therefore the excitation energies ω_c and ω_b would also change. A reasonable extrapolation for $B=4$ is shown in Table I.

5. To conclude, we have estimated the binding energies of dibaryons, tribaryons, and tetrabaryons with nonzero charm and bottom. For the top quantum number the necessary data for the meson masses are not available, but similar results can be obtained for it also. When the mass of the meson with $t=1$ was taken as $m_t=175$ GeV, the value of ω_t turned out to be close to 130 GeV; therefore, the energy of the top-baryons is smaller than it should be, by several tens of GeV. It also turned out that the state with $B=2$, $t=1$ is lower in energy than the baryon with $t=1$ by $\sim$1.5 GeV, and the hyperon Λ_t

could decay into the $B=2$ state with $t=1$ and an antinucleon. In view of considerable uncertainty of our approach this result should be checked in other variants of the model. Moreover, the large width of the t quark puts this issue in doubt.

The apparent drawback of the approach exploited in the present paper is that the motion of the system into the ''charm'' or ''bottom'' direction is considered independently from other motions. Therefore, consideration of baryonic systems with ''mixed'' flavors is not possible here; it demands a more complicated treatment.

Since the binding energies increase with increasing mass of the flavor, the charmed and bottom baryonic systems have a better chance of being bound than do strange baryonic systems. This is in agreement with the experimental fact that $c\bar{c}$ and $b\bar{b}$ quarkonia with $J^P=1^-$ are bound more strongly than $s\bar{s}$ relative to the lightest pseudoscalar mesons with the corresponding flavor. The nonzero quantum corrections to the energy of charmed (bottom) baryonic systems are expected to be smaller than for strange baryonic systems, because of the greater mass of charmed (bottom) quarks or mesons.

The rigid oscillator model of Kaplan, Klebanov, and Westerberg that we used here generally underestimates the masses of the quantized states if the masses of the nucleon and Δ isobar have been fitted to the start.[9,10] At the same time, the collective coordinates approach with the rigid or soft rotator variant of the model usually overestimates the masses of baryons.[3,11,18] One of the sources of this difference is the presence of the zero-modes contribution to the rotational energy, which is of the order of N_c/Θ_F (see Eq. (11)[13,11,18] and which is absent in the oscillator model.It was shown recently by Walliser for the $B=1$ sector[13] that this large contribution is cancelled almost completely by the 1-loop correction — the zero-point Casimir energy, which is of the same order, N_c^0 (Ref. 19). Anyway, since both approaches have led to similar results in the case of strange baryonic systems, we may expect the same for the case of charmlets and bottomlets, so that our results should be valid qualitatively, at least.

The production of states with $c=1$ and even $c=2$ will be available at accelerators like the future Japan Hadron Facility (energy ~ 50 GeV), but the production of bottomlets requires higher energy.

I am indebted to H. Walliser for helpful discussions of skyrmion quantization at arbitrary N_c and N_F.

This study was supported in part by the Russian Fund for Fundamental Research, Grant 95-02-03868a, and was presented at the Workshop on Science at Japan Hadron Facility (JHF98), KEK, March 3–7, 1998.

[1] J. K. Ahn *et al.*, KEK PS E224 Collaboration, AIP Conf. Proc. 412, 923–926 (1997).
[2] L. D. Faddeev and V. E. Korepin, Phys. Rep. **42**, 1 (1978).
[3] G. S. Adkins, C. R. Nappi, and E. Witten, Nucl. Phys. B **228**, 552 (1983); G. S. Adkins and C. R. Nappi, Nucl. Phys. B **233**, 109 (1984); G. Guadagnini, Nucl. Phys. B **236**, 35 (1984).
[4] J. T. Reed *et al.*, Phys. Rev. **168**, 1495 (1968).
[5] B. Sechi-Zorn *et al.*, Phys. Rev. **175**, 1452 (1968); G. Alexander *et al.*, Phys. Rev. **173**, 1452 (1968).
[6] V. B. Kopeliovich, Genshikaku Kenkyu **41**, 171 (1997);http://xxx.lanl.gov/abs/hep-ph/9712453; Nucl. Phys. A, in press; Zh. Éksp. Teor. Fiz. **112**, 1941 (1997) [JETP **85**, 1060 (1997)];Yad. Fiz. **56**, 160 (1993) [Phys. At. Nucl. **56**, 1084 (1993)].
[7] C. G. Callan and I. R. Klebanov, Nucl. Phys. B **262**, 365 (1985).
[8] N. Scoccola, H. Nadeau, M. Nowak, and M. Rho, Phys. Lett. B **201**, 425 (1988); C. G. Callan, K. Hornbostel, and I. R. Klebanov, Phys. Lett. B **202**, 269 (1988); J. P. Blaizot, M. Rho, and N. Scoccola, Phys. Lett. B **209**,

27 (1988); N. Scoccola, D. P. Min, H. Nadeau, and M. Rho, Nucl. Phys. A **505**, 497 (1989).
[9] D. Kaplan and I. R. Klebanov, Nucl. Phys. B **335**, 45 (1990).
[10] K. M. Westerberg and I. R. Klebanov, Phys. Rev. B **50**, 5834 (1994); I. R. Klebanov and K. M. Westerberg, Phys. Rev. D **53**, 2804 (1996).
[11] V. B. Kopeliovich, B. Schwesinger, and B. E. Stern, Nucl. Phys. A **549**, 485 (1992); V. B. Kopeliovich, Yad. Fiz. **47**, 1495 (1988) [Sov. J. Nucl. Phys. **47**, 949 (1988)]; Yad. Fiz. **51**, 241 (1990) [Sov. J. Nucl. Phys. **51**, 151 (1990)].
[12] V. B. Kopeliovich, Phys. Lett. B **259**, 234 (1991).
[13] H. Walliser, http://xxx.lanl.gov/abs/hep-ph/9710232.
[14] V. B. Kopeliovich and B. E. Stern, preprint 89/34 N, NORDITA-Copenhagen, 1989; JETP Lett. **45**, 203 (1987).
[15] E. Braaten, S. Townsend, and L. Carson, Phys. Lett. B **235**, 147 (1990).
[16] R. A. Battye and P. M. Sutcliffe, Phys. Lett. B **391**, 150 (1997); Phys. Rev. Lett. **79**, 363 (1997).
[17] M. Schvellinger and N. N. Scoccola, http://xxx.lanl.gov/abs/hep-ph/9801347.
[18] H. Walliser, Nucl. Phys. A **548**, 649 (1992).
[19] B. Moussalam, Ann. Phys. (N.Y.) **225**, 264 (1993); F. Meier and H. Walliser, Phys. Rep. **289**, 383 (1997).

Published in English in the original Russian journal. Edited by Steve Torstveit.

005811jtparasi
Erratum

Do excited states exist in a system of two neutrons?

D. V. Aleksandrov, E. Yu. Nikol'skiĭ, B. G. Novatskiĭ, and D. N. Stepanov
Kurchatov Institute Russian Science Center, 123182 Moscow, Russia

R. Wolski
Institute of Nuclear Physics, 31342 Kraków, Poland
(Submitted 23 April 1998)
67, No. 11, 860–865 (10 June 1998)
The interaction in a system of two neutrons (2n) in the reaction T(d, 3He) at energy Ed=31 MeV is investigated experimentally. Nuclear-unstable 2n, with a decay width $\Gamma=(1.1\pm0.2)$ MeV, is observed with a large transverse cross sections in the interval of angles from 6° to 13° ($d\sigma/d\Omega(6°)\sim10$ mb/sr in the center-of-mass system). Two wide energy peaks were observed in the 3He spectra. It is proposed that broad resonances with energies $E*=(3.6\pm0.3)$ and $E*\sim11.8$ MeV, populated in the reaction T(d, 3He), are excited in the n–n system. Their energy positions satisfy the interval rule $E4:E2\cong3.3$, indicating the possible existence of a ''rotational band'' with the characteristics 2+ and 4+. The ''radius'' of the dineutron is estimated from the relation $\Delta E=\hbar2l(l+1)/2\mu R2$ to be ~8 fm.
[S0021-3640(98)00511-8]

13.75.Cs

The question of the forces acting between two particles is a fundamental problem of classical and quantum physics. The solution of this problem has made it possible to understand the nature of electromagnetic and gravitational forces. It is well known that the existence of numerous excited states in the hydrogen atom was the key to the construction of the ‘‘planetary’’ model of the Bohr atom. Nuclear forces differ sharply from electromagnetic forces by their very short range, and the deuteron — the simplest nuclear system with an anomalously low binding energy (ϵ=2.22 MeV) — does not have excited bound states like the hydrogen atom. However, the experimental study of pn and pp scattering has firmly established an interaction in the final state in these systems with isospin T=1 and it has been shown that singlet d and 2p systems possess virtual levels near the decay threshold. In the 1960s and 1970s the hypothesis of the charge independence and symmetry of nucleon–nucleon interactions was checked experimentally in measurements of the scattering lengths. A small difference was found in the n–n and p–n interactions: $a_{nn}=-16.6$ fm and $a_{np}=-23.7$ fm (see, for example, the review in Ref. 1). In contrast to p–p and p–n scattering, because of the unavailability of neutron targets the main means of studying the n–n interaction have been the reactions D(n, p), T(n, d), D(d, 2p), T(d, ^{3}He), and T(t, ^{4}He). We note that in these investigations emphasis has been placed on confirmation of the hypothesis of charge independence and symmetry of the nuclear forces and not on a search for excited states of unstable 2n. As a rule, the spectra have been obtained in a narrow energy range near zero binding energy of the dineutron.2 On the other hand, in high-energy physics the searches have been conducted for ‘‘narrow’’ dibaryonic resonances (2p) with energies of tens and even hundreds of MeV, which are traditionally far from the excitation energies characteristic for low-energy nuclear physics.3

The objective of the present work was to search for excited states of the dineutron in the reaction T(d, ^{3}He) by the conventional methods of nuclear spectroscopy in the interval from the 2n ground state up to the maximum possible energies admissible under the experimental conditions ($E^*\sim 15$ MeV). Of the three variants of the search for dibaryonic resonances (2n,2p,np) the first one was chosen because a purely nuclear interaction of two identical particles occurs in this case.

the transverse cross sections
($d\sigma/d\Omega(6°) \sim 10$ mb/sr in the
center-of-mass system) and their sharp forward elongation. This is
evident from Fig. 3, where the experimental angular
distributions for the reaction T(d,
3He) are presented. The filled
circles indicate the differential cross sections for the
2n ground state, while the open circles
correspond to the resonance with
$E = 3.6$ MeV. Conversely, the
parasitic process T(d,
$^4He^*$), proceeding with
formation of unstable levels of
$^4He^*$ and their subsequent
dissociation into $^3He + n$, is more
complicated (two-nucleon pickup reaction). Moreover, as one can see
from the table of the decay widths presented in Ref. 6, the
dissociation of $^4He^*$
proceeds predominantly with the emergence of a triton and not a
3He nucleus.

The main results of this work are presented in Table
I, where the excitation energies of the hypothetical
resonances in 2n are given in the first
column, the proposed values of the spins and parities are given in the
second column, and estimates of their decay widths are given in the
third column. Nonetheless, we believe that additional experiments at
high incident deuteron energies (50–60 MeV) must be performed in order
to confirm the results obtained.

We thank M. V. Zhukov and I. M. Pavlichenkov for helpful discussions
and a number of valuable remarks, as well as SKTB ÉP of the
Ukrainian National Academy of Sciences for preparing the
titanium–tritium targets.

This work was supported by Russian Fund for Fundamental Research under
Grant 96-02-17298a.

B. Kühn, Fiz. Élem. Chastits
At. Yadra, 378 (1975) [Sov. J. Part. Nucl.
6(2), 139 (1976)].
E. Baumgartner, H. E. Conzett,
E. Shield, and R. J. Slobodrian,
Phys. Rev. Lett. 16, 105 (1966).
Yu. A. Troyan, A. V. Nikitin, V. N. Pechenov , Preprint
R1-90-78, JINR, Dubna, 1990; Yad. Fiz. 54,
1301 (1991) [Sov. J. Nucl. Phys. 54,
792 (1991)].
M. Ivanovich, P. G. Joung, and
G. G. Ohlsen, Nucl. Phys. A
110, 441 (1968).
H. T. Larson, A. D. Bacher,
K. Nagatini, and T. A. Tombrello,
Nucl. Phys. A 149, 161 (1970).

Cherenkov emission of magnons by a slow monopole

P. V. Vorob'ev[a)] and I. V. Kolokolov[b)]
G. I. Budker Institute of Nuclear Physics, Siberian Branch of the Russian Academy of Sciences, Novosibirsk State University, 630090 Novosibirsk, Russia

(Submitted 25 March 1998; resubmitted 6 May 1998)
Pis'ma Zh. Éksp. Teor. Fiz. **67**, No. 11, 866–868 (10 June 1998)

The energy losses due to Cherenkov emission of magnons during the interaction of a slow heavy monopole with magnetically ordered media are discussed. © *1998 American Institute of Physics.* [S0021-3640(98)00611-2]

PACS numbers: 14.80.Hv

The observation of slow, heavy monopoles[1,2] would be of fundamental significance for elementary particle physics and cosmology. However, most modern detectors possess a low efficiency when detecting slow monopoles with velocities $v/c<10^{-4}$ (Ref. 3). For this reason, for both detector physics and astrophysics it is of interest to consider different mechanisms of the interaction of monopoles with matter.

In the present letter we study the passage of a slow monopole through a magnetically ordered medium. In this case the main mechanism of kinetic energy loss is Cherenkov emission of magnons. This is because the phase velocities of magnons reach zero and the monopole–magnon coupling is linear and large.

For definiteness, we shall study a ferromagnet but the estimates obtained below are more general.

The magnon Hamiltonian in the presence of the magnetic field of a moving monopole can be written in the form

$$H=\sum_{\mathbf{k}} \hbar\omega_{\mathbf{k}} a_{\mathbf{k}}^{\dagger} a_{\mathbf{k}}+\sum_{\mathbf{k}} (f_{\mathbf{k}} e^{-i\Omega_{\mathbf{k}} t} a_{\mathbf{k}}^{\dagger}+\text{c.c.}), \tag{1}$$

where $a_{\mathbf{k}}^{\dagger}$ is the creation operator of a magnon with wave vector $\mathbf{k}$, $\omega_{\mathbf{k}}$ is the magnon dispersion law, $\Omega_{\mathbf{k}}=\mathbf{k}\cdot\mathbf{v}$, $\mathbf{v}$ is the monopole velocity vector, and $f_{\mathbf{k}}$ is the coupling coefficient between the monopole magnetic field $\mathbf{B}=g\nabla(1/r)$ and the magnon.

The energy of magnons emitted per unit time equals

$$\epsilon=\frac{2\pi}{\hbar}\sum_{\mathbf{k}} \omega_{\mathbf{k}}|f_{\mathbf{k}}|^2\delta(\Omega_{\mathbf{k}}-\omega_{\mathbf{k}}). \tag{2}$$

Let the velocity $\mathbf{v}$ of the monopole be directed along the spontaneous magnetization, fixing the direction of the Z axis.[c)] Then

$$f_{\mathbf{k}}=\frac{4\pi g\mu_B}{a^{3/2}\sqrt{V}}\sqrt{\frac{S}{2}}\frac{k_x-ik_y}{k^2}, \tag{3}$$

where a is the lattice constant, V is the volume of the sample, S is the spin at a lattice site, and μ_B is the Bohr magneton. Substituting expression (3) Eq. (2) for ϵ becomes

$$\epsilon=\frac{2g^2\mu_B^2 S}{a^3\hbar}\int d^3\mathbf{k}\omega_{\mathbf{k}}\frac{k_x^2+k_y^2}{k^4}\delta(k_z v-\omega_{\mathbf{k}}). \tag{4}$$

The integration in Eq. (4) extends over the first Brillouin zone.

If $v\geqslant u$, where u is the velocity of magnons near the boundary of the Brillouin zone, then the magnons with large $\mathbf{k}$ are important. Then

$$\epsilon\simeq\frac{\bar{\omega}g^2\omega_M}{v}, \tag{5}$$

where the frequency $\omega_M=4\pi\mu_B^2 S/\hbar a^3$ characterizes the magnetization of the medium,[4]

$$\bar{\omega}=\frac{1}{2\pi}\int\frac{d^2\mathbf{k}_\perp}{k_\perp^2}\omega_{k_\perp} \tag{6}$$

$\mathbf{k}_\perp=(\mathbf{k}_x,\mathbf{k}_y)$, and $\bar{\omega}$ is of the order of the maximum magnon frequency.

For $g^2\simeq 4700\cdot e^2$ we obtain

$$\epsilon\simeq 10^3\cdot \mathrm{Ry}\cdot\omega_M(\bar{\omega}\tau), \tag{7}$$

where $\tau=a/v$ is the characteristic interaction time.

Typical values for magnetically ordered dielectrics are $\bar{\omega}\simeq 10^{-13}$ s^{-1}, $\omega_M\simeq 10^{-11}$ s^{-1} and for $v/c\simeq 10^{-4}$ we have $\epsilon\simeq 10^{14}$ eV/s, which corresponds to losses per unit length $dE/dl\simeq 10^8$ eV/cm.

It is evident from Eq. (5) that the losses ϵ and dE/dl increase with decreasing velocity v of the monopole. When the velocity v becomes $v<u$, magnons from the bottom of the spectrum make the main contribution to the losses. For them $\omega_{\mathbf{k}}=\omega_{\mathrm{ex}}(ak)^2$, where ω_{ex} is the frequency characterizing the exchange interaction,[4,5] the expressions for the losses now become

$$\epsilon=g^2\frac{\omega_M v}{4\omega_{\mathrm{ex}}a^2}, \tag{8}$$

$$\frac{dE}{dl}=\frac{\epsilon}{v}=g^2\frac{\omega_M}{4\omega_{\mathrm{ex}}a^2}. \tag{9}$$

As one can see, as the velocity of the monopole decreases, the energy losses per unit length become constant. The characteristic values are $\omega_M/\omega_{\mathrm{ex}}\simeq 10^{-2}$, and for $v/c\simeq 10^{-4}$ and $a\simeq 10^{-8}$ cm we have $dE/dl\simeq 10^8$ eV/cm.

It is evident from these estimates that the level of the energy losses of a slow magnetic monopole in a magnetically ordered medium is comparable to that of the ionization losses of a fast monopole. This opens up new possibilities for constructing

detectors in the range $v/c<10^{-4}$. Conversion of spin waves into electromagnetic waves[5] makes it possible to register the passage of a monopole through a slab of magnetic material by standard radio electronic means.

A detailed analysis of other mechanisms of the interaction of a slow monopole with matter is given in Ref. 6.

We thank L. M. Barkov, I. B. Khriplovich, and V. V. Yanovskiĭ for their interest in this work and for helpful remarks.

[a)]e-mail: vorobyov@inp.nsk.su
[b)]e-mail: kolokolov@inp.nsk.su
[c)]The general case can be investigated completely analogously and the answer differs only by a numerical factor of the order of 1.

[1] A. P. Polyakov, JETP Lett. **20**, 194 (1974).
[2] G. 't Hooft, Nucl. Phys. B **79**, 276 (1974).
[3] H. V. Klapdor-Kleingrofthaus and A. Staudt, *Non-Accelerator Particle Physics*, IOP Publishers, 1994 [Russian translation, Nauka, Moscow, 1997].
[4] A. G. Gurevich, *Magnetic Resonance in Ferrites and Antiferromagnets* [in Russian], Nauka, Moscow, 1973.
[5] A. I. Akhiezer, V. G. Bar'yakhtar, and S. V. Peletminskiĭ, *Spin Waves*, North-Holland, Amsterdam, 1968 [Russian original, Nauka, Moscow, 1967].
[6] P. V. Vorob'ev, I. V. Kolokolov, and V. V. Yanovskiĭ, ''Interaction of slow magnetic monopoles with matter'' [in Russian], in *Proceedings of the 32nd Winter School of St. Petersburg Institute of Nuclear Physics*, Gatchina, February 21–28, 1998 (to be published).

Translated by M. E. Alferieff

Phase conjugation of linear signals and solitons of magnetostatic waves

A. L. Gordon, G. A. Melkov,[a] A. A. Serga, V. S. Tiberkevich, and A. V. Bagada
T. Shevchenko Kiev University, 252017 Kiev, Ukraine

A. N. Slavin
Department of Physics, Oakland University, Rochester, MI 48309, USA

(Submitted 6 April 1998)
Pis'ma Zh. Éksp. Teor. Fiz. **67**, No. 11, 869–873 (10 June 1998)

Phase conjugation of magnetostatic waves by a local longitudinal pump in yttrium iron garnet films is observed experimentally. Theoretical expressions are obtained which describe the experimental curves well.
 [S0021-3640(98)00711-7]

PACS numbers: 41.20.Gz

1. Phase conjugation (or wave-front reversal) has been well studied in the optical range, where it opens up new possibilities in adaptive optics, laser-driven fusion, correlation information processing, and so on.[1] In phase conjugation (PC) the nonlinear interaction of a signal wave with a complex amplitude a_1 and a reference (pump) wave with amplitude a_p gives rise to a wave with the complex-conjugate amplitude $a_2^* = \text{const} \times a_1$, which always propagates counter to the signal wave irrespective of the angle of incidence of the latter on the interaction region. This is equivalent to the time reversal operation: The signal wave is not reflected from the interaction region according to the laws of geometrical optics but rather it propagates backward away from the interaction region along the same trajectory along which it arrived; the wave front of the conjugate wave is the same as that of the signal wave, but propagating in the opposite direction.[2] One method of PC is the parametric method, in which a parametric wave and one or two pump waves, respectively, for parametric excitation of the first or the second orders, engender an idler wave with complex-conjugate amplitude relative to that of the signal wave.[2]

2. In the present work we investigated the phase conjugation of magnetostatic backward volume waves (MSBVWs) in yttrium iron garnet (YIG) ferrite films by parametric interaction of the waves with a local electromagnetic pump. The pump frequency ω_p was double the signal frequency ω_1, i.e., a first-order parametric process occurred. The experiment was performed on an ordinary magnetostatic delay line (Fig. 1), where, however, besides input and output transducers separated by 7.5 mm a third electrode was placed midway between these transducers for feeding the pump signal to the film.[3] All three transducers consisted of segments of microstrip transmission lines shorted at the end; the input and output transducers were 50 μm wide and the pump electrode was 200 μm wide; the YIG film was 4.9 μm thick and 1.6 mm wide.

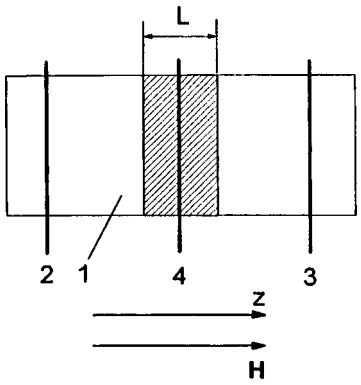

FIG. 1. Ferrite film *1* with input *2* and output *3* transducers and a pump-field transducer *4*. The active region where the magnetostatic waves interacted with a local pump field is located at the center of the hatched region. The phase conjugate signal is extracted from the input transducer *2*.

An external magnetic field $H=1015$ Oe was applied tangentially to the plane of the film and perpendicular to the axes of the transducers. This corresponds to operation of the magnetostatic delay line in the MSBVW regime. The experimentally measured delay time t_d of the MSBVW pulse in the linear regime for a 4686 MHz carrier frequency was equal to 336 ns, which agrees well with the theoretically computed values of the group velocity 2.22 cm/μs and delay time 338 ns. The total loss at the carrier frequency was $\approx$13 dB. The input signal pulse had a duration $\tau_s = 40$ ns and a square shape. The energy of the pump at frequency $\omega_p \simeq 2\omega_1$ was fed from a magnetron generator through a matching transformer to the central electrode at the moment when the signal pulse passed through the active region near this electrode (see Fig. 1). The pump pulse duration τ_p varied from 20 ns to 70 ns and the maximum pump power reached 6.7 W, which gave an amplitude h_p of the microwave magnetic field at the film of up to $h_p \simeq 30$ Oe.

3. To give a theoretical description of PC of MSBVWs in the experimental system (see Fig. 1) it is necessary to solve a one-dimensional problem of the interaction of a signal MSBVW with a local parametric pump. This problem belongs to the general class of problems of parametric interaction of three or four waves of different nature (optical, plasma, elastic, spin, and so on) in an active region of finite length L. For spin and magnetostatic waves the effect of the pump localization during the parametric interaction has been studied only in the stationary case of monochromatic signal and pump[4] and to find the thresholds for the excitation of the waves by local pumping.[4–6] The problem of local pumping has been investigated in greatest detail in Ref. 2, where, however, only the case of stationary pumping was considered. This is clearly unacceptable for a multiwave system, such as a ferrite film, where in principle pulsed pumping must be used in order to obtain any appreciable amplification and conversion of waves.[4]

We solved the nonstationary problem of the interaction of an arbitrary signal wave with a nonstationary uniform pump localized in the region of interaction of length L and having within L a constant amplitude a_p. The analysis was performed using the standard system of equations, derived by Bloembergen,[7,8] neglecting the back effect of parametric processes on the pump:

$$\left(\frac{\partial}{\partial t}+\Gamma_1+v_1\frac{\partial}{\partial z}\right)a_1=Va_pa_2^*+f_1(t,z),$$

$$\left(\frac{\partial}{\partial t}+\Gamma_2-v_2\frac{\partial}{\partial z}\right)a_2^*=V^*a_p^*a_1+f_2(t,z). \tag{1}$$

Here $a_1\equiv a_1(z,t)$, $a_2\equiv a_2(z,t)$ are the slow complex amplitudes (envelopes) of the signal wave, $\exp[i(k_1z+\omega_1t)]$, and the idler wave, $\exp[i(-k_2z+\omega_2t)]$; $k_1=k_2\equiv k$, $\omega_1+\omega_2=\omega_p$. Only the pump parameter Va_p takes into account the specific nature of the interacting waves; in the case of a parallel pump $Va_p=h_p[(\omega_p/2)^2-(gH)^2]/2\omega_pH$ (Ref. 9); $\Gamma_{1,2}$ are the relaxation parameters of the waves, $v_{1,2}$ are the group velocities of the waves, and g is the gyromagnetic ratio for electronic spin. The external forces f_1 and f_2 describe distributed sources acting in the interaction region in addition to the pump. These could be, for example, random thermodynamic disturbances, which were used in Refs. 6 and 10 to calculate the thresholds. In that case they can be assumed to be constants. In our case of the general formulation of the problem the thresholds can be calculated neglecting f_1 and f_2 from the condition of an infinite gain in the stationary regime. The initial and boundary conditions must be added to Eq. (1):

$$a_1(t=0)=a_1^0(z),\quad a_1(z=0)=a_1^S(t),$$

$$a_2^*(t=0)=a_2^{0*}(z),\quad a_2^*(z=L)=a_2^{S*}(t). \tag{2}$$

The solution Eqs. (1), taking account of Eqs. (2), was obtained by the method of Green's functions $G_{ij}(t,z,z')$;[11] an expression for the phase conjugate wave with the signal wave present only at the entrance $(z=0)$ is

$$a_2^*(t,z)=\int_0^t G_{21}(t-t',z,0)v_1a_1^S(t')dt'+\int_0^L G_{21}(t,z,z')a_1^0(z')dz', \tag{3}$$

$$G_{21}(t,z,z')=\frac{\rho}{\sqrt{v_1v_2}}K\left[\rho t+\mu\left(\frac{z}{L}-\frac{z'}{L}\right),\frac{z}{L},\frac{z'}{L}\right]\exp(-\omega_rt+k_r(z-z')),$$

$$K(\tau,\zeta,\zeta')=\frac{\sigma}{2}\sum_{n=0}^{\infty}[P_{2n}(\tau,\alpha_n)-P_{2n}(\tau,\beta_n)-P_{2n+2}(\tau,\gamma_n)+P_{2n+2}(\tau,\delta_n)],$$

$$P_n(\tau,\xi)=\Theta(\tau-\xi)\left(\frac{\tau-\xi}{\tau+\xi}\right)^{n/2}I_n(\sigma\sqrt{\tau^2-\xi^2}),$$

$\Theta(\tau)$ is the Heaviside unit function, $I_n(x)$ are Bessel functions with imaginary arguments; and,

$$\alpha_n=2n+|\zeta-\zeta'|,\quad \beta_n=2n+2-(\zeta+\zeta'),$$

$$\gamma_n=2n+(\zeta+\zeta'),\quad \delta_n=2n+2-|\zeta-\zeta'|,$$

$$\sigma=\frac{Va_pL}{\sqrt{v_1v_2}},\quad \rho=\frac{2v_1v_2}{(v_1+v_2)L},\quad \mu=\frac{v_1-v_2}{v_1+v_2},\quad \omega_r=\frac{v_1\Gamma_2+v_2\Gamma_1}{v_1+v_2},\quad k_r=\frac{\Gamma_2-\Gamma_1}{v_1+v_2}.$$

Formula (3) was used to construct the theoretical curves in Fig. 2. In accordance with the experimental conditions, it was assumed that $v_1=v_2=v$, $\Gamma_1=\Gamma_2=\Gamma$, and $v/\Gamma\gg L$.

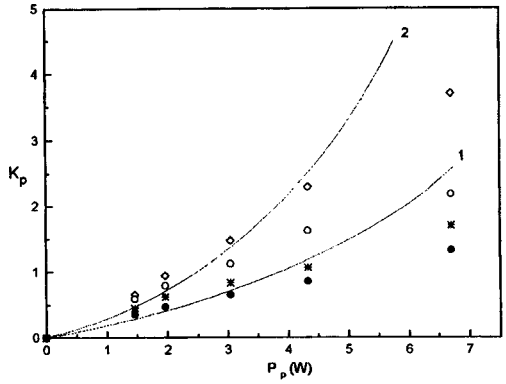

FIG. 2. Conversion ratio K_p, describing conversion of the incident signal into a phase conjugate signal, versus the pump power for the linear ($\diamond$, $*$) and soliton ($\circ$, $\bullet$) operating regimes of the delay line at pump pulse durations $\tau_p = 20$ ns ($*$, $\bullet$) and $\tau_p = 40$ ns ($\diamond$, $\circ$); solid curves *1* and *2* — theoretical calculation according to Eq. (3) for $\tau_p = 20$ and 40 ns, respectively.

Without dwelling here to analyze the solutions obtained, we note only that they depend strongly on the ratio η of the pump power P_p to the threshold power P_{th} determined by the damping of the MSBVWs, the size L of the active region, and the group velocities v_1 and v_2 (Refs. 4 and 10). For $\eta = P_p/P_{\text{th}} < 1$ a stationary phase-conjugation regime obtains and for $\eta > 1$ a nonstationary regime, accompanied by exponential buildup of the waves in time, obtains.

4. In the experiment the signal pulse with frequency ω_1 and duration $\tau_s = 40$ ns was fed into the input transducer of the delay line (see Fig. 1). The MSBVW packet excited by this pulse propagated along the YIG film to the output transducer. At the moment t_1 when the MSBVW packet passed through the active region a pump pulse with duration τ_p and frequency ω_p was applied to the film. As a result of the action of the pump, the first MSBVW packet, continuing along its path to the output transducer,[3] was amplified in the active region and a phase conjugate MSBVW packet was formed and appeared after a time $t_2 \simeq t_1$ near the input transducer, exciting in it an output electromagnetic signal which was delayed relative to the input signal by the time $t_1 + t_2 \simeq t_d$.

In the course of the experiment the pulse power P of the delayed phase conjugate signal at the input transducer was measured with different pump P_p and signal P_s powers and different pump durations τ_p. Next, the parametric conversion ratio K_p, describing the parametric conversion of the incident signal into the phase conjugate signal, was calculated. It equals the ratio of the power of the phase conjugate wave at the entrance into the active region to the power of the input signal at the same point of the delay line and is convenient for making comparisons with the theory. Figure 2 displays the experimental curves of K_p versus the pump power for two pump durations: $\tau_p = 20$ ns and 40 ns. At first the input signal power was equal to 5 mW and the delay line operated in the linear regime. The solid lines in Fig. 2 show the results of a theoretical calculation using Eq. (3). In this case, $P_{\text{th}} = 7.8$ W, i.e., in the entire range of pump powers at our disposal phase conjugation occurred in a stationary regime. Figure 2 shows good agreement between theory and experiment, though at the maximum power $P_p = 6.7$ W an appreciable decrease of the conversion factor relative to the expected values was observed. This could

be due to the multiwave nature of the spin system of the ferrite film: At high powers more and more spin waves are above the excitation threshold and impede transmission of pump power to MSBVWs.[4]

5. We also realized experimentally phase conjugation of MSBVW envelope solitons arising in the YIG film when the input signal level exceeded a certain critical level for the formation of solitons.[12] In our case this level was equal to $P_{cr}=140$ mW. The experimental results on phase conjugation of a signal with a power of 200 mW, for which a MSBVW soliton propagates in the film, are also presented in Fig. 2. One can see that the conversion ratio describing the conversion of a soliton into a phase conjugate signal is always less than for a weak linear signal, especially at high powers and with long pump pulses. This could be due to the stronger influence of parametrically excited higher order types of oscillations of the spin system, since now they are subjected to two powerful pulses — signal and pump. Of course, the circumstance that the soliton pulse is narrower and possesses internal frequency modulation also has an effect.

The thresholds for the formation of envelope solitons of the phase conjugate wave were calculated, using the conjugate wave profile obtained from Eq. (3), by the inverse-problem method with the aid of the nonlinear Schrödinger equation. We neglected the influence of nonlinear and dispersion effects in the pump region, making the assumption that the pump duration τ_p and the passage time of the signal through the active region were short compared with the nonlinear distortion and dispersion spreading times.[12] It turned out that the conditions of our experiment admit the existence of a phase conjugate wave soliton, but we were not able to observe it experimentally.

In summary, we have investigated experimentally and theoretically the phase conjugation of MSBVWs in YIG films by means of locally uniform parallel pumping. The pulse power of the phase conjugate signal at the start of the pump region was more than three times greater than the power of the low-amplitude input pulse. In the case of a powerful input signal, forming an envelope soliton, the conversion ratio describing the conversion of the incident signal into the phase conjugate signal was almost two times lower.

This work was supported by the Ukrainian Fund for Fundamental Research under Grant 2.4/707, and by the US National Science Foundation under Grant DMR-9701640.

[a)]e-mail: melkov@boy.rpd.univ.kiev.ua

[1] A. Yariv and P. Yeh, *Optical Waves in Crystals*, J. Wiley and Sons, New York, 1984 [Russian translation, Mir, Moscow, 1987].
[2] B. Ya. Zel'dovich, R. F. Pilipetskiĭ, and V. V. Shkunov, *Principles of Phase Conjugation*, Springer-Verlag, New York, 1985 [Russian original, Nauka, Moscow, 1085].
[3] A. V. Bagada, G. A. Melkov, A. A. Serga, and A. N. Slavin, Phys. Rev. Lett. **79**, 2137 (1997).
[4] G. A. Melkov and S. V. Sholom, Zh. Tekh. Fiz. **60**, 118 (1990) [Sov. Phys. Tech. Phys. **35**, 943 (1990)].
[5] V. S. L'vov and A. M. Rubenchik, Preprint No. 31 [in Russian], Institute of Atomic Energy, Siberian Branch of the Academy of Sciences of the USSR (1976).
[6] Yu. V. Gulyaev, P. E. Zil'berman, and A. V. Lugovskiĭ, Zh. Éksp. Teor. Fiz. **111**, 199 (1997) [JETP **84**, 109 (1997)].
[7] N. Bloembergen, *Nonlinear Optics*, W. A. Benjamin, Inc., New York, 1965 [Russian translation, Mir, Moscow, 1966].
[8] V. S. L'vov, *Nonlinear Spin Waves* [in Russian], Nauka, Moscow, 1987.
[9] A. G. Gurevich and G. A. Melkov, *Magnetic Oscillations and Waves* [in Russian], Nauka, Msocow, 1994.

[10] A. M. Gorbunov, Zh. Éksp. Teor. Fiz. **67**, 1386 (1974) [Sov. Phys. JETP **40**, 689 (1974)].
[11] V. S. Vladimirov, *Equations of Mathematical Physics* [in Russian], Nauka, Moscow, 1988.
[12] M. Chen, M. A. Tsankov, J. M. Nash, and C. E. Patton, Phys. Rev. B **49**, 12773 (1994).

Translated by M. E. Alferieff

Screw-type transparency in a three-level medium

I. V. Kazinets and B. G. Matisov
St. Petersburg State Technical University,[a] *195251 St. Petersburg, Russia*

I. E. Mazets
A. F. Ioffe Physicotechnical Institute, Russian Academy of Sciences, 194021 St. Petersburg, Russia

(Submitted 20 April 1998)
Pis'ma Zh. Éksp. Teor. Fiz. **67**, No. 11, 874–880 (10 June 1998)

A solution is obtained for the system of Maxwell–Schrödinger equations describing the propagation of a laser pulse through a three-level Λ medium in which the initial atomic populations are in a specially prepared coherent superposition of low-energy states. This solution describes a new type of transparency which is characterized by the presence of conversion of the frequency of the incident pulse and can be used, specifically, to produce ''optical keys'' and frequency converters for laser radiation. © *1998 American Institute of Physics.* [S0021-3640(98)00811-1]

PACS numbers: 42.50.Md

Several types of transparency in multilevel resonance media are now known. One type is called self-induced transparency (SIT) and was discovered in the mid-1960s by McCall and Hahn.[1] The essence of the SIT phenomenon is that the leading edge of the incident pulse transfers particles of the medium into an excited state, while the trailing edge of the incident pulse induces the particles to emit coherently, giving up energy to the field. If the area under the pulse (integral of the Rabi frequency over time) equals 2π, then such a process of taking energy away from the leading edge and transferring it to the trailing edge does not change the area of the pulse. Therefore the pulse propagates without loss in the medium. Self-induced transparency in multilevel media has been studied mainly by numerical methods. However, analytical solutions have also been obtained for stationary propagation of two-frequency pulses in three-level media, for example.[2]

Another, well-known mechanism for producing transparency in a medium consisting of multilevel atoms is electromagnetically induced transparency (EIT).[3] EIT is based on the fact that under the action of the leading edge of the incident pulses under certain conditions the atoms in the medium end up in a coherent superposition state which is not coupled to the excited state, and they stop interacting with the field. Resonance radiation in the medium propagates without losses and without dispersion distortions.

In the present letter we describe a new type of transparency in a coherent three-level medium that combines the effects characteristic of both SIT and EIT. Besides transparency, the phenomenon studied here includes a transformation of the frequency of the

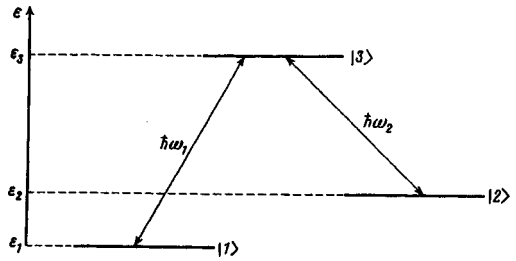

FIG. 1. Diagram of the energy levels of the Λ atoms in the medium.

incident radiation in the course of propagation. Under certain conditions this transformation can reduce to complete conversion of the frequency.

The significance of the term ''screw'' in the title is as follows: To observe transparency of this type a definite spatial periodicity of the initial nonuniform low-frequency coherence and initial populations of the low-energy levels of the medium (thread on a female screw) must correspond to the given frequency, maximum amplitude, and spatial width of the incident pulse of a prescribed form (thread on a male screw). This property of the phenomenon under study is interesting, in our view, in connection with the possibility of producing an optical key.

BASIC EQUATIONS

Let us consider a medium consisting of atoms with a Λ scheme of levels (Fig. 1). Let initial coherence between levels $|1\rangle$ and $|2\rangle$ be induced in this medium (today the production of such coherence does not present any experimental difficulties[4]), while the entire population is in the lower levels.

Let a pulse propagating along the z axis in resonance with the transition $|1\rangle \rightarrow |3\rangle$ be incident on a medium prepared in this manner. Coherence at the transition $|1\rangle \rightarrow |3\rangle$ is excited by this pulse, and on account of the presence of an initial coherence at the transition $|1\rangle \rightarrow |2\rangle$ radiation is induced in the medium at the frequency of the transition $|2\rangle \rightarrow |3\rangle$ and is likewise directed along the z axis. We shall assume that the system of atomic levels is such that $k_1 \cong k_2 = k$, where k_m is the wave number of the field at the transition $|m\rangle \rightarrow |3\rangle$ $(m = 1,2)$. Then the total field can be represented in the form

$$\mathbf{E} = E_1(z,t)\mathbf{e}_1 \exp(-i(\omega_1 t - kz)) + E_2(z,t)\mathbf{e}_2 \exp(-i(\omega_2 t - kz)) + \text{c.c}, \tag{1}$$

where $\omega_1 = (\epsilon_3 - \epsilon_1)/\hbar, \omega_2 = (\epsilon_3 - \epsilon_2)/\hbar$, and $\mathbf{e}_1$ and $\mathbf{e}_2$ are unit polarization vectors.

We shall write the wave function of an atom in the medium as

$$|\Psi\rangle = a_1(z,t)\exp\left(-i\frac{\epsilon_1}{\hbar}t\right)|1\rangle + a_2(z,t)\exp\left(-i\frac{\epsilon_2}{\hbar}t\right)|2\rangle + a_3(z,t)\exp\left(-i\frac{\epsilon_1}{\hbar}t\right)|3\rangle, \tag{2}$$

where $|1\rangle$, $|2\rangle$, and $|3\rangle$ are the eigenstates of the unperturbed Hamiltonian $\hat{H}_0$ ($\hat{H}_0|\mu\rangle = \epsilon_\mu|\mu\rangle$, $\mu = 1,2,3$) and a_μ is a probability amplitude ($\mu = 1,2,3$). We shall study the dynamics of such a three-level atom in the field (1) in the presence of a coherent interaction regime (neglecting spontaneous relaxation).

Under conditions of exact resonance and in the rotating wave approximation, from the Schrödinger equation we have for the nonstationary probability amplitudes

$$\frac{\partial}{\partial t}a_1(z,t)=i\Omega_1^*(z,t)a_3(z,t)\exp(-ikz),$$

$$\frac{\partial}{\partial t}a_2(z,t)=i\Omega_2^*(z,t)a_3(z,t)\exp(-ikz), \tag{3}$$

$$\frac{\partial}{\partial t}a_3(z,t)=i\Omega_1(z,t)a_1(z,t)\exp(ikz)+i\Omega_2(z,t)a_2(z,t)\exp(ikz),$$

where $\Omega_m(z,t)=\langle 3|\hat{\mathbf{d}}_m\cdot\mathbf{e}_m|m\rangle E(z,t)/\hbar$ is the Rabi frequency ($m=1,2$) and $\hat{\mathbf{d}}_1$ and $\hat{\mathbf{d}}_2$ are the dipole moment operators of the transitions $|1\rangle\rightarrow|3\rangle$ and $|2\rangle\rightarrow|3\rangle$, respectively.

Let us choose real Rabi frequencies and introduce the notation

$$\Omega(z,t)=\sqrt{\Omega_1^2(z,t)+\Omega_2^2(z,t)},\quad \frac{\Omega_1(z,t)}{\Omega(z,t)}=\sin\,\varphi(z,t),\quad \frac{\Omega_2(z,t)}{\Omega(z,t)}=\cos\,\varphi(z,t). \tag{4}$$

Instead of the amplitudes a_1, a_2, and a_3 we introduce s, r, and $\tilde{a}_3$:

$$s(z,t)=\frac{\Omega_1(z,t)a_1(z,t)+\Omega_2(z,t)a_2(z,t)}{\Omega(z,t)}\exp(ikz/2),$$

$$r(z,t)=\frac{\Omega_2(z,t)a_1(z,t)-\Omega_1(z,t)a_2(z,t)}{\Omega(z,t)}\exp(ikz/2), \tag{5}$$

$$\tilde{a}_3(z,t)=-ia_3(z,t)\exp(-ikz/2).$$

Then the system (3) acquires the form

$$\frac{\partial}{\partial t}r(z,t)=-\frac{\partial\varphi(z,t)}{\partial t}s(z,t),\quad \frac{\partial}{\partial t}s(z,t)=-\Omega(z,t)\tilde{a}_3(z,t)+\frac{\partial\varphi(z,t)}{\partial t}r(z,t),$$
$$\frac{\partial}{\partial t}\tilde{a}_3(z,t)=\Omega(z,t)s(z,t). \tag{6}$$

Next, assuming that the interaction is adiabatic[5]

$$|\partial\varphi/\partial t|\ll\Omega, \tag{7}$$

we have that the system of equations (6) decomposes into two independent subsystems:

$$\frac{\partial}{\partial t}r(z,t)=0,\quad \frac{\partial}{\partial t}s(z,t)=-\Omega(z,t)\tilde{a}_3(z,t),\quad \frac{\partial}{\partial t}\tilde{a}_3(z,t)=\Omega(z,t)s(z,t). \tag{8}$$

The solution of the system (8) has the form

$$r(z,t)=\text{const}=r_0,\quad s(z,t)=s_0\,\cos(\theta(z,t)/2),\quad \tilde{a}_3(z,t)=s_0\,\sin(\theta(z,t)/2), \tag{9}$$

where $\theta(z,t)=2\int_{-\infty}^{t}\Omega(z,t')dt'$ is the area of the total pulse and the fact that $\tilde{a}_3|_{t=-\infty}=0$ is taken into account. We also assume that the initial values of the amplitudes s and r do not depend on z, and we denote them by s_0 and r_0, respectively.

To take account of the change in the radiation field on account of the influence of the medium in which this radiation propagates, we write down the abridged Maxwell wave equations for the slowly varying amplitudes of the waves propagating along the z axis:

$$\left(\frac{\partial}{\partial z}+\frac{1}{c}\frac{\partial}{\partial t}\right)E_m(z,t)=2\pi iNkd_m a_3(z,t)a_m^*(z,t)\exp(-ikz)\ (m=1,2), \tag{10}$$

where $d_m=\langle 3|\hat{\mathbf{d}}_m\cdot\mathbf{e}_m|m\rangle$, and N is the number density of atoms in the medium. For simplicity we shall consider a medium in which $d_1\cong d_2=d$. Making the substitution of variables $\zeta=z$ and $\tau=t-z/c$, we obtain from Eqs. (10)

$$\frac{\partial}{\partial\zeta}\Omega(\zeta,\tau)=-\frac{2\pi}{\hbar}Nkd^2\tilde{a}_3(\zeta,\tau)s^*(\zeta,\tau). \tag{11}$$

Next, switching to the area of the combined pulse, we have

$$\frac{\partial}{\partial\zeta}\frac{\partial}{\partial\tau}\theta(\zeta,\tau)=-\alpha\ \sin\theta(\zeta,\tau), \tag{12}$$

where $\alpha=2\pi Nkd^2|s_0|^2/\hbar$.

Equation (12) is the sine-Gordon equation. Let us consider a particular solution in the form of a single soliton $\theta(z,t)=\theta(z-ut)$. Then the solution to Eq. (12) is

$$\theta(z,t)=4\tan^{-1}(\exp(-\nu(z-ut))), \tag{13}$$

where

$$\nu^2=\frac{\alpha}{u(1-u/c)}=\frac{2\pi kNd^2|s_0|^2}{\hbar u(1-u/c)}. \tag{14}$$

Hence we have for Ω

$$\Omega(z,t)=\frac{1}{2}\frac{\partial}{\partial t}\theta(z,t)=\nu u\cdot\mathrm{sech}(\nu(z-ut)). \tag{15}$$

Expression (15) is a particular solution of the equation describing the propagation of a pulse in resonance with the transition $|1\rangle\rightarrow|3\rangle$ in a medium prepared so that s_0 and r_0 would be independent of z. This is accomplished by prescribing a definite spatially nonuniform distribution of the initial populations $|a_1|^2$, $|a_2|^2$ and the coherence $\rho_{12}=a_1a_2^*$. It follows from Eq. (15) that if the pulse incident on the medium and in resonance with the transition $|1\rangle\rightarrow|3\rangle$ has the form of a hyperbolic secant (whose parameters correspond to the initial state of the medium), then as the pulse propagates in the medium, the electromagnetic field will vary in a manner so that the aggregate pulse will retain the initial form (15) and will consist of two pulses with two different carrier frequencies. The propagation velocity of such an aggregate pulse can be easily determined from the expression $\Omega_{\max}^2=\nu^2u^2$. Substituting Eq. (14) into this expression, we obtain

$$u=\frac{c}{1+2\pi\hbar\omega N|s_0|^2/E_{\max}^2}, \tag{16}$$

where $\omega = kc$ and $E_{\max}^2$ is the squared maximum value of the amplitude of the incident pulse.

The contribution of each spectral component to the aggregate pulse is characterized by the quantity $\varphi(z,t)$, which can be found simply by differentiating:

$$\frac{\partial}{\partial\zeta}\varphi(\zeta,\tau) = -\alpha\frac{r_0^*}{s_0^*\nu u}\cosh[\nu(z-ut)]\sin[2\tan^{-1}(\exp(-\nu(z-ut)))] \cong -\alpha\frac{r_0^*}{s_0^*\nu u}. \tag{17}$$

Since $\varphi(z=0) = \pi/2$ (the incident pulse has one carrier frequency ω_1), we obtain the solution to Eq. (17)

$$\varphi(z,t) = \frac{\pi}{2} - \alpha\frac{r_0^*}{s_0^*\nu u}z, \tag{18}$$

whence one can see that $\partial\varphi/\partial t = 0$, i.e., the adiabaticity condition (7) holds automatically.

Using Eqs. (4) and (5), we obtain the following expressions for the amplitudes a_1, a_2, and a_3:

$$\begin{aligned} a_1 &= \sin\,\varphi(z)\cdot s_0\,\cos\frac{\theta(z,t)}{2}\exp(-ikz) + \cos\varphi(z)\cdot r_0\,\exp(-ikz),\\ a_2 &= \cos\,\varphi(z)\cdot s_0\,\cos\frac{\theta(z,t)}{2}\exp(-ikz) - \sin\varphi(z)\cdot r_0\,\exp(-ikz),\\ a_3 &= is_0\,\sin\frac{\theta(z,t)}{2}\exp(ikz). \end{aligned} \tag{19}$$

From Eqs. (19) we find the initial populations and the low-frequency coherence which are required for the medium to be transparent:

$$\begin{aligned} |a_1|^2 &= \sin^2\varphi(z)\cdot|s_0|^2 + \cos^2\varphi(z)\cdot|r_0|^2 + \sin\varphi(z)\cdot\cos\varphi(z)\cdot(s_0r_0^* + s_0^*r_0),\\ |a_2|^2 &= \cos^2\varphi(z)\cdot|s_0|^2 + \sin^2\varphi(z)\cdot|r_0|^2 - \sin\varphi(z)\cdot\cos\varphi(z)\cdot(s_0r_0^* + s_0^*r_0),\\ |a_3|^2 &= 0,\quad \rho_{12} = a_1a_2^* = \sin\varphi(z)\cdot\cos\varphi(z)\cdot(|s_0|^2 - |r_0|^2)\\ &\quad - \sin^2\varphi(z)\cdot s_0r_0^* + \cos^2\varphi(z)\cdot s_0^*r_0. \end{aligned} \tag{20}$$

The constants s_0 and r_0 satisfy the condition $|s_0|^2 + |r_0|^2 = 1$ (see Eq. (5)) and they can be interpreted as probability amplitudes of the initial population of the superposition states $|s\rangle$ and $|r\rangle$, respectively.

DISCUSSION

Let us suppose that we have a medium with a prescribed density N and consisting of Λ atoms with the dipole moment of the transition $|1\rangle \to |3\rangle$ (Fig. 1) equal to d. Then a definite value of the amplitude s_0 (and therefore r_0 also), which is determined from expressions (14) and (16) as

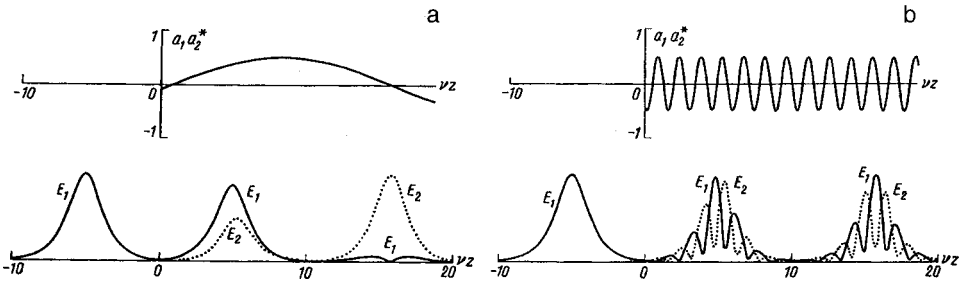

FIG. 2. Initial low-frequency coherence of the medium (top) and amplitudes of pulses with frequencies ω_1 and ω_2 — E_1 and E_2, respectively, at three successive moments in time (bottom) — left-most — incident pulse before entry into the medium; a) $r_0/s_0=0.1$; b) $r_0/s_0=2$ (this picture is observed if $2\pi\hbar\omega N/E_{\max}^2 \gg 1$).

$$|s_0|^2=\frac{E_{\max}^2}{2\pi\hbar\omega N}\left(\frac{\nu c\hbar}{dE_{\max}}-1\right), \tag{21}$$

corresponds to definite parameters (maximum amplitude $E_{\max}$ and spatial width ν^{-1}) of the hyperbolic secant pulse (15) incident on the medium and in resonance with the transition $|1\rangle\rightarrow|3\rangle$. The values of s_0 and r_0 correspond to a spatially nonuniform distribution of the initial populations $|a_1|^2$, $|a_2|^2$ and the coherence ρ_{12}, determined by expressions (20). Screw-type transparency is observed only when such a correspondence holds.

The phenomenon considered here has, in some sense, an analogy with a male and female screw or a lock and key. A concrete pulse (key) propagates transparently only in a medium prepared in an appropriate manner (lock). Therefore this phenomenon could find practical application for producing ''optical keys.''

For a deeper analysis of the mechanism of screw transparency we shall examine two limiting cases.

1. Let us suppose that the parameters of the incident pulse are such that as the pulse passes through an appropriately prepared medium a substantial portion of the population is in the upper level $|3\rangle$. This situation is realized for $s_0 \gg r_0$ (see Eq. (19)). The mechanism leading to the formation of transparency is similar to SIT. The shape of the envelope of the pulses with carrier frequencies ω_1 and ω_2 is close to that of the envelope of the incident pulse (Fig. 2a) (this is valid for $2\pi\hbar\omega N/E_{\max}^2 \gg 1$, which holds in all cases of practical interest). If the parameters of the incident pulse are such that $s_0=1$ $(r_0=0)$, then, as follows from Eq. (20), the medium should be in the following initial state: $|a_1|^2=1$, $|a_2|^2=0$, $\rho_{12}=0$. The population does not transfer into the $|2\rangle$ level and screw transparency completely degenerates into two-level SIT.

2. Let $s_0 \ll 1$. As one can see from Eq. (19), the upper state $|3\rangle$ is then virtually empty. Using the established terminology, we can say that the atoms of the medium are trapped in a superposition state $|r\rangle$ which does not interact with the field. This situation is similar to EIT. The envelope of pulses with carrier frequencies ω_1 and ω_2 has a strongly distorted shape (Fig. 2b) (for $2\pi\hbar\omega N/E_{\max}^2 \gg 1$) Degeneracy appears at $|s_0|^2=0$ and reduces to the following trivial situation: $|a_1|^2=0$, $|a_2|^2=1$, $\rho_{12}=0$. The pulse in resonance with the transition $|1\rangle\rightarrow|3\rangle$ does not affect the population in the level $|2\rangle$.

In all intermediate cases screw transparency is produced by two mechanisms. Part of the population is trapped in a superposition state $|r\rangle$ that does not interact with the field, while the other part of the population, located in the state $|s\rangle$, interacts with the field by a mechanism analogous to SIT.

The most complete conversion of the frequency of the incident pulse is observed in a medium whose thickness is a multiple of Z, determined by the condition $\varphi(Z)=0$ (see Eqs. (4) and (18)). One can see from Eq. (20) that the period of nonuniformity of the initial coherent superposition of low-energy states of the medium (coherence lattice spacing) equals $2Z$. As a result of the independence of φ from t, the time dependence of the envelope of the pulses with carrier frequencies ω_1 and ω_2 is the same at any point z of the medium.

In order for screw transparency to exist the parameters of the incident pulse must satisfy the conditions $0<|s_0|^2<1$, $\nu \ll k$, which together with Eq. (21) reduce to the inequalities

$$\frac{dE_{\max}}{c\hbar}<\nu\ll k, \quad \frac{E_{\max}^2}{2\pi\hbar\omega N}\left(\frac{\nu c\hbar}{dE_{\max}}-1\right)<1. \tag{22}$$

As an example we shall present some numerical estimates. Let us suppose that we have a medium with Λ-atom density $N=10^{15}$ cm^{-3} and dipole moment of the resonance transition $d=10^{-18}$ cgs esu; the frequency of the resonance transition is $\omega=10^{15}$ s^{-1}. Let a resonant pulse in the form of a hyperbolic secant with maximum intensity $I_m\sim 10$ W/cm^2 and spatial width $\nu^{-1}=10^{-2}$ cm be incident on such a medium. Then, proceeding from Eq. (21), we have $|s_0|^2\sim 0.1$. The propagation velocity of such a pulse in the medium is determined by expression (16) and equals $u\sim 2\times 10^6$ cm/s. The quantity $Z\sim 5\times 10^{-3}$ cm. Substituting the values obtained into Eq. (20) we find the initial state of the medium that is necessary for transparency of a given pulse.

It is also necessary to take into consideration the fact that the approach described in the present letter is valid only for times much shorter than the lifetime of the excited state $|3\rangle$. Assuming that the propagation time of a pulse in the medium does not exceed 10^{-6} s, we find that over this time the pulse can transverse a medium with thickness $z\sim 2$ cm.

The type of transparency studied above combines several currently known mechanisms of this kind. Now the actuation of one or another mechanism depends on the parameters of the incident pulse and the corresponding degree of nonuniformity of the initial coherent superposition of the low-energy states of the medium (coherence lattice spacing). This type of transparency has two distinguishing features: 1) for a coherent pulse in the form of a hyperbolic secant the screw transparency arises only in a medium specially prepared for this pulse and 2) besides transparency of the medium, frequency conversion of the incident pulse also occurs. Either total conversion of the frequency or a more complicated transformation of the incident pulse into two pulses with carrier frequencies equal to the frequencies of adjacent atomic transitions in the Λ medium can occur at the exit from the medium.

[a)]e-mail: quark@citadel.stu.neva.ru

[1] S. L. McCall and E. L. Hahn, Bull. Am. Phys. Soc. **10**, 1189 (1965); S. L. McCall and E. L. Hahn, Phys. Rev. Lett. **18**, 908 (1967); S. L. McCall and E. L. Hahn, Phys. Rev. **183**, 457 (1969).
[2] M. J. Konopnincki and J. H. Eberly, Phys. Rev. A **24**, 2567 (1981); M. J. Konopnincki, P. D. Drummond, and J. H. Eberly, Opt. Commun. **36**, 313 (1981); F. T. Hioe, Phys. Rev. A **26**, 1466 (1982); C. R. Stroud Jr. and D. A. Cardimona, Opt. Commun. **37**, 221 (1981); L. A. Bol'shov and V. V. Likhanskiĭ, Kvantovaya Élektron. (Moscow) **12**(7), 1339 (1985) [Sov. J. Quantum Electron. **15**, 889 (1985)].
[3] S. E. Harris, Phys. Rev. Lett. **70**, 552 (1993); S. E. Harris, Phys. Rev. Lett. **72**, 52 (1994); J. H. Eberly, M. L. Pons, and H. R. Haq, Phys. Rev. Lett. **72**, 56 (1994); E. Gerboneschi and E. Arimondo, Phys. Rev. A **52**, R1823 (1995).
[4] S. E. Harris, Phys. Today **50**(7), 36 (July 1997).
[5] J. H. Eberly, Quantum Semiclassic. Opt. **7**, 373 (1995).

Translated by M. E. Alferieff

Generation of quadrature-squeezed light during the propagation of a light wave in a birefringent fiber

S. A. Podoshvedov[a)]
Southern Urals State University, 454080 Chelyabinsk, Russia

(Submitted 9 January 1998; resubmitted 21 April 1998)
Pis'ma Zh. Éksp. Teor. Fiz. **67**, No. 11, 881–886 (10 June 1998)

It is shown that generation of quadrature-squeezed states of a vector electromagnetic field in which quantum fluctuations in one of the quadrature components are smaller than in the coherent state can occur in cubically nonlinear media (birefringent fibers) with efficient energy transfer between the polarization modes of the field. It is shown that for certain distributions of the initial total power between modes, light with suppressed quantum fluctuations in both polarization modes of the vector field is formed at the fiber exit. The optimal conditions for obtaining quadrature-squeezed light are determined. New analytical expressions are obtained for the degree of squeezing in the two polarization modes in the case when there is no energy transfer between the polarization components of the field propagating in the fiber (eigenmodes of two-wave mixing). © *1998 American Institute of Physics.*
[S0021-3640(98)00911-6]

PACS numbers: 42.50.Dy, 42.81.Gs

Possible ways of controlling the quantum fluctuations of laser fields are currently under intensive investigation, being of great interest both from the standpoint of implementing fundamental physical experiments and for producing a fundamentally new generation of computers — optical computers.[1] The key aspects of the current status of theoretical and experimental investigations of the formation of squeezed light in nonlinearly optical interactions are reflected in Refs. 2 and 3. A quantum analysis of optical processes on $\chi^{(3)}$ nonlinearities, and specifically taking energy transfer into account, can be found in Refs. 4–6.

Let us consider the propagation of two coupled, orthogonally polarized, modes in a cubically nonlinear medium (birefringent fibers or polarization-preserving optical waveguides in which a strong birefringence is produced deliberately and it is necessary to identify the slow and fast axes of the fiber) in the presence of a nonlinear correction to the refractive index ($n=n_0+n_2\cdot I$, where $n_2=3\chi^{(3)}_{xxxx}/8n_0=2.3\times 10^{-22}$ m^2/V^2 is the nonlinear refractive index and I is the intensity of the field inside the fiber). The three independent components of $\chi^{(3)}$ are related with $\chi^{(3)}_{xxxx}$ by the relation $\chi^{(3)}_{xxxx}=\chi^{(3)}_{xxyy}+\chi^{(3)}_{xyxy}+\chi^{(3)}_{xyyx}$. The relative magnitude of the three components depends on the specific physical mechanisms contributing to $\chi^{(3)}$. In quartz optical fibers, where $\chi^{(3)}$ is mainly of electronic origin, these three components are almost identical in magnitude.[7] When this

equation is taken into account, the operators describing the nonlinear dynamics of the vector field in a given medium have the form

$$\frac{d\hat{A}_x}{dz}=\frac{iR}{3}\hat{A}_x^+\hat{A}_y^2\,\exp(i\Delta k)+iR\left(\hat{A}_x^+\hat{A}_x+\frac{2}{3}\hat{A}_y^+\hat{A}_y\right)\hat{A}_x, \tag{1}$$

$$\frac{d\hat{A}_y}{dz}=\frac{iR}{3}\hat{A}_y^+\hat{A}_x^2\,\exp(-i\Delta kz)+iR\left(\frac{2}{3}\hat{A}_x^+\hat{A}_x+\hat{A}_y^+\hat{A}_y\right)\hat{A}_y, \tag{2}$$

where $\hat{A}_x$, $\hat{A}_y^+$ and $\hat{A}_y$, $\hat{A}_y^+$ are operators creating and annihilating photons polarized in the directions **x** and **y**; $R=\nu\sqrt{2\hbar\omega/\epsilon_0 V}$ is a nonlinear coupling coefficient, $\nu=n_2\omega/cA$, ω is the carrier frequency, A is the effective area of the fiber, $\Delta k=2(k_y-k_x)$ is the wave detuning, and k_x and k_y are the propagation constants of the modes.

Let us examine a model in which we determine the quantum operators of the vector field as

$$\hat{A}_x=\langle\hat{A}_x\rangle+\hat{a}_x, \tag{3}$$

$$\hat{A}_y=\langle\hat{A}_y\rangle+\hat{a}_y, \tag{4}$$

where $\langle\hat{A}_x\rangle$ and $\langle\hat{A}_y\rangle$ are the classical values of the intensities of the vector electromagnetic field; $\hat{a}_x$ and $\hat{a}_y$ are photon annihilation operators which describe the quantum fluctuations of the polarization modes. From Eqs. (3) and (4) we obtain $\langle\Delta\hat{A}_x^2\rangle=\langle\Delta\hat{a}_x^2\rangle$, $\langle\Delta\hat{A}_y^2\rangle=\langle\Delta\hat{a}_y^2\rangle$. Substituting expressions (3) and (4) into Eqs. (1) and (2) and retaining in Eqs. (1) and (2) only terms which are linear in $\hat{a}_x$ and $\hat{a}_y$, we obtain to zero order in $\hat{a}_x$ and $\hat{a}_y$ the standard nonlinear equations which describe the evolution of the classical intensities of the vector electromagnetic field. We shall represent this system as

$$\frac{d\psi}{ds}=\frac{1}{3}(1-2\eta)\cos(2\psi)+\frac{2}{3}\eta-\frac{1}{3}+\frac{k}{2}, \tag{5}$$

$$\frac{d\eta}{ds}=\frac{2}{3}\eta(1-\eta)\sin(2\psi), \tag{6}$$

where $|q_y|^2=\eta=|\langle\hat{A}_y\rangle|^2/N$; $|q_x|^2=|\langle\hat{A}_x\rangle|^2/N$; $\varphi_x(s)$, $\varphi_y(s)$ — phases of $\langle\hat{A}_x(s)\rangle$, $\langle\hat{A}_y(s)\rangle$; $\psi=\varphi_y-\varphi_x+ks/2$; $k=\Delta kL_{nl}$; $s=z/L_{nl}$; $L_{nl}=1/RN$; $|\langle\hat{A}_x\rangle|^2+|\langle\hat{A}_y\rangle|^2=N=\text{const}$. The system of equations (5) and (6) can be represented in the Hamiltonian form[8,9] for two canonically conjugate quantities η and ψ: $d\eta/ds=-\partial H/\partial\psi$ and $d\psi/ds=\partial H/\partial\eta$ with the Hamiltonian H given by

$$H=\frac{1}{3}\eta(1-\eta)\cos(2\psi)+\frac{1}{3}\eta^2-\frac{1}{3}\eta+\frac{k}{2}\eta. \tag{7}$$

Correspondingly, to first order in $\hat{a}_x$ and $\hat{a}_y$ we obtain a system of linearized equations for the quantum operators $\hat{a}_x$ and $\hat{a}_y$. From the practical standpoint the analysis is easiest to follow if the equations are transformed into equations for quadrature operators. We shall determine the quadrature operators of the polarization modes by the expressions

$$\hat{X}_x(s)=\frac{1}{2}(\hat{a}_x(s)\exp(-i\varphi_x(s))+\hat{a}_x^+(s)\exp(i\varphi_x(s))), \tag{8}$$

$$\hat{Y}_x(s)=\frac{1}{2i}(\hat{a}_x(s)\exp(-i\varphi_x(s))-\hat{a}_x^+(s)\exp(i\varphi_x(s))), \tag{9}$$

$$\hat{X}_y(s)=\frac{1}{2}(\hat{a}_y(s)\exp(-i\varphi_y(s))+\hat{a}_y^+\exp(i\varphi_y(s))), \tag{10}$$

$$\hat{Y}_y(s)=\frac{1}{2i}(\hat{a}_y(s)\exp(-i\varphi_y(s))-\hat{a}_y^+(s)\exp(i\varphi_y(s))). \tag{11}$$

Performing the algebraic transformations, we obtain a system of equations that describes the dynamics of the quadrature operators:

$$\frac{d\hat{X}_x}{ds}=-\frac{1}{3}|q_y|^2\ \sin(2\psi)\hat{X}_x+\frac{2}{3}|q_y|^2\ \cos(2\psi)\hat{Y}_x$$
$$-\frac{2}{3}|q_x||q_y|\sin(2\psi)\hat{X}_y-\frac{2}{3}|q_x||q_y|\cos(2\psi)\hat{Y}_y, \tag{12}$$

$$\frac{d\hat{Y}_x}{ds}=2|q_x|^2\hat{X}_x+\frac{1}{3}|q_y|^2\ \sin(2\psi)\hat{Y}_x+\frac{2}{3}|q_x||q_y|$$
$$\times(2+\cos(2\psi))\hat{X}_y-\frac{2}{3}|q_x||q_y|\sin(2\psi)\hat{Y}_y, \tag{13}$$

$$\frac{d\hat{X}_y}{ds}=\frac{2}{3}|q_x||q_y|\sin(2\psi)\hat{X}_x-\frac{2}{3}|q_x||q_y|\cos(2\psi)\hat{Y}_x+\frac{1}{3}|q_x|^2$$
$$\times\sin(2\psi)\hat{X}_y+\frac{2}{3}|q_x|^2\ \cos(2\psi)\hat{Y}_y, \tag{14}$$

$$\frac{d\hat{Y}_y}{ds}=\frac{2}{3}|q_x||q_y|(2+\cos(2\psi))\hat{X}_x+\frac{2}{3}|q_x||q_y|$$
$$\times\sin(2\psi)\hat{Y}_x+2|q_y|^2\hat{X}_y-\frac{1}{3}|q_x|^2\ \sin(2\psi)\hat{Y}_y. \tag{15}$$

We shall assume that $\hat{a}_x$ and $\hat{a}_y$ are in the vacuum state. Using this, we obtain the following relations between the average combinations of the quadrature components of the polarization modes of the light field:

$$\langle\hat{X}_i(0)\rangle=\langle\hat{Y}_i(0)\rangle=0, \tag{16}$$

$$\langle\hat{X}_i(0)\hat{X}_j(0)\rangle=\frac{1}{4}\delta_{ij},\quad \langle\hat{Y}_i(0)\hat{Y}_j(0)\rangle=\frac{1}{4}\delta_{ij}, \tag{17}$$

$$\langle\hat{X}_i(0)\hat{Y}_j(0)\rangle=\langle\hat{Y}_i(0)\hat{X}_j(0)\rangle=0,\quad i\neq j, \tag{18}$$

$$\langle \hat{X}_i(0)\hat{Y}_i(0)\rangle + \langle \hat{Y}_i(0)\hat{X}_i(0)\rangle = 0, \tag{19}$$

where $i=x$ and $j=y$. The linearized quadrature-operator equations (12)–(15) can be written in the form

$$\frac{d\hat{X}}{ds} = G\hat{X}, \tag{20}$$

where $\hat{X}=(\hat{X}_x,\hat{Y}_x,\hat{X}_y,\hat{Y}_y)^T$ is a column vector, while the form of the matrix G can be obtained using Eqs. (12)–(15). From the theory of linear differential equations it is known that the solution of Eq. (20) can be represented as $\hat{X}(s)=S(s)\hat{X}(0)$, where $\hat{S}(s)$ is a 4×4 matrix with real elements $S_{ij}(s)$. The equation for the matrix $S_{ij}(s)$ has the form $dS/ds=G(s)S(s)$. We introduce the following quantities:

$$S_{xx}=\sum_{j=1}^{4} S_{1j}^2(s), \quad S_{yx}(s)=\sum_{j=1}^{4} S_{2j}^2(s), \quad S_{xy}(s)=\sum_{j=1}^{4} S_{3j}^2(s), \quad S_{yy}(s)=\sum_{j=1}^{4} S_{4j}^2(s).$$

To find the degree of quadrature squeezing in the polarization modes we shall determine the quadrature operators $\hat{\tilde{X}}_x$, $\hat{\tilde{Y}}_x$, $\hat{\tilde{X}}_y$, $\hat{\tilde{Y}}_y$ with arbitrary phases $\tilde{\varphi}_x$ and $\tilde{\varphi}_y$. As an example, let us consider the quadrature operator $\hat{\tilde{X}}_x=(\hat{a}_x \exp(-i\tilde{\varphi}_x) + \hat{a}_x^{+} \exp(i\tilde{\varphi}_x))/2$. Similar expressions can be obtained for the remaining quadrature operators. With the aid of algebraic calculations, we write $\hat{\tilde{X}}_x$ in the form $\hat{\tilde{X}}_x=\hat{X}_x \cos\psi_x + \hat{Y}_x \sin\psi_x$, where $\psi_x=\tilde{\varphi}_x-\varphi_x$. Calculations give for the variances of the quadrature operator $\hat{\tilde{X}}_x$

$$\langle \hat{\tilde{X}}_x^2\rangle = S_{xx}\cos^2\psi_x + S_{yx}\sin^2\psi_x + S_{xxy}\sin(2\psi_x), \quad S_{xxy}=\sum_{j=1}^{4} S_{1j}S_{2j}.$$

The procedure for finding the phase ψ_x for which the variance $\langle \hat{\tilde{X}}_x^2\rangle$ assumes extremal values ($\partial\langle \hat{\tilde{X}}_x^2\rangle/\partial\psi_x=0$) leads to the following results:

$$\tan(2\psi_x)_{(\max,\min)}=\frac{2S_{xxy}}{S_{xx}-S_{yx}}, \tag{21}$$

$$\sin(2\psi_x)_{(\max,\min)}=\pm\frac{2S_{xxy}}{\sqrt{(S_{xx}-S_{yx})^2+4S_{xxy}^2}}. \tag{22}$$

Let us examine Eq. (22) with the minus sign. Then, introducing the normalized variance of the quadrature component $\hat{X}_x$ as $S_x=\langle \hat{\tilde{X}}_x^2(s)\rangle/\langle \hat{\tilde{X}}^2(0)\rangle$, we obtain an analytical expression for the minimum normalized variance of a light wave polarized along **x** (squeezing):

$$S_x=\frac{1}{2}(S_{xx}+S_{yx}-\sqrt{(S_{xx}-S_{yx})^2+4S_{xxy}^2}). \tag{23}$$

Correspondingly, for a given value of the phase ψ_x the normalized variance of $\hat{Y}_x$ will be maximum (desqueezing — plus sign in front of the square root in Eq. (23)). Taking $\sin(2\psi)$ with a plus sign in Eq. (22), we have the directly opposite picture. The normal-

ized variance of $\hat{Y}_x$ will be minimum while that of $\hat{X}_x$ will be maximum. Similar expressions can be obtained for both the minimum and maximum normalized variances in the **y**-polarization mode in the particular case that $\sin(2\psi_y)=\pm 2S_{yxy}/\sqrt{(S_{yx}-S_{yy})^2+4S_{yxy}^2}$:

$$S_y=\frac{1}{2}(S_{xy}+S_{yy}-\sqrt{(S_{xy}-S_{yy})^2+4S_{yxy}^2}). \tag{24}$$

We obtain an expression for D_y from Eq. (24) by replacing the minus sign by a plus sign in front of the square root.

The solution of the classical equations (5) and (6) can be obtained in terms of the Jacobi elliptic functions. It is impossible to solve the linearized quadrature-operator equations (12)–(15) analytically in the most general case. Let us consider the stable eigenmodes (5) and (6),[8,9] which are extremal points of the Hamiltonian (7) and are determined from the conditions $d\psi/ds=d\eta/ds=0$. A stability analysis shows that there exist two stable eigenmodes (η_e,ψ_e) which are determined as $\eta=\frac{1}{2}(1-\frac{3}{4}k)$, $\psi=\pi/2$ and $\eta=\frac{1}{2}(1-\frac{3}{4}k)$, $\psi=3\pi/2$. For this distribution of the total power between the polarization modes of the light wave and ratio of the phases, there is no energy transfer between the modes, despite the presence of the parametric term in Eqs. (5) and (6). In this case the solution of Eqs. (12)–(15) can be written in the form

$$\hat{X}_x=\frac{1}{2}(1+\cos(U))\hat{X}_{x0}-\frac{|q_y|}{2|q_x|}\sin(U)\hat{Y}_{x0}+\frac{|q_y|}{2|q_x|}(1-\cos(U))\hat{X}_{y0}+\frac{1}{2}\sin(U)\hat{Y}_{y0}, \tag{25}$$

$$\hat{Y}_x=\left(\frac{4}{3}|q_x|^2s+\frac{|q_x|}{2|q_y|}\sin(U)\right)\hat{X}_{x0}+\frac{1}{2}(1+\cos(U))\hat{Y}_{x0}$$
$$+\left(\frac{4}{3}|q_x||q_y|s-\frac{1}{2}\sin(U)\right)\hat{X}_{y0}+\frac{|q_x|}{2|q_y|}(1-\cos(U))\hat{Y}_{y0}, \tag{26}$$

$$\hat{X}_y=\frac{|q_x|}{2|q_y|}(1-\cos(U))\hat{X}_{x0}+\frac{1}{2}\sin(U)\hat{Y}_{x0}$$
$$+\frac{1}{2}(1+\cos(U))\hat{X}_{y0}-\frac{|q_x|}{2|q_y|}\sin(U)\hat{Y}_{y0}, \tag{27}$$

$$\hat{Y}_y=\left(\frac{4}{3}|q_x||q_y|s-\frac{1}{2}\sin(U)\right)\hat{X}_{x0}+\frac{|q_y|}{2|q_x|}(1-\cos(U))\hat{Y}_{x0}$$
$$+\left(\frac{4}{3}|q_y|^2s+\frac{|q_y|}{2|q_x|}\sin(U)\right)\hat{X}_{y0}+\frac{1}{2}(1+\cos(U))\hat{Y}_{y0}, \tag{28}$$

where $U=(4|q_x||q_y|s)/3$, $\hat{X}_{i0}=\hat{X}_i(s=0)$, and $\hat{Y}_{i0}=\hat{Y}_i(s=0)$. The calculations give for S_{xx}, S_{yx}, S_{xy}, S_{yy}, S_{xxy}, and S_{yxy}

$$S_{xx}=\frac{1}{2}(1+\cos(U))+\frac{|q_y|^2}{2|q_x|^2}(1-\cos(U)), \tag{29}$$

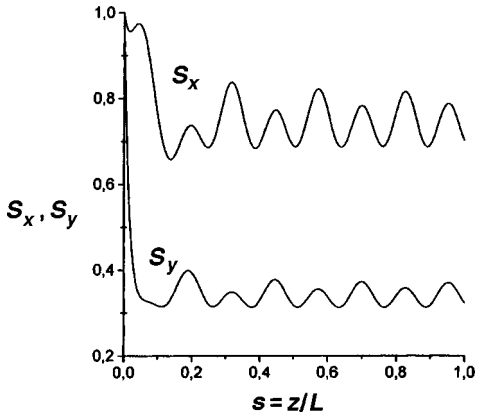

FIG. 1. Minimum values of the normalized variances $S_x(s)$ and $S_y(s)$ in the eigenmodes of two-wave mixing as a function of the normalized distance $s=z/L$ $(L/L_{nl}=40;\ k=-0.5)$.

$$S_{yx}=\frac{16}{9}|q_x|^2s^2+\frac{4|q_x|}{3|q_y|}(|q_x|^2-|q_y|^2)s\ \sin(U)+\frac{1}{2|q_y|^2}+\frac{|q_y|^2-|q_x|^2}{2|q_y|^2}\cos(U), \tag{30}$$

$$S_{xxy}=\frac{2}{3}s+\frac{|q_x|^2-|q_y|^2}{2|q_x||q_y|}\sin(U)+\frac{2}{3}(|q_x|^2-|q_y|^2)s\ \cos(U). \tag{31}$$

The expressions for S_{xy}, S_{yy}, and S_{yxy} can be obtained from Eqs. (29)–(31) by interchanging x and y. Figure 1 shows plots of S_x and S_y versus the fiber length, normalized to half the fiber length (L is the fiber length) for $k=-0.5$ (the value of the stable eigenmode $\eta_e=11/16$). For the present case $k=2\omega L_{nl}(n_y-n_x)/c=-0.5$ we have that the **y** component of the light field is polarized along the fast axis while the **x** component is polarized along the slow axis of the fiber. As one can see from Fig. 1, the minimum values of the normalized variances of $\hat{a}_x$ and $\hat{a}_y$ drop sharply to a certain level at the initial stage of propagation and then oscillate around it. One can see from Fig. 1 that a stronger suppression of quantum noise in the fast mode than in the slow mode of the vector field can be observed at the fiber exit.

Let us consider a different limiting case for $k=-0.5$. Let $\eta(0)=0.375$, $|q_x(0)|^2=0.625$, $\psi(0)=\pi/2$ or $\psi(0)=3\pi/2$. The value of the Hamiltonian (7) for this unstable mode with $\eta=1$ will be $H=-0.25$. The corresponding solution (5), (6) can be represented in the form of combinations of hyperbolic functions:

$$|q_x(s)|^2=0.625\ \mathrm{sech}^2(U),\quad |q_y(s)|^2=1-0.625\ \mathrm{sech}^2(U), \tag{32}$$

$$\cos(2\psi(s))=\frac{0.25-0.625\ \mathrm{sech}^2(U)}{1-0.625\ \mathrm{sech}^2(U)},\quad \sin(2\psi(s))=\frac{\sqrt{0.9375}\ \tan(U)}{1-0.625\ \mathrm{sech}^2(U)}, \tag{33}$$

where $U=0.3227s$. Solving the system of equations (20) numerically, where $|q_x(s)|$, $|q_2(s)|$, $\cos(2\psi(s))$ and $\sin(2\psi(s))$ evolve according to Eqs. (32) and (33), we observe dependences $S_x(s)$ and $S_y(s)$ of the form presented in Fig. 2. One can see from Fig. 2 that as the fiber length increases, $S_x(s)$ approaches zero, while $S_y(s)\to 0.15$. Correspond-

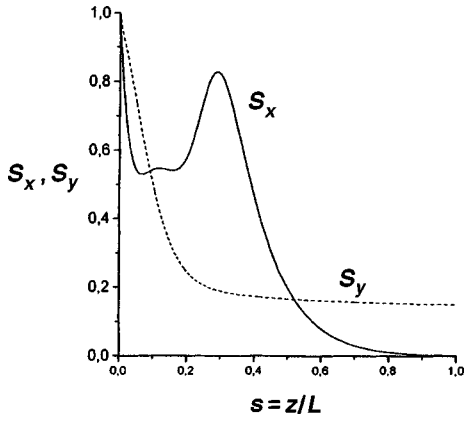

FIG. 2. $S_x(s)$ and $S_y(s)$ as a function of $s=z/L$ ($L/L_{nl}=20$; $k=-0.5$) for the case of total energy transfer from the slow to the fast mode.

ingly, as follows from Eqs. (32) and (33), $|q_x(s)|^2 \to 0$, while $|q_y(s)|^2 \to 1$. Linearly polarized light with strongly suppressed quantum noise exits from the fiber.

In the present letter a quantum theory of two-mode interaction in a birefringent fiber was developed. Two new problems were solved. It was shown that it is possible to achieve suppression of quantum fluctuations in polarization modes of a vector field which interact with one another through a cubic nonlinearity of the fiber.

[a)]e-mail: sergei@nlo.tu-chel.ac.ru

[1] S. A. Akhmanov (ed.), *New Physical Principles of Optical Information Processing* [in Russian], Nauka, Moscow, 1990.
[2] J. Opt. Soc. Am. B **4**, No. 10 (1987).
[3] D. F. Smirnov and A. S. Troshin, Usp. Fiz. Nauk **153**, 233 (1987) [Sov. Phys. Usp. **30**, 851 (1987)].
[4] A. S. Chirkin, A. A. Orlov, and D. Yu. Parashchuk, Kvantovaya Élektron. (Moscow) **20**, 999 (1993) [Quantum Electron. **23**, 870 (1993)].
[5] A. P. Alodzhants, G. A. Dzheĭranyan, L. P. Gevorkyan, and S. M. Arakelyan, Kvantovaya Élektron. (Moscow) **20**, 786 (1993) [Quantum Electron. **23**, 680 (1993)].
[6] A. P. Alodzhants, S. M. Arakelyan, and A. S. Chirkin, Zh. Éksp. Teor. Fiz. **108**, 63 (1995) [JETP **81**, 34 (1995)].
[7] G. P. Agrawal, *Nonlinear Fiber Optics*, Academic Press, New York, 1989 [Russian translation, Nauka, Moscow, 1996].
[8] S. A. Podoshvedov, Pis'ma Zh. Tekh. Fiz. **23**, 61 (1997) [Tech. Phys. Lett. **23**, 562 (1997)].
[9] S. A. Podoshvedov, Opt. Commun. **142**, 79 (1997).

Translated by M. E. Alferieff

Multifrequency photon echo generated by extremely short pulses

A. Yu. Parkhomenko
Tomsk State University, 634050 Tomsk, Russia

S. V. Sazonov
Kaliningrad State Technical University, 236000 Kaliningrad, Russia

(Submitted 23 April 1998)
Pis'ma Zh. Éksp. Teor. Fiz. **67**, No. 11, 887–891 (10 June 1998)

A photon echo in a multilevel quantum medium excited by two extremely short pulses with durations of less than one period of oscillation of the light is investigated theoretically. It is shown that Q echo signals (Q is the number of allowed transitions) can form at each frequency of the allowed transitions, and the number of echo responses for all the allowed transitions equals Q^2. Of these, $Q(Q-1)$ signals are separated in both time and space. The other Q echo signals of all the allowed frequencies all arise at the time $2\tau_{21}$ (τ_{21} is the time interval between application of the first and second pulses to the medium) and are collinear with one another. © *1998 American Institute of Physics.* [S0021-3640(98)01011-1]

PACS numbers: 42.50.Md, 42.65.Re

The possibility of generating extremely short pulses (ESPs) in the optical range under laboratory conditions has engendered great interest in investigations of the interaction of such pulses with matter.[1–3] Since ESPs contain roughly one period of the electromagnetic oscillations (i.e., they are video pulses), here the slowly-varying-amplitude and rotating-wave approximations,[4] which have proven themselves in the optics of monochromatic resonance pulses (MRPs), cannot be used in the wave and material equations. Inasmuch as self-induced transparency, which is a resonance effect, has an analog for ESPs,[5,6] there are grounds for believing that the photon echo effect,[7,8] which, like self-induced transparency, is a nonstationary optical phenomenon, should have an analog with its characteristic features in the case of excitation of a medium by ESPs. In Refs. 9 and 10 the primary and stimulated one-frequency photon echoes arising in a medium excited by a combination of extremely short and monochromatic signals were examined for the example of a two-level medium. Since an ESP is of short duration, its spectrum is quite wide, and for this reason several quantum transitions, characterizing the optical properties of the medium in the frequency region covered by the spectrum of the pulse, can be drawn simultaneously into interaction with the pulse. As a result, echo signals with the corresponding frequencies can arise at the given transitions. Echo effects

accompanying the action of resonance pulses with different frequencies on a medium have been investigated in many works (see Ch. 5 of Ref. 11 and the references cited therein).

The present letter is devoted to an investigation of the multifrequency photon echo accompanying the action of wide-band ESPs on a multilevel quantum medium. It is assumed that the quantum levels of interest are far removed from the continuous spectrum of the medium, so that ionization processes can be neglected. Evidently, transitions lying in the infrared region of the spectrum can satisfy this condition.[5,6] We write the spectral overlap condition[12] as

$$|\omega_{mr}|\tilde{\tau}_p \ll 1, \tag{1}$$

where $\omega_{mr}=-\omega_{rm}$ is the frequency of an allowed transition between the mth and rst levels ($\omega_{mr}>0$ for $m<r$), and $\tilde{\tau}_p$ is the characteristic time scale of the ESP. The system of material equations for the elements ρ_{mr} of the density matrix $\hat{\rho}$ of the medium, neglecting irreversible relaxation, has the form

$$\dot{\rho}_{mr}=i\omega_{mr}\rho_{mr}+i[\hat{A},\hat{\rho}]_{mr}, \tag{2}$$

where $m,\ r=1,2,\ldots,N$, N is the number of quantum levels studied, $\hat{A}$ is the transition matrix with elements $A_{mr}=d_{mr}E/\hbar$, d_{mr} is the projection of the matrix element of the dipole moment operator $\hat{d}$ of the $m\leftrightarrow r$ transition onto the electric field vector $\mathbf{E}$ of the ESP, and $\hbar$ is Planck's constant.

To investigate the excitation of the medium we assume, on the basis of Eq. (1), that $\omega_{mr}\approx 0$. Therefore we find from Eq. (2)

$$\dot{\hat{\rho}}=i[\hat{A},\hat{\rho}]. \tag{3}$$

Echo signals form during the free evolution ($\hat{A}=0$) of atomic dipole moments. Therefore

$$\rho_{mr}(t)=\rho_{mr}(t_j)\exp[i\omega_{mr}(t-t_j)], \tag{4}$$

where t_j is the time at which the action of the nth ESP ceases.

Under the condition $[\hat{A},\int_{t_0}^{t}\hat{A}\,dt]=0$ (t_0 is the time at which the action of the ESP starts),[13] which holds, in particular, for linearly polarized signals,[14] the solution of Eq. (3) can be represented in the form

$$\hat{\rho}(t)=\exp\left(i\frac{\hat{\theta}}{2}\right)\hat{\rho}(t_0)\exp\left(-i\frac{\hat{\theta}}{2}\right), \tag{5}$$

where $\hat{\rho}(t_0)$ is the density matrix of the medium prior to the action of the ESP, and $\hat{\theta}=2\int_{t_0}^{t}\hat{A}\,dt'$. Applying relations (4) and (5) n times in succession, we obtain an expression for the dipole moment $D\equiv$ Tr $(\hat{\rho}\hat{d})$ of an atom after the action of n pulses:

$$D=2id_{pq}U^{(n)}\rho_{ll}\sin[\omega_{pq}(t-\tau_{n,n-1})+\ldots+\omega_{kj}\tau_{32}+\omega_{mr}\tau_{21}], \tag{6}$$

where

$$U^{(n)}=U^{(n)}_{pt}\ldots U^{(2)}_{km}U^{(1)}_{ml}U^{*(1)}_{lr}U^{*(2)}_{rj}\ldots U^{*(n)}_{hq},\quad U^{(s)}_{pk}=[\exp(i\hat{\theta}^{(s)}/2]_{pk}$$

are the matrix elements of the evolution operator after the action of the sth ESP, which are determined by the profile of the latter and by the scheme of allowed quantum transitions, ρ_{ll} are the matrix elements of the equilibrium density matrix, $\tau_{s,s-1}$ is the time interval between neighboring exciting pulses ($s=2,3,\ldots,n$), and n is the number of pulses applied to the medium. Summation from 1 to N is performed over all the subscripts except the subscripts of τ.

Given the form factor of the inhomogeneous-broadening contour for each allowed transition $g_{mk}\equiv g_{mk}(T^*_{mk},\omega_{mk}-\omega_{mk0})$ (T^*_{mk} is the dephasing time of the atomic dipoles at the $m\leftrightarrow k$ transition, and ω_{mk0} is the center frequency of the $m\leftrightarrow k$ transition, corresponding to a maximum of the form factor g_{mk}), the polarization P of the medium as a response to the action of a sequence of ESPs can be found.

In the case of two-pulse action ($n=2$) we find from Eq. (6) the times $t_{kj}^{(mr)}$ at which the echo signals appear at frequency $|\omega_{kj}|$($kj(mr)$ echo signals):

$$t_{kj}^{(mr)}=\left(1+\left|\frac{\omega_{mr0}}{\omega_{kj0}}\right|\right)\tau_{21}. \tag{7}$$

In expression (7) the ω_{mr0} in the numerator in the argument of the modulus operation are the center frequencies of all the allowed transitions. Therefore, in the general case, the number S_ω of echo signals at each frequency equals the number Q of allowed transitions. If, for example, in an N-level system all the transitions are allowed, then at each possible frequency $S_\omega=N(N-1)/2$. The total number of echo responses at all the frequencies is $S=Q^2$. At the same time, it is known that when two MRPs with different frequencies act on a medium, only one echo signal at the difference frequency forms in the medium.[11] Therefore a much larger number of echo signals can be formed with ESPs than with MRPs. It follows from Eq. (7) that Q echo signals of different frequencies form at time $2\tau_{21}$ (with $|\omega_{mr0}|=|\omega_{kj0}|$ in Eq. (7)). The remaining $Q(Q-1)$ signals appear at different times. The characteristic time duration of an echo pulse at frequency $|\omega_{kj0}|$ is of the order of T^*_{kj}. Then in order for two neighboring echo signals at the same frequency $|\omega_{kj0}|$ to be resolvable, the time interval Δt_{kj} between them must satisfy the condition $\Delta t_{kj}>2T^*_{kj}$.

Following the method for determining the wave vector of an echo,[11] we find for the $kj(mr)$ echo signal

$$\mathbf{k}_{kj}^{(mr)}=\mathbf{k}_{kj}^{(2)}+\mathbf{k}_{mr}^{(2)}-\mathbf{k}_{mr}^{(1)}. \tag{8}$$

The left-hand side of expression (8) corresponds to wave vectors of echo signals of frequency $|\omega_{kj0}|$ which are emitted at time $t_{kj}^{(mr)}$ (see Eq. (7)). The wave vectors on the right-hand side of Eq. (8) are to be understood as the spectral components of the ESPs applied to the medium. The superscript 1 or 2 in parentheses corresponds to the number of the video pulse in sequence. The direction $\mathbf{k}_{pq}^{(s)}$ ($s=1,2$) is also the direction of application of the sth ESP. Here $|\mathbf{k}_{pq}^{(s)}|=|\omega_{pq0}|/c$, where $|\omega_{pq0}|$ is the center frequency of one of the allowed $p\leftrightarrow q$ transitions. Following Refs. 9 and 10, we associate to each ESP a quasi-indistinct directed wave vector with characteristic magnitude $(c\tilde{\tau}_p)^{-1}$. By virtue of Eq. (1) the ESP contains all of the resonance spectral components. Maxima of the intensities of the emitted echo signals should be observed in directions determined by Eq. (8).[9] One can see from Eq. (8) that Q echo signals which have equal frequencies and are formed at the time $2\tau_{21}$ are collinear with one another. Their wave vectors are determined

by the expressions $\mathbf{k}_{kj}^{(kj)}=2\mathbf{k}_{kj}^{(2)}-\mathbf{k}_{kj}^{(1)}$ in the case when the exciting ESPs are applied in noncollinear directions. The remaining $Q(Q-1)$ echo responses are separated in space.

Let us illustrate relations (7) and (8) for the example of a three-level medium for which all three transitions are allowed. The states 1, 2, and 3 correspond to energies W, 0, and $-\epsilon W$, where ϵ is a nonequidistance parameter.[11] From Eq. (7) we find the emission times of the echo signals at each allowed frequency:

$$t_{12}^{(12)}=2\tau_{21},\quad t_{12}^{(13)}=(2+\epsilon)\tau_{21},\quad t_{12}^{(23)}=(1+\epsilon)\tau_{21};$$

$$t_{13}^{(12)}=\left(1+\frac{1}{1+\epsilon}\right)\tau_{21},\quad t_{13}^{(13)}=2\tau_{21},\quad t_{13}^{(23)}=\left(1+\frac{\epsilon}{1+\epsilon}\right)\tau_{21}; \tag{9}$$

$$t_{23}^{(12)}=\left(1+\frac{1}{\epsilon}\right)\tau_{21},\quad t_{23}^{(13)}=\left(2+\frac{1}{\epsilon}\right)\tau_{21},\quad t_{23}^{(23)}=2\tau_{21}.$$

From Eq. (8) we obtain wave vectors determining the direction of emission of the corresponding echo signals:

$$\mathbf{k}_{12}^{(12)}=2\mathbf{k}_{12}^{(2)}-\mathbf{k}_{12}^{(1)},\quad \mathbf{k}_{12}^{(13)}=\mathbf{k}_{12}^{(2)}+\mathbf{k}_{13}^{(2)}-\mathbf{k}_{13}^{(1)},\quad \mathbf{k}_{12}^{(23)}=\mathbf{k}_{13}^{(2)}-\mathbf{k}_{23}^{(1)};$$

$$\mathbf{k}_{13}^{(12)}=\mathbf{k}_{13}^{(2)}+\mathbf{k}_{12}^{(2)}-\mathbf{k}_{12}^{(1)},\quad \mathbf{k}_{13}^{(13)}=2\mathbf{k}_{13}^{(2)}-\mathbf{k}_{13}^{(1)},\quad \mathbf{k}_{13}^{(23)}=\mathbf{k}_{13}^{(2)}+\mathbf{k}_{23}^{(2)}-\mathbf{k}_{23}^{(1)}; \tag{10}$$

$$\mathbf{k}_{23}^{(12)}=\mathbf{k}_{13}^{(2)}-\mathbf{k}_{12}^{(1)},\quad \mathbf{k}_{23}^{(13)}=\mathbf{k}_{23}^{(2)}+\mathbf{k}_{13}^{(2)}-\mathbf{k}_{13}^{(1)},\quad \mathbf{k}_{23}^{(23)}=2\mathbf{k}_{23}^{(2)}-\mathbf{k}_{23}^{(1)}.$$

We note that the 12(13), 12(23), 13(13), 23(12), and 23(13) echo responses have been detected with two-frequency (two- and three-pulse) resonance actions on a three-level medium with the aid of MRPs.[11] Here (see Eqs. (9) and (10)), however, all possible $kj(mr)$ echo signals, including those listed in Ref. 11, appear under the action of only two ESPs.

To determine the intensity of different echo signals it is necessary to calculate the matrix elements $U_{mr}^{(s)}$ $(s=1,2)$ of the evolution operator, which in the general case is a very difficult problem. Let us assume that in the N-level system under study only transitions which have one common quantum level with number μ are allowed. There are many physical realizations of this model. For example, for $N=3$ and $N=4$ the model describes the optical properties of wide-gap insulators ($\mu=2$ and $\mu=3$ for $N=3$, $\mu=2$ for $N=4$).[15,16] Taking account of the interaction of the vibrational and electronic terms in molecules leads to a three-level model ($N=3$, $\mu=3$).[15] In this case, in the symmetric matrix $\hat{\theta}$ only the elements of the μth row and μth column are nonzero, except for the element $\theta_{\mu\mu}=0$. Expanding $\exp(i\hat{\theta}/2)$ in a Taylor series in powers of $\hat{\theta}$, and summing, we obtain

$$U_{kp}^{(j)}=\delta_{kp}-\frac{(\hat{\theta}_j^2)_{kp}}{\theta_j^2}\left(1-\cos\frac{\theta_j}{2}\right)+i\frac{(\hat{\theta}_j)_{kp}}{\theta_j}\sin\frac{\theta_j}{2},\quad j=1,2, \tag{11}$$

where δ_{kp} is the Kronecker delta,

$$\theta_j=2(D_\mu/\hbar)\int_{t_j}^{t}E_j dt',\quad D_\mu^2=\sum_{i=1}^{N}d_{i\mu}^2$$

(the subscript j corresponds to the number in sequence of the ESP applied to the medium), and t_j is the time at which the jth ESP is applied. We note that the ''area'' θ_j of an ESP is expressed not in terms of an envelope, which cannot be introduced in present case, but rather in terms of the electric field E itself.

Assume that prior to the action of the first ESP the medium is in a state of equilibrium, where the diagonal elements $\rho_{kk}(0)$ $(k=1,2,\ldots,N)$ are proportional to the corresponding Boltzmann factors. After substituting expressions (11) into Eq. (6) and separating out the parts of the dipole moment $D_{\mu k}^{(mr)}$ that contribute to the echo at frequency $|\omega_{\mu k0}|$, we find the corresponding expressions for the polarization $P_{\mu k}^{(\mu r)}$ at the times $t_{\mu k}^{(\mu r)}$:

$$P_{\mu k}^{(\mu r)}=\frac{4\rho}{D_\mu^3}d_{\mu k}^2 d_{\mu r}^2 L_{\mu r}^{(1)}\cos\frac{\theta_2}{2}\sin^2\frac{\theta_2}{4} \quad \text{for } k<\mu<r \text{ and } r<\mu<k,$$

$$P_{\mu k}^{(\mu r)}=\frac{2\rho}{D_\mu^3}d_{\mu k}^2 d_{\mu r}^2 L_{\mu r}^{(1)}\sin^2\frac{\theta_2}{2} \quad \text{for } \mu<k,\ r \text{ and } \mu>k,r. \tag{12}$$

Here

$$L_{\mu r}^{(1)}=\sin\frac{\theta_1}{2}\left(\cos\frac{\theta_1}{2}\rho_{\mu\mu}-\rho_{rr}+\frac{2}{D_\mu^2}\sin^2\frac{\theta_1}{4}\sum_{l=1}^{N}d_{\mu l}^2\rho_{ll}\right), \tag{13}$$

where ρ is the density of atoms. Given $P_{\mu k}^{(\mu r)}$, the intensity $I_{\mu k}^{(\mu r)}$ of the corresponding echo responses can be calculated as

$$I_{\mu k}^{(\mu r)}\cong\frac{2\omega_{\mu k}^4}{3c^3}V^2(P_{\mu k}^{(\mu r)})^2$$

(V is the volume of the radiating sample).

It follows from Eq. (12) that the intensity of the first group of echo signals ($k<\mu<r$ or $r<\mu<k$) is maximum for $\theta_2=2\pi$; echo pulses of the second group ($\mu<k,r$ or $\mu>k,r$) do not arise. At the same time, if $\theta_2=\pi$, the echo signals of the first group are suppressed, while the intensity of the responses in the second group is maximum. The dependence of the amplitude of the echo signals on the ''area'' θ_1 of the first ESP is determined by relation (13). For example, for V transitions in a three-level system ($\mu=3$) and when only the ground state is initially populated ($\rho_{33}=1$), we find from Eq. (13) that $L_{3r}^{(1)}(\sin\theta_1)/2\pi$. Then the amplitude of the echo signals is maximum when $\theta_1=\pi/2$. Then all the echo signals belong the second group, the maximum intensity of which corresponds to $\theta_2=\pi$. In the cases of Λ transitions ($\mu=1$) and cascade excitation ($\mu=2$) of a three-level medium, the corresponding analysis likewise reduces to searching for the maximum values of $P_{\mu k}^{(\mu r)}$ as a function of θ_1 and θ_2.

In summary, even in the case when two pulses are applied to a multilevel quantum medium a large number of echo signals, both at one frequency and at frequencies of different allowed transitions, can be generated by means of ESPs. Multipulse action ($n>2$) is capable of both increasing the number of echo responses and expanding the

possibilities for controlling them by varying the parameters θ_j $(j=1,2,\ldots,n)$. Following Refs. 9 and 10, echo responses of a multilevel medium excited by combined sequences of ESPs and MRPs can be investigated. This should expand the potential applications of photon echoes in different systems for online information processing, as well as fundamental echo-spectroscopic investigations.

[1] D. H. Auston, K. P. Cheung, I. A. Valdmanis, and D. A. Kleinmann, Phys. Rev. Lett. **53**, 1555 (1984).
[2] J. T. Darrow, B. B. Hu, X. C. Chang, and D. H. Auston, Opt. Lett. **15**, 323 (1990).
[3] P. C. Becker, H. L. Fragnito, J. Y. Bigot *et al.*, Phys. Rev. Lett. **63**, 505 (1989).
[4] A. Allen and J. Eberly, *Optical Resonance and Two-Level Atoms*, Wiley, New York, 1975 [Russian translation, Mir, Moscow, 1978].
[5] É. M. Belenov and A. V. Nazarkin, JETP Lett. **51**, 288 (1990).
[6] É. M. Belenov, A. V. Nazarkin, and V. A. Ushchapovskiĭ, Zh. Éksp. Teor. Fiz. **100**, 762 (1991) [Sov. Phys. JETP **73**, 422 (1991)].
[7] U. Kh. Kopvillem and V. R. Nagibarov, Fiz. Met. Metalloved. **15**, 313 (1963).
[8] N. A. Kurnit, I. D. Abella, and S. R. Hartmann, Phys. Rev. Lett. **6**, 567 (1964).
[9] V. Yu. Man'kov, A. Yu. Parkhomenko, and S. V. Sazonov, Kvantovya Élektron. (Moscow) **24**, 934 (1997).
[10] V. Yu. Man'kov, A. Yu. Parkhomenko, and S. V. Sazonov, Izv. Akad. Nauk Ser. Fiz. **62**, 287 (1998).
[11] É. A. Manykin and V. V. Samartsev, *Optical Echo Spectroscopy* [in Russian], Nauka, Moscow, 1984.
[12] É. M. Belenov, V. A. Isakov, and A. V. Nazarkin, Kvantovaya Elektron. (Moscow) **20**, 1045 (1993) [Quantum Electron. **23**, 911 (1993)].
[13] I. A. Lappo-Danilevskiĭ, *Applications of Matrix Functions in the Theory of Linear Systems of Ordinary Differential Equations* [in Russian], Gostekhizdat, Moscow, 1957.
[14] S. V. Sazonov, Izv. Akad. Nauk Ser. Fiz. **58**, 129 (1994).
[15] R. Braunstain, Phys. Rev. **125**, 475 (1962).
[16] G. B. Al'tshuler, Opt. Spektrosk. **55**, 83 (1983) [Opt. Spectrosc. **55**, 47 (1983)].

Translated by M. E. Alferieff

Reduced magnetohydrodynamics of a toroidal plasma with flows

V. P. Pastukhov[a)]
Kurchatov Institute Russian Science Center, 123182 Moscow, Russia

(Submitted 8 January 1998; resubmitted 27 April 1998)
Pis'ma Zh. Éksp. Teor. Fiz. **67**, No. 11, 892–897 (10 June 1998)

A simplified system of MHD equations describing the nonlinear dynamics of a toroidal plasma in a high magnetic field is obtained by correct elimination of the fast magnetosonic oscillations. In contrast to earlier analogs (Kadomtsev–Pogutse, Strauss, and other equations), the symmetries and the corresponding conservation laws characteristic of the initial complete system of MHD equations are preserved in the system of equations obtained here. This makes it possible to use the system obtained here to analyze the dynamics of plasma with flow and to avoid error accumulation in the analysis of the long-time evolution of disturbances. © *1998 American Institute of Physics.* [S0021-3640(98)01111-6]

PACS numbers: 52.30.−q, 52.55.Dy

Motions in which the magnetic field is perturbed relatively weakly are characteristic for the dynamics of plasma in a high magnetic field ($\beta \equiv 8\pi p/B^2 \ll 1$). The strongest disturbance of the magnetic field energy is due to magnetosonic oscillations with characteristic frequency $\omega \sim k_\perp C_A$ (C_A is the Alfvén velocity), while the most interesting dynamic processes, specifically, magnetohydrodynamic (MHD) instabilities, correspond to disturbances which are strongly extended along the magnetic field ($k_\parallel \ll k_\perp$) and have characteristic frequencies which are typical for Alfvén waves $\omega \sim k_\parallel C_A$ or lower. In such processes the fast magnetosonic degrees of freedom are essentially not excited, so that it is desirable to exclude them at the outset and to study a simpler (reduced) system of equations.

The idea of reduced MHD equations was first advanced and implemented in application to a tokamak by Kadomtsev and Pogutse.[1,2] Their approach was based on expansion of the initial system of equations in terms of the small ratio of the poloidal and toroidal magnetic fields or the reciprocal of the aspect ratio $\epsilon = B_p/B_T \sim a/R$, where a and R are, respectively, the small and large radii of the toroidal plasma. The small but finite value of β and the longitudinal ion-sound oscillations were taken into account in a series of subsequent works.[3–6] However, these works were all inconsistent to some degree. They neglected completely the disturbance of the longitudinal field $\tilde{B}_\parallel$ and $\nabla \cdot \mathbf{V}_\perp$, which is valid only in the leading order. A correct reduction of the equations of motion assuming $\omega \leqslant \epsilon k_\perp C_A$ and $k_\parallel \leqslant \epsilon k_\perp$ requires equating to zero the disturbances of the force terms both in the leading order and in order ϵ. The quantities $\tilde{B}_\parallel \sim \epsilon \tilde{B}_\perp$ and

$\nabla \cdot \mathbf{V}_\perp \sim \epsilon k_\perp V_\perp$ cannot vanish simultaneously and must be retained in the reduced equations. The inadequate correctness of the reduced equations obtained in Refs. 1–6 is even more clearly evident in the fact that these equations do not admit stationary states of plasma with flows, which are characteristic of the initial MHD system. This is due to the fact that the symmetries of the starting equations are destroyed. In later works[7,8] modified versions of the reduced equations were proposed for describing the dynamics of plasma with stationary flows directed along the magnetic field. However, the above-indicated drawbacks are present even in these versions. Specifically, they do not admit stationary flows of a general form.

In the present letter a reduced system of equations for an ideal MHD model is obtained by systematic separation of the fast and slow motions. This approach is similar to determining the adiabatic invariants and constructing adiabatic equations of motion in classical Lagrangian mechanics. To this end, let us consider a variation of the standard Lagrangian of a one-fluid MHD model:[9]

$$\delta\mathcal{L}=\int d\mathbf{r}\left(\rho\mathbf{V}\cdot\delta\mathbf{V}+\frac{V^2}{2}\delta\rho-\frac{\delta p}{\gamma-1}-\mathbf{B}\cdot\delta\mathbf{B}\right). \tag{1}$$

(Here and below the coefficient $1/4\pi$ is included in the normalization of **B**). In this expression the variations of the physical quantities are not completely independent, since constraints are imposed on them in the form of freezing-in equation, the continuity equation, and the adiabatic equation:

$$\partial_t\mathbf{B}=\nabla\times[\mathbf{V}\times\mathbf{B}], \tag{2}$$

$$\partial_t\rho+\nabla\cdot\rho\mathbf{V}=0, \tag{3}$$

$$\partial_t s+\mathbf{V}\cdot\nabla s=0, \tag{4}$$

where $s=p/\rho^\gamma$ is the entropy function. The equations (2)–(4) are the local conservation laws in the sense that the corresponding Lie derivatives vanish.[10] According to Ref. 9, the equations (2)–(4) can be integrated in general form by introducing three independent Lagrangian coordinates with a nondegenerate Jacobian. In the present letter we consider magnetic systems with the topology of toroidally imbedded magnetic surfaces (tokamaks, stellarators, and so on). Following Refs. 11 and 12, where the dynamics of such systems is studied in greatest detail, we choose as the Lagrangian coordinates the poloidal flux ψ, the poloidal angle θ, and the toroidal angle ζ, which correspond to a coordinate system with straight flux lines. Then **B**, ρ, and s, which satisfy Eqs. (2)–(4), can be represented in the form

$$\mathbf{B}=[\nabla\psi\times(q\nabla\theta-\nabla\zeta)],\quad \rho=J\hat{\rho}(\psi,\theta,\zeta),\quad s=s(\psi), \tag{5}$$

where $q(\psi)$ is the conventional coefficient of ''margin of stability,'' while $J=\nabla\psi\times[\nabla\theta\times\nabla\zeta]\neq 0$, like ρ, satisfies Eq. (3). The system of coordinates introduced above engenders contravariant $\nabla\psi$, $\nabla\theta$, and $\nabla\zeta$ and covariant

$$\mathbf{e}_\psi=[\nabla\theta\times\nabla\zeta]/J,\quad \mathbf{e}_\theta=[\nabla\zeta\times\nabla\psi]/J,\quad \mathbf{e}_\zeta=[\nabla\psi\times\nabla\theta]/J$$

bases, in which the velocity assumes the form

$$\mathbf{V}=-\mathbf{e}_\psi\dot{\psi}-\mathbf{e}_\theta\dot{\theta}-\mathbf{e}_\zeta\dot{\zeta}, \tag{6}$$

where an overdot denotes ∂_t. The expressions presented above make it possible to write down explicitly the Lagrangian of system in terms of independent Lagrangian coordinates and their first time and space derivatives.

In Refs. 12 and 13 it was shown that in systems with the topology of imbedded toroidal magnetic surfaces there exists a labeling transformation of the Lagrangian coordinates (relabeling) that does not change the Lagrangian of the system. This symmetry transformation fixes the structure of the neutral flows that can be present in the stationary state of the system also. In Refs. 12 and 13 the dynamical conservation laws which are engendered by these transformations in accordance with Noether's theorem[10] were also found. In the present letter a similar procedure is used to separate fast and slow motions and to derive the reduced equations of motion. Specifically, we shall seek transformations of the independent variables that leave the Lagrangian (1) unchanged in zeroth and first orders in the small parameter ϵ but can change it in order ϵ^2. With respect to the fast motion these transformations play the role of approximate symmetry transformations. These transformations prescribe the structure of the adiabatic flows which do not excite the fast degrees of freedom, similarly to the way the above-mentioned symmetry transformations prescribe the structure of neutral flows. If the motion corresponding to the fast degrees of freedom is stable (this is the case of interest to us) and these degrees of freedom were not excited in the initial state of the system, then the presence of adiabatic flows in the initial state will not lead to excitation of fast degrees of freedom in the process of the further evolution in accordance with the principle of construction of these flows. Here there is a complete analogy with neutral flows which do not drive a stable system out of the stationary state. Therefore the problem of reducing the MHD equations reduces to finding the structure of adiabatic flows and obtaining the dynamical equations describing their evolution. It is important to note here that general adiabatic transformations should include symmetry transformations as a subclass, since the latter leave the Lagrangian unchanged in all orders in ϵ. Therefore the symmetries of the initial equations are automatically preserved in the reduced equations obtained in this manner.

To simplify the equations below, we shall confine our attention to systems with axisymmetric stationary states (of the tokamak type), that is systems in which all physical quantities (specifically, $\hat{\rho}$) in the stationary state are independent of ζ. For such systems the velocity of neutral flows can be written in the form[12]

$$\mathbf{V}_0=\kappa(\psi)\frac{\mathbf{B}}{\rho}-\Phi_0'(\psi)\mathbf{e}_\zeta=\frac{\mathbf{B}}{qJ}\left(\kappa\frac{qJ}{\rho}-\Phi_0'\right)+\frac{1}{qJ}[\nabla\zeta\times\nabla\Phi_0], \tag{7}$$

where $\kappa(\psi)$ and $\Phi_0(\psi)$ are arbitrary functions which prescribe the transverse profile of the flow. As one can see from expression (7), the Lagrangian coordinates make it possible to describe adequately the structure of the neutral flows. For this reason, it is natural to endeavor to describe the structure of adiabatic flows in terms of the same coordinates. Together with the real physical quantities $\mathbf{B}$, ρ, and p, neutral flows do not change the basis vectors $\nabla\psi$ and $\mathbf{e}_\zeta$. However, in the presence of neutral flows the remaining basis vectors depend on the time even in the stationary state. This is inconvenient for further analysis. For this reason, we shall employ below somewhat modified (pseudo-Lagrangian) angular coordinates satisfying the equations

$$\dot{\psi}+\mathbf{v}\cdot\nabla\psi=0,\quad \dot{\theta}+\mathbf{v}\cdot\nabla\theta=0,\quad \dot{\zeta}+\mathbf{v}\cdot\nabla\zeta=0, \tag{8}$$

where $\mathbf{v}=\mathbf{V}-\mathbf{V}_0$. Such a change of variables makes it possible to eliminate from them terms which are secular in time and are associated with the presence of neutral flows. The relations (5) and (7) retain their form, while in expression (6) $\mathbf{V}$ is replaced by $\mathbf{v}$.

Taking account of the relations (5), the dominant term in the variation of the Lagrangian (1) assumes the form

$$\mathbf{B}\cdot\delta\mathbf{B}=\frac{B^2}{q}(\mathbf{e}_\psi\cdot\nabla(q\,\delta\psi)+\mathbf{e}_\theta\cdot\nabla(q\,\delta\theta-\delta\zeta))$$
$$-J\mathbf{B}\cdot\mathbf{e}_\theta\left(\frac{q'}{q}\,\delta\psi+\frac{1}{qJ}(\mathbf{B}\cdot\nabla)(q\,\delta\theta-\delta\zeta)\right)-\mathbf{B}\cdot\mathbf{e}_\psi(\mathbf{B}\cdot\nabla\,\delta\psi). \tag{9}$$

In expression (9) the first term dominates. The adiabatic transformation of the independent variables that makes this term vanish has the form

$$\delta\psi_a=\frac{1}{q}\mathbf{e}_\theta\cdot\nabla\,\delta\alpha,\quad \delta\theta_a=-\frac{1}{q}\mathbf{e}_\psi\cdot\nabla\,\delta\alpha+\frac{\delta\zeta}{q}, \tag{10}$$

where $\delta\alpha$ and $\delta\zeta$ are arbitrary functions of the coordinates and time. By analogy to Refs. 10–12, this transformation can be written in the form of an infinitesimal displacement vector

$$\boldsymbol{\xi}_a=\frac{1}{qJ}[\nabla\zeta\times\nabla\,\delta\alpha]-\frac{1}{qJ}\mathbf{B}\delta\zeta. \tag{11}$$

It is easily to see by comparing with Eq. (7) that for $\delta\alpha=\Phi_0(\psi)\tau$ and $\delta\zeta=(\kappa qJ/\rho-\Phi_0')\tau$ the transformation (11) becomes a symmetry transformation. The residual term in expression (9) under the adiabatic transformation (11) assumes the form

$$\mathbf{B}\cdot\delta_a\mathbf{B}=\mathbf{B}\left[\nabla\zeta\times\nabla\frac{\mathbf{B}\cdot\nabla\,\delta\alpha}{qJ}\right] \tag{12}$$

and for $|\nabla_\parallel\delta\alpha|\sim\epsilon|\nabla_\perp\delta\alpha|$ it is of order ϵ^2. Since $\nabla_\perp qJ\sim\epsilon qJ/a$, we obtain the estimate $\nabla\cdot\boldsymbol{\xi}_a\sim\epsilon k_\perp\xi_a$. Then, assuming similarly to Refs. 1–8, that $\beta/k_\perp a\sim\epsilon^2$, we have $\delta_a p\sim B^2k_\perp\xi\beta/k_\perp a\sim O(\epsilon^2)$. Assuming $V\leqslant c_s$, the term $V^2\delta_a\rho$ is of the same order of magnitude. The term $\rho\mathbf{V}\cdot\delta\mathbf{v}$ in arbitrary (nonreduced) motion is of order of ϵ, since $\boldsymbol{\xi}$, generally speaking, depends on the fast time so that $\delta\mathbf{v}\sim k_\perp C_A\xi$. To check the order of smallness of this term, in accordance with the order of the other reduced terms, let us consider $\delta_a\mathbf{v}$, which, since $\delta\mathbf{v}=\dot{\boldsymbol{\xi}}+(\mathbf{v}\cdot\nabla)\boldsymbol{\xi}-(\boldsymbol{\xi}\cdot\nabla)\mathbf{v}$, assumes the form

$$\delta\mathbf{v}=\frac{1}{qJ}[\nabla\zeta\times\nabla(\dot{\delta\alpha}+\mathbf{v}\cdot\nabla\,\delta\alpha)]-\frac{\mathbf{B}}{qJ}(\dot{\delta\zeta}+\mathbf{v}\cdot\nabla\,\delta\zeta). \tag{13}$$

The quantity $\delta_a\mathbf{v}$ is of the correct order of magnitude if $\dot{\delta_a\alpha}+\mathbf{v}\cdot\nabla\,\delta_a\alpha\sim\epsilon k_\perp C_A\delta_a\alpha$, while $\dot{\delta_a\zeta}+\mathbf{v}\cdot\nabla\,\delta_a\zeta\sim\epsilon k_\perp C_A\delta_a\zeta$, i.e., with respect to the fast motion the functions $\delta_a\alpha$ and $\delta_a\zeta$ should approximately fulfill the role of a relabeling transformation. By analogy to neutral flows[12] such infinitesimal adiabatic transformations correspond to adiabatic flows of the form

$$\mathbf{v}_a=\frac{1}{qJ}[\nabla\zeta\times\nabla\phi]-\frac{1}{qJ}\mathbf{B}\dot{\zeta}, \tag{14}$$

which do not excite the fast degrees of freedom. Here ϕ and $\dot{\zeta}$ are arbitrary functions of the coordinates and the slow time.

Expression (14) gives the general structure of the velocity field of the desired reduced MHD equations. The equations themselves can be obtained from Hamilton's least-action principle (see, for example, Ref. 9, 10, and 12) by substituting into it the ''adiabatic'' variation of the Lagrangian (1). The vanishing of the coefficient of $\delta\zeta$, taking into account the pseudo-Lagrangian nature of ρ/qJ and $s=s(\psi)$, leads to a differential conservation law for the cross helicity $\chi=\mathbf{V}\times\mathbf{B}$:

$$\partial_t\chi+\nabla\cdot\left\{\mathbf{V}\chi-\mathbf{B}\left(\frac{V^2}{2}-\frac{\gamma}{\gamma-1}\frac{p}{\rho}\right)\right\}=0. \tag{15}$$

This conservation law is also valid for the initial nonreduced MHD model and can be obtained by multiplying the equation of motion by $\mathbf{B}/\rho$. It implies, in particular, the first of the integral invariants (29) of Ref. 12. The vanishing of the coefficient of $\delta\alpha$ gives a second dynamical equation of the reduced MHD model:

$$\partial_t\Omega^{\zeta}+\nabla\cdot\left\{\mathbf{V}\Omega^{\zeta}-\frac{\mathbf{B}}{\rho}\nabla\cdot[\mathbf{B}\times\nabla\zeta]-\frac{1}{\rho}[\nabla\zeta\times\nabla p]-[\mathbf{V}\times\nabla(\mathbf{V}_0\cdot\nabla\zeta)]+\left[\mathbf{B}\times\nabla\frac{qJ}{\rho}\right]\right\}=0, \tag{16}$$

whose form is formally that of a conservation law for the contravariant ζ component of the vorticity $\Omega^{\zeta}=\nabla\zeta\cdot\nabla\times\mathbf{V}$. This equation can also be derived as a direct consequence of the nonreduced vector equation of motion, but in contrast to the latter the scalar pair of equations (15) and (16) contains only terms of order ϵ^2 or higher. In view of the definitions of χ, $\mathbf{V}_0$, and $\dot{\zeta}$ it is convenient to rewrite expression (14) for the total velocity of the adiabatic motion as

$$\mathbf{V}=\frac{1}{B^2}\left[\mathbf{B}\times\left(\nabla\Phi-\nabla\zeta\frac{\mathbf{B}\cdot\nabla\Phi}{qJ}\right)\right]+\mathbf{B}\frac{\chi}{B^2}, \tag{17}$$

where $\Phi=\phi+\Phi_0$ is the electrical potential, while the relation

$$\partial_t\mathbf{A}=-\nabla\zeta\frac{(\mathbf{B}\cdot\nabla\Phi)}{qJ}$$

determines the adiabatic variation of the vector potential.

The equations (15)–(17), replacing the complete vector equation of motion, constitute the basis of the proposed reduced MHD model. These equations are similar to the corresponding equations of the well-known reduced models,[1–8] but in contrast to the latter the symmetries of the initial system are preserved in Eqs. (15)–(17), since a symmetry transformation is a subclass of the adiabatic transformation (11). Specifically, the system (15)–(17) admits a stationary state with flows of the type (7). At the same time, the velocity field (17), in the general case, is not a subclass of the exact flows of the initial system of MHD equations. In this sense the proposed reduced MHD model is a new, relatively independent, system of equations, and the question of the complete set of its symmetries and the corresponding invariants requires further investigation, which falls outside the scope of the present letter. We note only that the second integral invariant of the complete system of MHD equations (see expression (29) of Ref. 12)

$$I_2=\int \eta(\psi)\rho\mathbf{V}\cdot\mathbf{e}_\zeta d^3\mathbf{r}, \tag{18}$$

as expected, is also an invariant of the reduced system (15)–(17) with arbitrary $\eta(\psi)$.

In Refs. 1–8 the quantities **B**, ρ, and p appearing in the reduced equations of motion were determined from Eqs. (2)–(4) by substituting into them the expressions for the reduced velocity field. The equation for **B** was usually approximately integrated taking account of the relatively small perturbation of the magnetic field, but in such an integration, as a rule, the condition $\nabla\cdot\mathbf{B}=0$ was violated. So as not to introduce additional errors associated with the inexact satisfaction of the local conservation laws (2)–(4), it is useful to employ for **B**, ρ, and p, expressions (5) as a result of exact integration, and to substitute the velocity (17) into the simpler equations (8) to determine ψ, θ, and ζ. Finally, we write out explicitly an equation relating the functions Φ and Ω^ζ:

$$\Omega^\zeta=\nabla\cdot\left\{\frac{qJ}{B^2}\nabla\Phi+[\mathbf{B}\times\nabla\zeta]\frac{\chi}{B^2}-\nabla\zeta\frac{(\mathbf{B}\cdot\nabla\Phi)}{B^2}-\mathbf{B}\left(\frac{\nabla\zeta\cdot\nabla\Phi}{B^2}-\frac{(\nabla\zeta)^2(\mathbf{B}\cdot\nabla\Phi)}{qJB^2}\right)\right\}. \tag{19}$$

In principle, to solve specific problems a number of terms which are higher-order infinitesimals can be dropped in expressions (17) and (19). However, this must be done accurately enough so as not to destroy the self-consistency and intrinsic symmetry of the system of equations obtained.

In summary, Eqs. (15) and (16) supplemented by expressions (5) and (17) and by Eqs. (8) and (19) form a closed self-consistent system of equations of ideal reduced magnetohydrodynamics that is suitable for describing the relatively slow (adiabatic) dynamics of a toroidal plasma and, specifically, for analyzing the stability of stationary plasma states with flows of a general type. In contrast to previous analogs,[1–8] the system derived here preserves the symmetries of the initial nonreduced system of equations. This is of fundamental importance for analysis of the dynamics of plasma with flows and it also makes it possible to avoid error accumulation in calculations of the long-time evolution of disturbances.

I thank V. I. Il'gisonis for helpful discussions and constructive criticism. This work was supported in part by the Russian Fund for Fundamental Research under Projects 97-02-17238 and 96-15-96815 and the international association INTAS under Grant INTAS-94-3802.

[a)]e-mail: past@qq.nfi.kiae.su

[1] B. B. Kadomtsev and O. P. Pogutse, Zh. Éksp. Teor. Fiz. **65**, 575 (1973) [Sov. Phys. JETP **38**, 283 (1973)].
[2] B. B. Kadomtsev and O. P. Pogutse, Zh. Éksp. Teor. Fiz. **66**, 2056 (1973) [Sov. Phys. JETP **39**, 1012 (1973)].
[3] R. White, D. Monticello *et al.*, *Fifth International Conference on Plasma Physics and Controlled Nuclear Fusion Research*, IAEA, Vienna (1975), Vol. 1, p. 495.
[4] H. Strauss, Phys. Fluids **19**, 134 (1976).
[5] H. Strauss, Phys. Fluids **20**, 1354 (1977).
[6] H. Strauss, Nucl. Fusion **23**, 649 (1983).
[7] R. D. Hazeltine, M. Kotschenreuther, and P. J. Morrison, Phys. Fluids **28**, 2466 (1985).
[8] H. Strauss, J. Plasma Phys. **57**, 83 (1996).
[9] W. Newcomb, Nucl. Fusion Suppl. **2**, 451 (1962).

[10] V. I. Arnol'd, *Mathematical Methods of Classical Mechanics* [in Russian], Nauka, Moscow, 1974.
[11] V. I. Il'gisonis and V. P. Pastukhov, JETP Lett. **61**, 189 (1995).
[12] V. I. Il'gisonis and V. P. Pastukhov, Fiz. Plazmy **22**, 228 (1996) [Plasma Phys. Rep. **22**, 208 (1996)].
[13] V. I. Il'gisonis and V. P. Pastukhov, Dokl. Akad. Nauk **355**, 38 (1997) [Phys. Dokl. **42**, 577 (1997)].

Translated by M. E. Alferieff

Pseudodipole interaction in exchange-frustrated antiferromagnets

S. V. Maleev[a)]

B. P. Konstantinov St. Petersburg Institute of Nuclear Physics, Russian Academy of Sciences, 188350 Gatchina, Russia

(Submitted 16 April 1998)
Pis'ma Zh. Éksp. Teor. Fiz. **67**, No. 11, 898–903 (10 June 1998)

It is shown that the pseudodipole interaction explains the experimentally observed noncollinear magnetic structure of the compounds U_2Pd_2X (X=In, Sn) and $PrBa_2Cu_3O_{6+x}$, which consist of two spin subsystems which are noninteracting in the mean-field approximation if there is only isotropic exchange between them. © *1998 American Institute of Physics.* [S0021-3640(98)01211-0]

PACS numbers: 75.30.Et, 75.50.Ee

A large number of antiferromagnets whose magnetic structure is characterized by the following features has now been observed experimentally. 1. The set of all magnetic sublattices divides into two parts (subsystems) which do not interact in the mean-field approximation if there is only an isotropic exchange interaction between them. We shall term such antiferromagnets exchange-frustrated. 2. The magnetic structure as a whole is noncollinear. This general assertion is illustrated by the following examples: 1) The compounds R_2CuO_4, where R=Pr, Nd, Sm, and Eu.[1–5] Below T_N the copper spins in neighboring CuO_2 planes are mutually perpendicular. Moreover, at low temperatures the magnetic moments of the rare-earth ions are also ordered noncollinearly (see Ref. 6 and references cited therein). 2) The weak antiferromagnet $Sr_2Cu_3O_4Cl_2$ with a center of inversion.[7] The magnetic structure of these compounds has been explained by assuming the existence of a pseudodipole interaction (PDI) between neighboring ions.[6–9] In the present letter it is shown that the PDI makes it possible to explain the noncollinear magnetic structure observed experimentally in the compounds U_2Pd_2X, where X=In, Sn,[10] and $PrBa_2Cu_3O_{6+x}$ below the temperature $T_{\rm Pr}$ of the appearance of magnetic order in the praseodymium subsystem.[11–13] Thus we arrive at the conclusion that PDI plays an important role in the cases where the conventional magnetic interactions are suppressed for one reason or another. In the case of exchange-frustrated antiferromagnets such a reason is the symmetry-forbiddenness of exchange interaction in the mean-field approximation.

The PDI was postulated by Van Vleck in 1937.[14] The first microscopic derivation of the PDI was given in the famous paper by Moriya.[15] For rare-earth metals the PDI was analyzed in Ref. 16, and in Ref. 17 it was used to describe the spectra of spin waves in praseodymium. In Ref. 18 it was shown that the PDI in rare-earth metals and actinides is due to a skew scattering of conduction electrons by localized orbital moments of the *f*

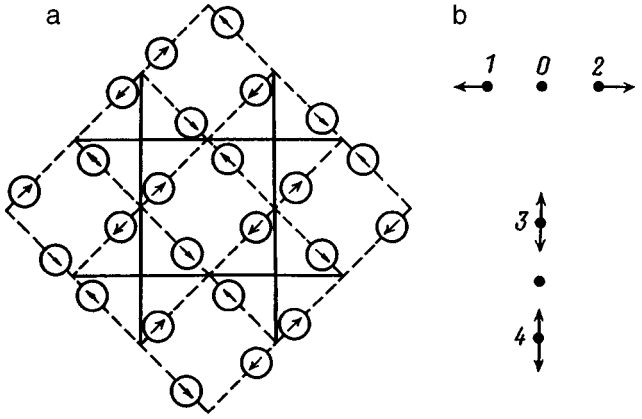

FIG. 1. a) Experimentally determined magnetic structure in the $c=0$ plane.[10] Only the uranium atoms are shown; the arrows indicate the direction of their spins. b) Two exchange-frustrated pairs of uranium atoms. The solid and dashed arrows correspond to two possible directions of the spins of the pair of ions 3 and 4 with the same exchange energy.

electrons. A microscopic calculation of the PDI between the spins of Cu^{2+} ions in CuO_2 planes is contained in Refs. 19 and 20 (see also the references cited therein). However, the gap width, computed on the basis of these calculations, in the spin-wave spectra was found to be an order of magnitude smaller than the value determined experimentally in Pr_2CuO_4 (Ref. 9) and $YBa_2Cu_3O_{6+x}$ (Ref. 21). This discrepancy is apparently due to the influence of the ions surrounding the CuO_2 planes in these compounds.

We shall employ the following expression for the PDI:[6,9]

$$H_{PD}=\frac{1}{2}\sum_{n,n'} Q_{n,n'}(\mathbf{S}_n\cdot\hat{R}_{n,n'})(\mathbf{S}_{n'}\cdot\hat{R}_{n,n'}), \tag{1}$$

where $\hat{R}_{n,n'}$ is a unit vector in the direction connecting the spins $\mathbf{S}_n$ and $\mathbf{S}_{n'}$, and the constants $Q_{n,n'}$, which can have either sign, fall off with increasing distance more rapidly than $R_{n,n'}^{-3}$. We also note that for brevity we shall always employ below the term ''ion spin,'' without specifying the real nature of the localized moment.

We begin with an analysis of the compounds U_2Pd_2X, where the uranium atoms lie in the basal plane $c=0$. The magnetic structure appearing at $T_N=41$ K and 36 K for X $=$Sn and In, respectively, is shown in Fig. 1a. Evidently, in the exchange approximation neighboring pairs of ions do not interact and the system is exchange-frustrated. However, the PDI between neighboring ion pairs gives rise to long-range magnetic order. Indeed, let consider two neighboring pairs of ions, shown in Fig. 1b. Confining ourselves, for the time being, to ions 1, 2, and 3, we find

$$E_{PD}=-\frac{2Q}{\rho^2+r^2}(\mathbf{S}\cdot\boldsymbol{\rho})(\mathbf{S}_3\cdot\mathbf{r}), \tag{2}$$

where $\mathbf{S}_1=-\mathbf{S}_2=\mathbf{S}$, $\boldsymbol{\rho}$ and $\mathbf{r}$ are the coordinates of ions 1 and 3, respectively, and $\mathbf{S}\|\boldsymbol{\rho}$ and $\mathbf{S}_3\perp\boldsymbol{\rho}$. For $Q>0$ this energy is minimum if $\mathbf{S}_3\|\mathbf{r}$, and we obtain the experimentally

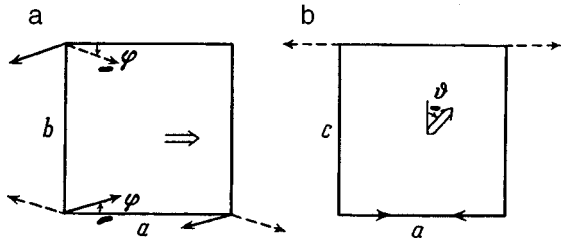

FIG. 2. Magnetic structure of $PrBa_2CuO_3O_{6+x}$ below T_{Pr} according to the data of Ref. 12. a) Direction of copper spins lying in the basal plane ab and belonging to two neighboring CuO_2 planes, and the projection of the praseodymium spins on the ab plane. The solid and dashed arrows show the direction of the copper spins in the bottom and top planes, respectively. Double arrows show the projection of the praseodymium spins. b) Projections of the copper and praseodymium spins on the ac plane.

determined structure shown in Fig. 1a. At the same time, for the magnetic dipole interaction $Q_m=-3(g\mu_B)^2(\rho^2+r^2)^{-3/2}<0$, and in the absence of the PDI, the structure corresponding to the dashed arrows in Fig. 1b correspond should materialize.[10] Evidently, taking into account the magnetic dipole interaction of the pair of spins 1 and 2 with the spin 4 does not change this result. Thus we can see that in the case of the compounds U_2Pd_2X it is impossible to explain the observed magnetic structure without taking the PDI into account. A possible mechanism leading to the appearance of PDI is skew scattering of the conduction electrons, already mentioned above, by the f electrons of uranium. If this is so, then an anomalous Hall effect associated with such scattering[22] should be observed in the compounds U_2Pd_2X above T_N.

Let us now turn to the problem of magnetism in $PrBa_2Cu_3O_{6-x}$. As is well known, this compound is an insulator at all values of x. Below $T_N\simeq 300$ K the Cu^{2+} spin subsystem exhibits antiferromagnetism with the same structure as in $YBa_2Cu_3O_6$.[11–13] However, at an x-dependent temperature T_{Pr}, which lies in the interval 10–20 K, antiferromagnetism also appears in the praseodymium subsystem, and a noncollinear magnetic order is established which, according to Ref. 12, has the form shown in Fig. 2. It is obvious that the system as a whole is exchange-frustrated, i.e., in the corresponding approximation there is no interaction between the copper and praseodymium ions.

Our goal is to demonstrate that the PDI makes it possible to give a qualitative explanation for the observed noncollinear magnetic structure. It should be noted that at present it is hardly possible to give a quantitative description, since the nature of the ground state of the Pr ions is unclear.[13,23] Moreover, below T_{Pr} the real magnetic structure is very sensitive to the presence of the trace impurities Al and Sr.[12,13] We also note that a symmetry analysis of the possible magnetic structures in the compounds $RBa_2Cu_3O_{6+x}$ is contained in Ref. 24.

Before proceeding, we shall present the main characteristics of the magnetic structure of $PrBa_2Cu_3O_{6+x}$ for the two values of x investigated in Ref. 12: $T_N=266$ K, $T_{Pr}=19\pm 0.5$ K, $\varphi=30\pm 5°$, $\vartheta=35\pm 20°$ and $T_N=347$ K, $T_{Pr}=11\pm 0.5$ K, $\varphi=20\pm 5°$, $\vartheta=52\pm 6°$ for $x=0.92$ and $x=0.35$, respectively; the angles ϑ and φ are shown in Figs. 2a and 2b.

We shall confine our attention below to the noncollinear magnetic structure in pairs of neighboring CuO_2 planes and the planes between them containing praseodymium ions

(see Fig. 2). An investigation of the ordering of such strongly coupled triplets along the c axis is not part of our problem. That ordering is due to weaker interactions and apparently depends strongly on the impurities.[12,13]

We proceed from the following model: The strong exchange interaction is responsible for collinear antiferromagnetism in the CuO_2 planes and also in the praseodymium plane. The relative orientation of the copper and praseodymium spins and their orientation relative to the axes of the crystal are determined by the weaker interactions. We shall describe the orientation of the copper spins in the planes 1 and 2 and the praseodymium spins by spherical coordinates $(\eta_{1,2};\varphi_{1,2})$ and (ϑ,ψ), respectively, choosing as the z and x axes the directions c and a (see Fig. 2). Then the ground state energy can be expressed as follows:

$$E=S^2J_\perp[\sin\ \eta_1\sin\ \eta_2+\cos\ \eta_1\cos\ \eta_2\sin(\varphi_1-\varphi_2)]+AS^2$$
$$\times(\cos^2\eta_1+\cos^2\eta_2)+\frac{P}{4}(\sin^4\eta_1\sin^2 2\varphi_1+\sin^4\eta_2\sin^2 2\varphi_2)$$
$$+BK^2\cos^2\vartheta+\wedge\sin\vartheta[\sin\ \eta_1\sin(\psi+\varphi_1)+\sin\ \eta_2\ \sin(\psi+\eta_2)]. \tag{3}$$

Here the first term describes the exchange interaction of copper spins ($S=1/2$) of neighboring planes along the c axis, the second term describes their uniaxial anisotropy, and the third term is the quadratic anisotropy energy in the CuO_2 planes, which, as is well known, plays an important role in cuprates.[9,19,21] The uniaxial anisotropy energy K of the praseodymium spins is determined by the fourth term. Finally, the last term is the pseudodipole interaction of the copper and praseodymium spins. It can be easily derived from the general formula (1) in the nearest-neighbor interaction approximation and $\wedge=4QSKa^2(2a^2+z^2)^{-1}$, where z is the distance between the CuO_2 planes.

The energy (3) is a function of six variables and five parameters. Although a complete investigation of its extrema for an arbitrary ratio of the parameters is impossible, it is not really necessary. For our purposes it is sufficient to show that for a definite ratio between the parameters the minimum of the energy (3) corresponds to a noncollinear structure close to that determined in Ref. 12.

We note first that the equations $\partial E/\partial\eta_{1,2}=0$ have a solution $\eta_{1,2}=\pi/2$, and for sufficiently large anisotropy $A>0$ the copper ion spins lie in the ab plane. As a result, we obtain instead of Eq. (3)

$$E=S^2J_\perp\cos(\varphi_1-\varphi_2)+\frac{P}{4}(\sin^2 2\varphi_1+\sin^2 2\varphi_2)BK^2\cos^2\vartheta$$
$$+\wedge[\sin(\psi+\varphi_1)+\sin(\psi+\varphi_2)]\sin\ \vartheta. \tag{4}$$

The extrema of this energy are determined by the expressions

$$-S^2J_\perp\sin(\varphi_1-\varphi_2)+P\sin\ 2\varphi_1\cos\ 2\varphi_1+\wedge\cos(\psi+\varphi_1)=0\,, \tag{5}$$

$$S^2J_\perp\sin(\varphi_1-\varphi_2)+P\sin\ 2\varphi_2\ \cos\ 2\varphi_2+\wedge\cos(\psi+\varphi_2=0\,, \tag{6}$$

$$\{-2BK^2\sin\ \vartheta+\wedge[\sin(\psi+\varphi_1)+\sin(\psi+\varphi_2)]\}\cos\vartheta=0\,, \tag{7}$$

$$[\cos(\psi+\varphi_1)+\cos(\psi+\varphi_2)]\sin\ \vartheta=0\,. \tag{8}$$

The solutions of this system can be divided into three classes: 1) $\cos\vartheta=0$, 2) $\sin\vartheta=0$, and 3) the angle $\vartheta\neq 0,\ \pi/2$. Evidently, only the last case corresponds to the experimental situation of interest to us, and we shall investigate it in greater detail.

From Eqs. (7) and (8) we find $\varphi_1=\varphi,\ \varphi_2=\pi-2\psi-\varphi$. As a result, from Eqs. (5) and (6) implies that $\psi=\pi n/4$, where n is an integer. The experimentally observed structure corresponds to $\psi=0$, and we obtain

$$\sin\vartheta=(\wedge/BK^2)\sin\varphi, \tag{9}$$

$$\cos 2\varphi=-[S^2J_\perp+\wedge^2/2BK^2]P^{-1}. \tag{10}$$

The energy (4) as a function of φ and ϑ under the conditions (9) and (10) and with $\psi=0$ has a minimum if

$$P<0;\quad B<0\,. \tag{11}$$

These conditions signify that the directions [1,1,0] and [0,0,1] are easy axes for the copper and praseodymium spins, respectively. Therefore in the absence of the last, pseudodipole term in Eq. (4), the copper spins should orient along the directions $[\pm 1,\pm 1,0]$, while the praseodymium spins should be parallel to the c axis. However, the PDI couples the orientations of the spins of these two subsystems and leads to the noncollinear structure shown in Fig. 2.

Using Eqs. (9) and (10), the ground state energy can be represented in the form

$$E=-S^2J_\perp+P/2+BK^2-P/2(1+2\sin^2\varphi)\cos 2\varphi. \tag{12}$$

Here the first three terms are the energy of the structure with the spins oriented along the corresponding easy axes. The last term has appeared as a result of the pseudodipole interaction, which caused the spins to tilt away from the directions of easy magnetization. It is obvious that by virtue of the conditions (11) one has $\cos 2\varphi<0$, i.e., $\varphi>45°$.

The result obtained does not agree with the experimentally determined values of the angles φ (see above). This is apparently due to the following circumstances: 1) The model employed is crude — in particular, it neglects the real structure of the ground state of the praseodymium ions in the crystal field (see above and Refs. 13 and 23), and 2) we have ignored quantum fluctuations, which should give an additional φ- and ϑ-dependent contribution to the ground state energy. At the same time, the main result is of a qualitative nature: in exchange-frustrated antiferromagnets the PDI can result in a noncollinear magnetic structure with the spins tilting away from the easy axes.

Let us now discuss some consequences of the results obtained.

1. The noncollinearity of the neighboring CuO_2 planes attests to the smallness of the exchange interaction $J_\perp$ between the copper spins along the c axis. On the strength of Eq. (10), this interaction should not exceed the quadratic anisotropy in the ab plane. At the same time, in $YBa_2Cu_3O_{6+x}$ this interaction is strong: $J_\perp\simeq 100$ K.[25] Such a strong decrease in $J_\perp$ is apparently due to the hybridization, studied in Ref. 23, of the $4f$ and $02p$ orbitals of Pr. It is necessary to make a direct determination of $J_\perp$ in $PrBa_2Cu_3O_{6+x}$ by the method of neutron scattering by optical spin waves at $T>T_{Pr}$.

2. In most cuprates the copper spins are oriented along the [1,0,0] direction.[1–5,21] At the same time, according to Eq. (11), in $PrBa_2Cu_2O_{6+x}$ the [1,1,0] direction is apparently the direction of easy magnetization. Elastic scattering of neutrons at $T>T_{Pr}$ in

magnetic fields directed along [1,1,0] and [1,0,0] would make it possible to determine the type of magnetic anisotropy[1–5] and find the value of P, just as was done in Ref. 23 for YBCO. A theoretical analysis of this problem is given in Ref. 9.

In summary, we have demonstrated for two new examples that the PDI explains the noncollinear magnetic structure of exchange-frustrated antiferromagnets. Taking into account the results of Refs. 6–9, we can assert that the PDI should play an important role in cases where the traditional magnetic interactions cannot explain the observed magnetic structure for one reason or another (for example, because the symmetry is too high).

In closing, I wish to thank A. T. Boothroyd for calling to my attention the problem of the structure of $PrBa_2Cu_3O_{6+x}$ and for providing a preprint.[24] This work was supported by the Russian Fund for Fundamental Research under Grant 96-2-18037a, the State Program ''Statistical Physics'' under Grant VIII–2, and the Russian Program ''Neutron Investigation of Matter.''

[a)]e-mail: Maleyev@thd.pnpi.spb.ru

[1] I. W. Sumarlin, J. W. Lynn, T. Chattopadnyay *et al.*, Phys. Rev. B **51**, 5824 (1995).
[2] D. Petitgrand, A. H. Moudden, G. Galez, and P. Boutrouille, J. Less-Common Met. **164–165**, 768 (1990).
[3] S. Skanthakumar, J. W. Lynn, J. L. Peng, and Z. Y. Li, Phys. Rev. B **47**, 6173 (1993).
[4] S. Skanthakumar, J. W. Lynn, J. L. Peng, and Z. Y. Li, J. Appl. Phys. **73**, 6326 (1993).
[5] T. Chathopadhyay, J. W. Lynn, N. Rosov *et al.*, Phys. Rev. B **49**, 9944 (1994).
[6] R. Sachidanandam, T. Yildirim, A. B. Harris *et al.*, Phys. Rev. B **56**, 260 (1997).
[7] G. C. Chou, A. Aharony, R. J. Birgeneau *et al.*, Phys. Rev. Lett. **78**, 535 (1997).
[8] P. Bourges, L. Boundarene, and D. Petitgrand, Physica B **180–181**, 128 (1992).
[9] D. Petitgrand, S. V. Maleyev, Ph. Bourges, and A. Ivanov, Phys. Rev. B (to be published).
[10] A. Purwanto, R. A. Robinson, L. Havel *et al.*, Phys. Rev. B **50**, 6792 (1994).
[11] S. Skanthakumar, J. W. Lynn, N. Rosov *et al.*, Phys. Rev. B **55**, R3406 (1997).
[12] A. T. Boothroyd, A. Longmore, N. H. Andersen *et al.*, Phys. Rev. Lett. **78**, 130 (1997).
[13] S. Uma, W. Schelle, E. Gmelin, *et al.*, J. Phys.: Condens. Matter **10**, L33 (1998).
[14] J. Van Vleck, Phys. Rev. **52**, 1178 (1937).
[15] T. Moriya, Phys. Rev. **120**, 91 (1960).
[16] T. A. Kaplan and D. H. Lyons, Phys. Rev. **129**, 2072 (1963).
[17] P.-A. Lindgård, Phys. Rev. Lett. **78**, 4641 (1997).
[18] S. V. Maleev, JETP Lett. **61**, 44 (1995).
[19] T. Yildirim, A. B. Harris, A. Aharony, and O. Entin-Wohlman, Phys. Rev. B **52**, 10239 (1995).
[20] O. Entin-Wohlman, A. B. Harris, and A. Aharony, Phys. Rev. B **53**, 11661 (1996).
[21] P. Burlet, J. Y. Henry, and L. P. Regnault, Physica C **296**, in press, 1998.
[22] J. Kondo, Prog. Theor. Phys. **27**, 772 (1962).
[23] R. Fehrenbacher and T. M. Rice, Phys. Rev. Lett. **70**, 3471 (1993).
[24] A. T. Boothroyd, Physica C, in press (1998).
[25] S. Shamoto, M. Sato, J. M. Tranquada, and B. J. Sternlib, Phys. Rev. B **48**, 13817 (1993).

Translated by M. E. Alferieff

Dynamics of first- and second-order phase transitions in amorphous magnetooptic TbFeCo films

M. B. Agranat, S. I. Ashitkov, A. V. Kirillin, and V. E. Fortov
Scientific-Research Institute of the Thermophysics of Pulsed Actions, Joint Institute of High Temperatures, Russian Academy of Sciences, 127412 Moscow, Russia

S. I. Anisimov
L. D. Landau Institute of Theoretical Physics, Russian Academy of Sciences, 142432 Chernogolovka, Moscow Region, Russia

A. B. Granovskiĭ
M. V. Lomonosov Moscow State University, 119899 Moscow, Russia

P. S. Kondratenko
Institute of Problems in the Safe Development of Nuclear Power, Russian Academy of Sciences, 113191 Moscow, Russia

(Submitted 17 April 1998)
Pis'ma Zh. Éksp. Teor. Fiz. **67**, No. 11, 904–909 (10 June 1998)

The dynamics of phase transformations in thin amorphous TbFeCo films under the action of ~ 1 ps laser pulses is investigated. The films are heated to the Curie temperature in the amorphous state (T_{C1}), to the crystallization temperature (T_{ac}), and to the Curie temperature in the crystalline phase (T_{C2}). The change in magnetization is detected by Faraday magnetooptic effect during and after the action of the heating pulse. A static external magnetic field $H \sim 1-12$ kOe, whose flux lines are directed perpendicular to the plane of the film, is used in the experiments. Amorphous TbFeCo films possess a perpendicular magnetic anisotropy, which on crystallization becomes reoriented in the plane of the film. It is observed that crystallization and magnetization reorientation occur during the heating pulse (within ~ 1 ps). The spin subsystem is heated to the Curie temperature several picoseconds after the end of the laser pulse. The characteristic spin relaxation time is ~ 10 ps. A model of the dynamics of the electronic, spin, and phonon subsystems that makes it possible to explain the experimental results is proposed on the basis of the data obtained. [S0021-3640(98)01311-5]

PACS numbers: 75.70.Ak, 75.30.Kz, 78.20.Ls

The question of the interaction of an ultrashort laser pulse with the electronic, spin, and phonon subsystems of a ferromagnet was first studied in Ref. 1 for the example of a thin Ni film. The section of the film heated by a ~ 10 ps pulse could not be demagnetized, even with a laser power density corresponding to melting of the lattice. Hence it was concluded that there is not enough time for the spin subsystem to heat up to the Curie

temperature during the characteristic cooling time of the electron gas and the lattice to this temperature. This agreed with both the theoretical estimates[1,2] and data on ferromagnetic resonance in Ni at temperatures above room temperature, according to which the characteristic spin–electron relaxation time is of the order of 0.1–0.5 ns.[3] It should be underscored that the characteristic spin–electron and spin–lattice relaxation times determined according to the width of the ferromagnetic resonance line can differ substantially from the values of these parameters averaged over all spin-wave modes.[2]

Similar investigations with picosecond heating pulses[4–6] performed later on different ferromagnets (Gd, Fe, CoPt, GdTbFe) confirmed the conclusion of Ref. 1 that the magnetization relaxation process is prolonged.

Recent studies have appeared[7,9,10] in which the dynamics of the spin subsystem in Ni was studied using femtosecond laser pulses. It was observed that in the subpicosecond range partial demagnetization of the Ni film occurs after the action of a femtosecond heating laser pulse. In Ref. 7 it is concluded on the basis of these results that the characteristic times τ_{es} and τ_{ls} are of the order of 1 ps. We underscore that, as shown in experiments on the effect of a strong pulsed magnetic field of an electron beam (see, for example, Ref. 8), reorientation of the magnetic moment can occur in ultrashort times ~ 1 ps, which by no means contradicts the times τ_{es} and τ_{ls} of the order of 1 ns. This result concerning the values of τ_{es} and τ_{ls} does not agree either with preceding works or with the fact that in Ref. 7, just as in Ref. 1, Ni could not be demagnetized. In Ref. 9, where the total demagnetization time of the film was also measured ($\sim 0.1-1$ ns), it was hypothesized that ultrafast spin dynamics is associated with Stoner excitations, which are characteristic for ferromagnets with collectivized electrons, a class which includes Ni, and it should be absent in ferromagnets with localized magnetic moments. A slow spin dynamics (~ 0.1 ns) was identified in Ref. 9 with spin–lattice relaxation under the assumption that the electron–spin relaxation is of the same order of magnitude.

In our view, the different interpretation of the results obtained for the dynamics of the spin subsystem in Ni is due to the fact that in all spin-dynamics investigations performed thus far by the methods of pulsed laser actions the evolution of the lattice temperature was not directly detected.

In the present letter we report the results of experimental investigations of the dynamics of first- and second-order phase transitions in magnetooptic TbFeCo films, which are amorphous ferromagnets with easy magnetization axis along the normal to the plane of the film (perpendicular magnetic anisotropy). At a temperature $T_{C1} \approx 150$ °C the film passes into the paramagnetic state. At $T_{ac} \approx 300$ °C two phase transitions (first- and second-order) occur, to a ferromagnetic crystal with magnetic anisotropy parallel to the film plane. At $T_{C2} \approx 450$ °C there is a transition to a paramagnetic crystal, and at $T_m \sim 900$ °C melting occurs, whereupon the crystalline state is unrecoverable.

A ~ 100 nm thick TbFeCo film was placed between the poles of a magnet capable of producing a constant magnetic field with vector **H** oriented perpendicular to the surface and varying in magnitude H from 1 to 15 kOe. A ~ 500 μm in diameter region of the film was heated by a ~ 1 ps laser pulse with wavelength 780 nm and a nearly Gaussian energy distribution in the focusing spot up to temperatures in the intervals $T_{C1} < T < T_{ac}$, $T_{ac} < T < T_{C2}$, and $T > T_{C2}$.

During the action of the heating pulse the change in magnetization was measured

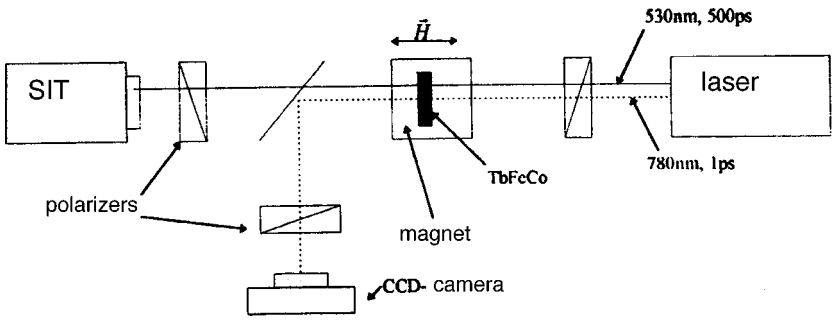

FIG. 1. Optical scheme of the measurements.

with the region of interest illuminated by the heating pulse itself ($\tau \sim 1$ ps) and a CCD camera, which was used to record an image of the heated region using the Faraday effect.

The magnetization dynamics after the action of the heating pulse was studied with a ~ 500 ps probe pulse with wavelength 530 nm and a 100 μm focusing spot, the Faraday magnetooptic effect, and a streak image tube (SIT) (time resolution ~ 2.5 ps).

The optical scheme of the measurements is presented in Fig. 1. In both measurement methods calibration of the dependence of the magnetization on the intensity of the signal due to rotation of the plane of polarization in the Faraday scheme was performed with the aid of magnetization reversal of the film, i.e., by measurements of the magnetic hysteresis loop. The calibration measurements showed that a change in magnetization by 10–15% of the value corresponding to complete demagnetization was reliably detected in both methods. The dynamics of the formation of the paramagnetic state at a transition through T_{C2} was investigated by applying of a high ($\sim 10-15$ kOe) magnetic field, which prevented the spin moments from becoming oriented in the film plane. The experimental results showed the following.

1. In the case of heating to temperatures $T_{C1} < T < T_{ac}$, the phase transition of the amorphous film to the paramagnetic state when the film was heated up to the Curie temperature (T_{C1}) was studied by magnetizing the film with a weak magnetic field (~ 1 kOe). When the heated region was imaged using a CCD camera with the heat pulse itself as the probe, the polarizer and analyzer in the Faraday scheme were initially crossed, i.e., the Faraday shutter operated in the opening mode, which made it possible to detect a useful signal even if it arrived at the end of the heating pulse. The measurements showed that no changes in the magnetization are observed during the action of the heating pulse. However, one can see that after the experiment the heated region of the film was completely demagnetized. Figure 2a shows a time profile of the variation of the magnetization obtained with the SIT. It should be noted that the time resolution of this device (2.5 ps) makes it possible to detect a time delay only with an accuracy no higher than 5 ps. The results of the measurements show that the heated region becomes completely demagnetized in a time $\approx 5-10$ ps after the start of the heating pulse (the reference point 0 on the ordinate corresponds to complete demagnetization, the Faraday scheme operated in the closing mode, i.e., in the initial state the polarizer and analyzer were uncrossed by an angle corresponding approximately to complete demagnetization).

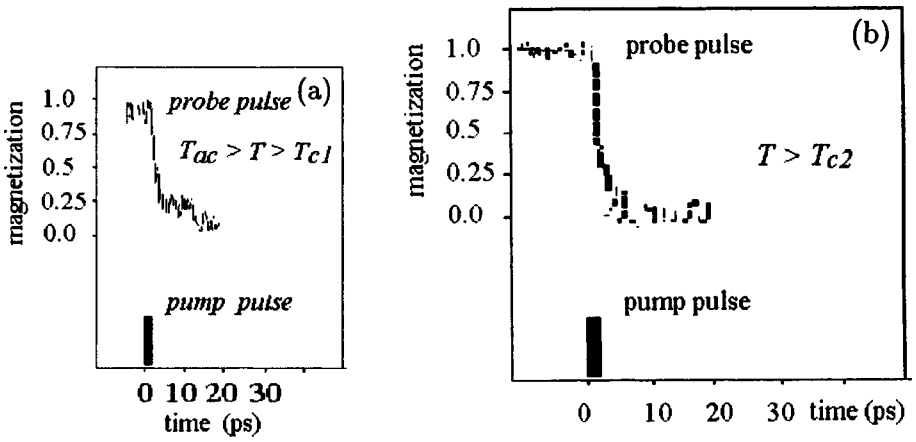

FIG. 2. Results of measurements of the dynamics of the magnetization change accompanying heating of an amorphous TbFeCo film up to temperatures T_{C1} (a) and T_{C2} (b).

2. In the case of heating up to temperatures $T_{ac}<T<T_{C2}$ the transition of the heated region of the amorphous film to the crystalline state was investigated during the action of the heating pulse by using the illumination of the region of interest by the heating pulse itself, a CCD camera, and premagnetization of the film by a weak magnetic field ($\sim$1 kOe). It was observed that during the heating laser pulse only a transition from the amorphous to the crystalline state with a change in orientation of the magnetic anisotropy in the film plane is observed at the center of the focal spot ($\sim$100 μm). This change is identified after cooling by applying a strong magnetic field that ''pulls'' the spins out of the film plane (Fig. 3a). After cooling, a paramagnetic state due to a transition through T_{C1} (Fig. 3b) is observed at the periphery of the focal spot, where the heating temperature is below T_{ac} (in accordance with the Gaussian energy distribution in the focal spot). When the film is magnetized by a weak magnetic field ($\sim$1 kOe), it is evident (Fig. 3c) that there remains only a region of the crystalline phase of the same size as the region in Fig. 3a. Therefore these results show that a first-order phase transition (amorphous state–crystalline state) in TbFeCo films, crystallization, and a change in the direction of the magnetic anisotropy occur during the action of the heating pulse (within

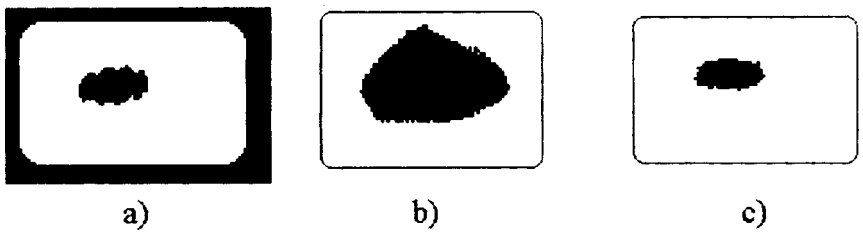

FIG. 3. Results of measurements of the dynamics of the magnetization change accompanying a phase transition of an amorphous film to the crystalline state: a) during the action of a heating pulse, b) after cooling, c) after cooling with $H\sim$1 kOe.

~ 1 ps). With such ultrafast heating this transition occurs without the formation of a paramagnetic state in the amorphous phase.

3. In the case of heating up to temperatures $T > T_{C2}$ to study the transition through the temperature T_{C2} in the crystalline film, the experimental region either was preheated up to temperature T_{ac} to transform the amorphous film into a crystalline state or, on the basis of preceding experiments, the heating was performed from the amorphous phase. The dynamics of the formation of the paramagnetic state accompanying a transition through T_{C2} was investigated by applying a high ($\sim 10-15$ kOe) magnetic field that prevented the spin moments from becoming oriented in the film plane. These experiments were performed with a probe pulse and a streak image tube. The experimental results were found to be practically identical to the results of measurements of a transition through the first Curie point (Fig. 2b).

Our results correspond to ''slow''[9] spin dynamics, occurring under conditions of thermodynamic equilibrium between the electronic subsystem and the lattice. Since energy transfer between the spin subsystem and the electrons and lattice occurs on the basis of the spin–orbit interaction, the electron–spin (α_{es}) and spin–phonon (α_{ls}) heat transfer constants are small compared with the electron-phonon interaction constant:

$$\alpha_{es}, \alpha_{ls} \ll \alpha_{el}. \tag{1}$$

Analysis of the system of three energy balance equations[11,1] for the temperatures T_s, T_e, and T_l shows that at the end of a ~ 1 ps laser pulse, when the lattice temperature reaches its maximum value $T_{l\,\max}$ and $T_e \approx T_l$, the spin temperature T_{s1} is determined by the expression

$$T_{s1} = T_0 + \frac{c_l \alpha_{es}}{c_s \alpha_{el}} (T_{l\,\max} - T_0), \tag{2}$$

where T_0 is the initial temperature and c_l and c_s are the lattice and spin specific heats. At the next stage the spin temperature relaxes to the temperature of the lattice, which is in equilibrium with the electrons. The characteristic time of this relaxation is

$$\tau_s = c_s / (\alpha_{es} + \alpha_{ls}). \tag{3}$$

The maximum temperature reached by the spin subsystem depends on the ratio of the spin relaxation time and the lattice cooling time due to heat conduction into the sample $\tau_c \approx d^2/4\chi$, where d is the depth of heating and χ is the smaller of the thermal diffusivities of the film and substrate. For $\tau_s \ll \tau_c$ the maximum temperature of the spin subsystem equals the maximum lattice temperature, while $T_{sl} < T_{s\,\max} < T_{l\,\max}$ for $\tau_s > \tau_c$. In our experiment the cooling time of the TbFeCo films, according to Ref. 12, is of the order of 100 ps. For this reason, on the time scale where the magnetization changes substantially it can be assumed that $T_l = T_{l\,\max}$, and then the evolution of the spin temperature after the laser pulse ends can be described by the expression

$$T_s = T_{s1} + (T_{l\,\max} - T_{s1})(1 - e^{-t/\tau_s}). \tag{4}$$

Since demagnetization and therefore also heating of the spin subsystem up to temperature T_{C1} occur in 3–5 ps when the lattice is heated to temperatures in the interval $T_{C1} < T < T_{ac}$, we obtain from Eq. (4), taking account of the numerical values of T_{C1} and T_{ac} and also the comparative smallness of the temperature difference $T_{s1} - T_0$, the estimate

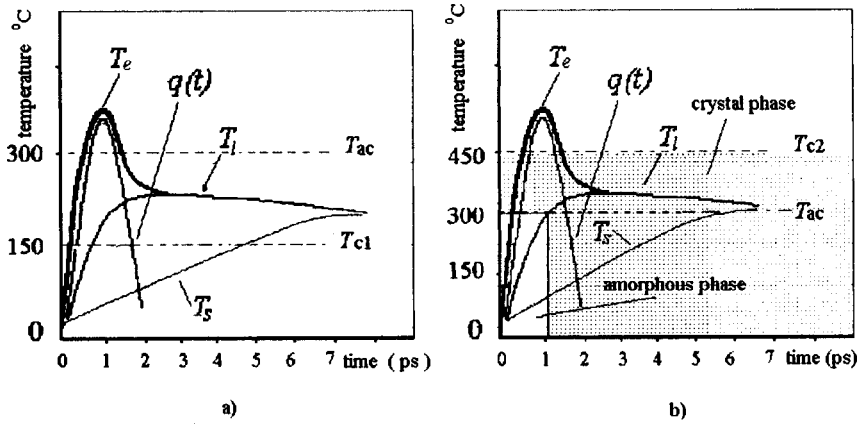

FIG. 4. Dynamics of the relaxation of the electronic, phonon, and spin subsystems accompanying heating of a TbFeCo film up to temperatures: a) $T_{ac}>T>T_{C1}$, b) $T_{C2}>T>T_{ac}$.

$$\tau_s \approx 10 \text{ ps}. \tag{5}$$

We note that this estimate is much shorter than the spin–lattice relaxation time in Ni. In our view this difference is due to the strong increase in the spin–orbit interaction with increasing atomic number, on account of which the presence of the rare-earth element Tb in the experimental films increased the time τ_s substantially. The results obtained can be represented in the form displayed in Fig. 4. Such a dynamics of the electronic, spin, and phonon subsystems is characteristic, in our opinion, for transition metals also.

This work was supported by the Russian Fund for Fundamental Research under Grants 96-02-18495a and 96-02-18494a.

[1] M. B. Agranat, S. I. Ashitkov, A. B. Granovskiĭ, and G. I. Rukman, Zh. Éksp. Teor. Fiz. **86**, 1376 (1984) [Sov. Phys. JETP **59**, 804 (1984)].
[2] E. A. Turov, Izv. Akad. Nauk SSSR, Ser. Fiz. **19**, 462 (1955).
[3] S. M. Bhagat and P. Lubitz, Phys. Rev. B **10**, 179 (1974).
[4] D. Guarisco, R. Burgermeister, C. Stamm, and F. Meier, Appl. Phys. Lett. **68**, 1729 (1996).
[5] A. Vaterlaus, D. Guarisco, M. Lutz, M. Aeschlimann *et al.*, J. Appl. Phys. **67**, 5661 (1990).
[6] A. Vaterlaus, T. Beutler, and F. Meier, Phys. Rev. Lett. **67**, 3314 (1991).
[7] E. Beaurepaire, J.-C. Merle, A. Daunois, and J.-Y. Bigot, Phys. Rev. Lett. **76**, 4250 (1996).
[8] J. Heidmann, D. Weller, H. Siegmann *et al.*, *Abstracts of the 40th MMM Conference*, Philadelphia (1995), p. 473.
[9] A. Scholl, L. Baumgarten, R. Jacquemin, and W. Eberhardt, Phys. Rev. Lett. **79**, 5146 (1997).
[10] J. Hohlfield, E. Matthias, R. Knorren, and K. H. Bennemann, Phys. Rev. Lett. **78**, 4861 (1997).
[11] S. I. Anisimov, B. L. Kapelovich, and T. L. Perel'man, Zh. Éksp. Teor. Fiz. **66**, 776 (1974) [Sov. Phys. JETP **39**, 375 (1974)].
[12] W. Mihael and D. Treves, J. Appl. Phys. **40**, 303 (1969).

Translated by M. E. Alferieff

Isothermal desorption of hydrogen molecules from a W(110) surface at temperature ~5 K

V. D. Osovskiĭ,[a] Yu. G. Ptushinskiĭ, V. G. Sukretnyĭ, and B. A. Chuĭkov
Institute of Physics, Ukrainian National Academy of Sciences, 252650 Kiev, Ukraine

(Submitted 23 April 1998)
Pis'ma Zh. Éksp. Teor. Fiz. **67**, No. 11, 910–915 (10 June 1998)

Isothermal desorption of hydrogen molecules from a W(110) surface at $T_s \sim 5$ K upon rapid shuttering of the molecular beam is observed in a ''black chamber'' type of ultrahigh-vacuum apparatus. Desorption was detected from three different states, identified as a multilayer condensation state and physisorbed states in the form of a two-dimensional gas and a two-dimensional condensate. The distribution of the physisorbed molecules between these states depends on the intensity of the flux of molecules on the surface; this appears to be responsible for the anomalous decrease of the number of isothermally desorbed molecules as the flux increases. © *1998 American Institute of Physics.*
[S0021-3640(98)01411-X]

PACS numbers: 68.45.Da

In previous studies of the low-temperature adsorption of hydrogen molecules by molecular-beam and thermal-desorption spectroscopy methods,[1–6] in addition to obtaining data on the spectrum of weakly bound adsorption states we also observed isothermal desorption of hydrogen molecules at substrate temperature $T_s \sim 5$ K.[1,3] Isothermal desorption was manifested in the fact that when the molecular beam was rapidly shuttered (in a time $\leqslant 50$ ms) the ion current of the mass-spectrometric desorbed-molecule detector did not drop instantaneously but rather over a time much greater than the time constant of the detecting apparatus. The present work is devoted to a more detailed investigation of isothermal desorption of hydrogen molecules from a W(110) surface at $T_s \sim 5$ K, with the expectation that this investigation will shed additional light on the characteristic features of the low-temperature adsorption of hydrogen isotopes.

Investigation of the interaction of hydrogen with solid surfaces is of great interest in connection with the fact that hydrogen participates in important catalytic reactions, e.g., the synthesis of ammonia, and also because hydrogen is a promising environmentally clean fuel. The study of hydrogen adsorption at very low temperatures makes it possible to observe weakly bound molecular adsorption states, which can serve as prestates in the process of dissociative adsorption. Moreover, differences in the quantum properties of hydrogen isotopes can be expected to appear at low temperatures. As far as we know, isothermal desorption of hydrogen at $T_s \sim 5$ K has not been previously investigated.

The experiments were performed in a ''black chamber'' type of ultrahigh-vacuum

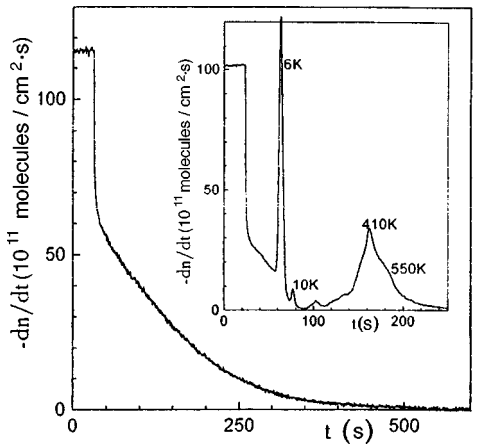

FIG. 1. Isothermal desorption of H_2 molecules from an adsorbed layer formed with flux intensity $\sim 10^{13}$ molecules/cm$^2 \cdot$ s. Inset: Thermal desorption spectrum.

apparatus, in which a molecular beam was formed from an effusion source and a single-transit regime of desorbed molecules was realized.[4,7] In the working regime with the sample manipulator filled with liquid helium and the molecular beam switched on, the residual-gas pressure in the apparatus was $\sim 10^{-12}$ torr and the flux of molecules on the surface from the molecular beam was 10^4 times greater than the background flux. The procedure for measuring isothermal desorption consists of the following. Hydrogen was adsorbed to saturation, indicated by the stabilization of the value of the ion current of the desorbed-molecule detector, from a molecular beam onto a clean W(110) surface cooled to $T_s \sim 5$ K. After saturation was reached, a dynamic equilibrium between the fluxes of adsorbing and desorbing molecules was established in the adsorbed film. After equilibrium was established the molecular beam was quickly shuttered and the time dependence of the ion current $I(t)$ of the detector was measured. After determining the proportionality coefficient α between the detector current and the desorption rate, we obtained the time dependence of the desorption rate and the number of molecules desorbed in the time interval $t_1 - t_2$:

$$n(t) = \alpha \int_{t_1}^{t_2} I(t)dt. \tag{1}$$

The quantity α was determined from a calibration experiment, in which the desorption (in the form of molecules) of a saturated adsorbed atomic layer of hydrogen, containing, according to Ref. 8, $\sim 1.4 \times 10^{15}$ atoms/cm^2 or $\sim 0.7 \times 10^{15}$ molecules/cm^2, was detected. The correctness of such a calibration can in principle be affected by the difference between the spatial distributions of the particles desorbing from the molecular and atomic adsorbed layers as well as the difference in the substrate temperatures at which these adsorbed layers desorb. Control experiments showed that these factors do not greatly affect the measurement results.

Figure 1 shows the desorption rate as a function of time after a molecular beam with intensity $\sim 1 \times 10^{13}$ molecules/cm$^2 \cdot$ s is shuttered. In accordance with the rate of decrease

of the desorption rate, the process can be conventionally divided into a fast stage, which is completed in several seconds, and a slow stage, which lasts for hundreds of seconds. Very few molecules desorb in the fast stage as compared with the slow stage ($<1\%$ of the total number of desorbed molecules). We believe that the fast stage consists of the desorption of a very small (dynamically equilibrium with the flux switched on) number of hydrogen molecules, probably in a multilayer condensation state. We do not mean by this that a continuous multilayer film of condensed hydrogen is formed on the surface, but rather we mean that the heat of desorption of the molecules is close to the heat of sublimation of hydrogen.

The inset in Fig. 1 shows the thermal desorption spectrum measured some time after the onset of the slow stage of desorption. The temperature of the sample increases at a rate of 0.7 K/s in the interval 50–100 s and ~ 7 K/s in the interval 125–250 s. Thermal desorption of molecularly adsorbed hydrogen occurs in the first interval and thermal desorption of atomically adsorbed hydrogen occurs in the second interval.[8] According to our estimate, the temperatures of the first and second peaks due to desorption of molecularly adsorbed hydrogen are close to 6 and 10 K, respectively. In the case of deuterium similar peaks were observed at 8 and 15 K.[5] We note that, in contrast to hydrogen, one does not observe appreciable isothermal desorption of deuterium at $T_s \sim 5$ K. It is clear why the desorption characteristics of hydrogen and deuterium are different, since the levels of the zero-point vibrations of the hydrogen and deuterium molecules in the physisorption potential well are different.[5] A similar interpretation of the difference between the adsorption properties of hydrogen and deuterium on a Ru(001) surface is given in Ref. 9. As one can see from the thermal desorption spectrum in Fig. 1, most hydrogen molecules desorb from the 6 K state. Fewer than 3% of the total number of desorbed molecules are in the 10 K state.

The Polyani–Wigner equation is usually used to describe thermal desorption:

$$-dn/dt = \nu n^a \exp(-E_d/kT_s), \tag{2}$$

where ν is a pre-exponential factor, n is the surface density, a is the order of the desorption reaction, E_d is the desorption activation energy, and k is Boltzmann's constant. Let us represent Eq. (2) in logarithmic form:

$$\log(-dn/dt) = \log \nu + a \log n - 0.43E_d/kT_s. \tag{3}$$

The function $\log(-dn/dt)$ versus $\log n$ (Fig. 2) can be approximated by two linear segments AB and CD with substantially different slopes and correspondingly different desorption reaction orders: a is close to 1 for AB and close to zero for CD. These results attest to the fact that the isothermal desorption of hydrogen molecules occurs from two different states. We believe that the section AB represents isothermal desorption from a two-dimensional (2D) gas state, while the section CD represents desorption with participation of islands of a 2D condensed phase. Under conditions when the desorption rate becomes very low as a result of the depletion of the 2D gas phase, a mechanism whereby the gas phase is replenished by 2D evaporation of islands of a 2D condensate, stabilizing for some time the surface concentration in the gas phase, starts to play an important role. This stabilization causes the order of desorption to approach zero. Apparently, the H_2 molecules in both states are localized in the same first physisorbed monolayer, since their total number ($\sim 1 \times 10^{15}$ molecules/cm^2) is less than a monolayer. A hypothetical model

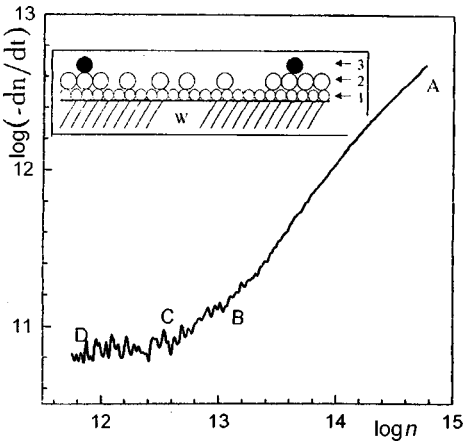

FIG. 2. Rate of desorption of H_2 molecules versus the surface density on a logarithmic scale. Inset: Hypothetical model of an adsorbed hydrogen film: *1* — hydrogen atom, *2* — H_2 molecule in a state of physisorption, *3* — H_2 molecule in a multilayer condensation state.

of such an adsorbed hydrogen film is shown in the inset in Fig. 2. The first monolayer from the metal surface is a chemisorbed atomic layer and the second monolayer is a physisorbed molecular layer. The third layer contains a very small number of H_2 molecules in a multilayer condensation state. A two-phase structure of the physisorbed H_2 layer (2D gas + condensate) was also invoked in Ref. 9 in an investigation of the system $H_2/\mathrm{Ru}(001)$.

We shall now discuss the question of the correspondence between the character of observed isothermal desorption and the thermal desorption spectrum. A multilayer condensation type state does not appear in the thermal desorption spectrum, since the H_2 molecules desorb very rapidly from this state after the molecular beam is shuttered, and this state is already empty at the moment when measurements of the thermal desorption spectrum begin. The 6 K peak represents desorption of molecules from a 2D gas state and corresponds to the section *AB* of the curve in Fig. 2. A rough estimate of the lifetime of a hydrogen molecule in this adsorption state at $T_s \sim 5$ K, under the assumption that at $T_s \sim 6$ K the lifetime equals 1 s, gave ~ 200 s, which is consistent with the experimental data presented in Fig. 1.

At first glance it is tempting to associate the second peak (10 K) in the thermal desorption spectrum to the section *CD* of the curve in Fig. 2, representing desorption with participation of islands of a 2D condensed phase. However, the temperature of this peak and the corresponding binding energy of the molecules in this state are too high to detect desorption at $T_s \sim 5$ K. What is the origin of the molecular desorption peak at $T_s \sim 10$ K? We believe that this peak corresponds to desorption of H_2 molecules from the center of islands of a 2D condensate, where the binding energy should be much greater than in the 2D gas phase and at the edge of an island. As a result of the dynamic character of the experiment, when measuring the thermal desorption spectrum (the temperature of the sample increases continuously at the rate 0.7 K/s) there comes a time when the desorption rate from sections with a high binding energy becomes higher than from sections with a lower binding energy (on account of the steeper dependence on T_s). In

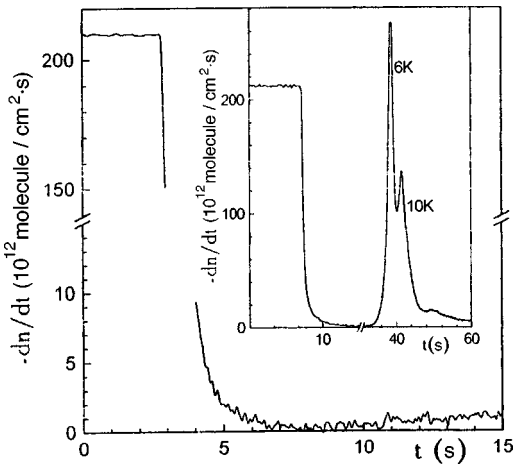

FIG. 3. Isothermal desorption of H_2 molecules from an adsorbed layer formed with flux intensity $\sim 2 \times 10^{14}$ molecules/cm$^2 \cdot$ s. Inset: Thermal desorption spectrum.

other words, when the temperature rises comparatively rapidly there is not enough time for 2D evaporation of the islands to occur, and the molecules desorb into the vacuum from the center of the islands.

Therefore to interpret the observational results on the isothermal desorption of H_2 molecules at $T_s \sim 5$ K we invoked the idea of the existence of islands of a 2D condensed phase. For this reason, we thought it would be useful to perform experiments with an adsorbed H_2 film formed with a substantially higher flux of molecules on the surface. It is reasonable to expect that as the flux increases, the probability of formation of islands of a 2D condensate will increase and correspondingly the fraction of the surface covered by this phase will increase. It is known that the critical size of the nuclei of the condensed phase decreases as supersaturation increases, i.e., as the flux of molecules on the surface increases. In addition, a gas–condensate phase transition is more likely to occur during the experiment.

Let us now examine the results obtained when the flux of H_2 molecules was increased to approximately 2×10^{14} molecules/cm$^2 \cdot$ s. Figure 3 shows a curve of isothermal desorption of H_2 molecules after the molecular beam was switched off. Comparing Figs. 1 and 3 we can see that in the latter case the slow phase of isothermal desorption is virtually absent and the total number of desorbed molecules (proportional to the area under the desorption curve) is more than 50 times smaller. The inset in Fig. 3 shows the low-temperature part of the thermal desorption spectrum, measured 20 s after the molecular beam was shuttered. The same 6 K and 10 K states as in the case of a low-intensity flux are present in the spectrum, but in contrast to the latter case the number of molecules desorbed from the 6 K and 10 K states are comparable. Therefore the main distinction of the high-flux experimental results are the very small number of isothermally desorbed molecules and the large number of molecules in the 10 K state. According to our estimates, the total number of molecules desorbed from the 6 K and 10 K states as the sample temperature increases corresponds to a complete monolayer.

We believe that the absence of substantial isothermal desorption at $T_s \sim 5$ K in the case of a high flux is due to the fact that the overwhelming majority of the H_2 molecules is adsorbed in a 2D condensed phase, while in the case of a low flux a very small portion of the adsorbed molecules is contained in islands of the condensed phase. The large increase in the 10 K peak in the thermal desorption spectrum likewise attests to more intense formation of a 2D condensed phase as the flux of molecules increases.

Finally, let us discuss one other observation. In the experiment with a high flux we noticed that after the desorption rate rapidly decreased to virtually zero after the molecular beam was shuttered, the desorption rate was observed to increase slowly (Fig. 3). We made sure that the pressure in the chamber remained stable and this increase of the detector current is not caused by an increase in the background, but rather it in fact reflects an increase in the desorption rate of hydrogen molecules. We think that the increase in the rate of isothermal desorption is due to pitting of the 2D condensed phase, which is accompanied by lengthening of the ''edge line'' and fosters the transition of an increasingly larger number of molecules into the 2D gas phase, whence, as one can see from Fig. 1, appreciable isothermal desorption occurs.

In conclusion, we shall summarize the main results. Isothermal desorption of physisorbed hydrogen molecules from a W(110) surface at $T_s \sim 5$ K was observed. The results attest to a two-phase structure of the physisorbed H_2 monolayer. We presumed that these phases are states of a 2D gas and a 2D condensate. The relative content of H_2 molecules in these phases depends on the flux of molecules onto the surface. For a low flux ($\sim 10^{13}$ molecules/cm$^2 \cdot$s) the overwhelming majority of the molecules is in a thermally less stable 2D gas state, while for high fluxes ($\sim 2 \times 10^{14}$ molecules/cm$^2 \cdot$s) the majority of the molecules is in a 2D condensate state. For this reason, in the latter case ~ 50 times fewer H_2 molecules than in the first case are isothermally desorbed in the time of the experiment at $T_s \sim 5$ K. In contrast to hydrogen, isothermal desorption of deuterium molecules at $T_s \sim 5$ K was not observed. This is explained by the fact that the zero-point vibrational level of the deuterium molecules lies deeper in the physisorbed potential well.

We express our sincere appreciation to the Ukrainian Ministry and INTAS for financial support. We thank A. G. Naumovets for helpful discussions.

[a)]e-mail: osov@marion.iop.kiev.ua

[1] V. V. Dvurechenskikh, V. D. Osovskiĭ, Yu. G. Ptushinskiĭ *et al.*, JETP Lett. **54**, 40 (1991).
[2] V. V. Dvurechenskikh, V. D. Ososvskiĭ, Yu. G. Ptushinskiĭ *et al.*, Ukr. Fiz. Zh. **37**, 716 (1992).
[3] B. A. Chuikov, V. V. Dvurechenskikh, V. D. Osovskii *et al.*, Surf. Sci. **285**, 75 (1993).
[4] V. D. Osovskiĭ, Yu. G. Ptushinskiĭ, V. G. Sukretnyĭ, and B. A. Chuĭkov, Fiz. Nizk. Temp. **19**, 570 (1993) [Low Temp. Phys. **19**, 406 (1993)].
[5] V. D. Osovksiĭ, Yu. G. Ptushinskiĭ, V. G. Sukretnyĭ, and B. A. Chuĭkov, JETP Lett. **60**, 586 (1994).
[6] V. D. Osovksiĭ, Yu. G. Ptushinskiĭ, V. G. Sukretnyĭ, and B. A. Chuĭkov, Fiz. Nizk. Temp. **23**, 773 (1997) [Low Temp. Phys. **23**, 587 (1997)].
[7] B. A. Chuikov, V. D. Osovskii, Yu. G. Ptushinskii, and V. G. Sukretnyi, Surf. Sci. **213**, 359 (1989).
[8] P. W. Tamm and L. D. Schmidt, J. Chem. Phys. **54**, 4775 (1971).
[9] W. Frieb, H. Schlichting, and D. Menzel, Phys. Rev. Lett. **74**, 1147 (1995).

Translated by M. E. Alferieff

On the observation of a single paramagnetic center in experiments with a scanning tunneling microscope

F. I. Dalidchik and S. A. Kovalevskiĭ
N. N. Semenov Institute of Chemical Physics, Russian Academy of Sciences, 117977 Moscow, Russia

(Submitted 24 April 1998)
Pis'ma Zh. Éksp. Teor. Fiz. **67**, No. 11, 916–921 (10 June 1998)

It is shown that exchange splitting is observed in the field emission resonance spectrum when a paramagnetic center is present in the contact of a scanning tunneling microscope. The effect makes it possible to detect single electron spins. © *1998 American Institute of Physics.* [S0021-3640(98)01511-4]

PACS numbers: 61.16.Ch, 71.70.Gm, 61.72.Ji

Scanning tunneling microscopes (STMs) are widely used in modern investigations of current-conducting materials.[1] The impressive achievements of STM methods in the solution of problems of the physics and chemistry of surfaces are well known. The development of this device has made it possible not only to obtain images of surface structures, but it has also made it possible to change purposefully the composition, structure, and location of individual surface complexes.[2] In recent years many elementary events of fundamental heterogeneous processes — adsorption,[3] desorption,[4] dissociation,[5] and others — have become accessible to direct observation. At the same time the deficiencies of the modern STM methods are also known. First and foremost, STM methods are insensitive to the chemical structure of surface complexes. The problem of identifying topographic images, especially images of point defects in adsorbed particles, still remains as one of the central problems in STM physics. This problem is difficult to solve by theoretical methods. The difficulties are due to both a lack of information about the structure of the working tip of an STM and the lack of sufficiently accurate methods for calculating the electronic wave functions of a surface at large distances ($z \geqslant 5$ Å) in high fields ($f \geqslant 10^7$ V/cm). New ''dynamic'' methods of scanning tunneling spectroscopy (STS), which are sensitive to the vibrational spectra, spins, and electronic transition energies of surface complexes, are now required in order to identify single point defects and adsorbed particles. Such methods have been intensively sought in recent years.[2,6]

One direction of these searches are attempts to repeat directly in experiments with an STM the spectroscopic measurements that are usually employed in studying macroscopic systems. However, this approach is still not successful enough. Attempts to measure vibrational spectra according to a vibrational tunneling spectroscopy scheme,[7] i.e., by detecting threshold features of STM currents at voltages $eV = \hbar\omega \leqslant 0.5$ eV ($\hbar\omega$ is the vibrational quantum), have not been successful.[6] Attempts to detect ESR signals from single paramagnetic centers (PCs) of oxidized silicon were made in Refs. 8–10. In these

works it was reported that weak radio frequency variations of STM tunneling currents were observed at room temperature at distances 3–6 Å from a single point defect. The mechanism leading to the appearance of ''single atom'' ESR with equal population of the Zeeman levels is not known at present. The coordinate dependence of the effects described in Refs. 8–10 is anomalous. The question of the possibility of detecting single PCs by ESR remains open.

The objective of the present letter is to propose a new method for detecting single PCs in experiments with an STM. The method described below is based on a quantum-size effect which is unobservable under macroscopic conditions.

It is well known (see, for example, Refs. 11–13) that in experiments with an STM the quantum-size effect is ordinarily manifested as oscillations of the conductance $\sigma(V)=\partial J/\partial V$ which appear at voltages $eV>\phi\sim 5$ eV (ϕ is the work function of the tip). The periodic growth of the conductance of an STM operating in a field emission mode can be lucidly explained by the formation of electron standing electron waves (ESWs) in a nanoscale resonator formed by the surface and the field barrier bounding on the tip side the region of the classically allowed motion (we assume the polarity of the sample to be positive). Taking account of the interactions of the electrons with the vibrational and internal degrees of freedom of the surface atoms leads to new effects. The characteristic features produced in the STM currents by vibrational transitions were predicted and observed in Refs. 14–17. In these works, specifically, it was shown that for a sufficiently long delay of an electron in a resonator (for $\omega\tau_e\geqslant 1$, τ_e is the delay time) the interaction of the ESWs with local surface vibrations is manifested as a series of electronic–vibrational field emission resonances, which were observed in the current–voltage characteristics of an STM scanning an oxidized titanium surface. The effect observed in measurements of $J(V)$ ''in air''[14,17] were later also observed under high-vacuum conditions.[16,18]

The surfaces of oxides and oxidized metals contain a small number of PCs.[19] Some of these centers play the role of ''active centers'' in catalysis and are being intensively studied on powders by ESR method.[20] This approach gives spectroscopic information averaged over an ensemble of $N\geqslant 10^{12}$ particles. Spectroscopic information about single PCs is accessible only by methods employing an STM. We shall show that in experiments with an STM single PCs can be observed according to a very simple indicator — exchange splitting of field emission resonances. For this, we note that the ESW spectrum is determined not only by the field of the forces repelling an electron from the tip but also by the scattering amplitudes (phases) of electrons scattered by surface atoms. For paramagnetic centers, because of the contributions of the exchange mechanism, the scattering amplitude depends only on the total spin $j=s\pm 1/2$ (s is the spin of a paramagnetic particle).[21] For oxygen, for example, for electron energies $\epsilon\sim(eV-\phi)\sim 2-5$ eV a severalfold difference in the amplitudes $A_j(\epsilon)$ is possible.[22]

Hence it follows that when a PC is present beneath the STM tip exchange splitting $\delta\epsilon_{j,n}$ (n is the number of the electronic level in the resonator) should be observed in the ESW spectrum. The magnitude of the splitting can be easily estimated using the Fermi pseudopotential approximation:[21]

$$\delta\epsilon_{j,n}\sim 2\pi\delta A_j(0)\left|\Phi_n(\mathbf{R})\right|^2\geqslant 2\pi\delta A_j(0)/\Omega. \tag{1}$$

Here $\delta A_j(0)=|A_{s+1/2}-A_{s-1/2}(0)|$, Φ_n is the wave function of an electron in the state of the nth standing wave, $\mathbf{R}$ is the coordinate of the PC, and Ω is the volume of the resonator:

$$\Omega \sim \frac{eV-\phi}{eV} dS. \tag{2}$$

Here d is the distance between the tip and the surface and S is a characteristic scale of the scanned surface. Let $S \sim a_x a_y$ ($a_{x,y}$ are the periods of the surface lattice). Then for $\delta A_j(0) \sim (0.5\text{–}1)$ Å, $V=8$ V, $\phi=5$ eV, $a_x \approx 3$ Å, $a_y \approx 6.5$ Å, which corresponds to titanium oxide,[23] we have

$$\delta\epsilon_{j,n} \geqslant (0.1-0.2) \text{ eV}, \tag{3}$$

which is greater than (or comparable to) the half-widths of the field emission resonances observed in Refs. 14–17 ($\Gamma \leqslant 0.05\text{–}0.1$ eV). The long delay of an electron near the oxide surface ($\tau_e \sim \hbar/\Gamma \sim 10^{-4}$ s), which was not observed in experiments with beams (current densities $\sim 10^{-1}$ electrons/Å^2), indicates that the volume charge that accumulates in the oxide layer beneath the tip and relaxes over a time $\tau_Q > 10^{-11}$ s plays a substantial role in experiments with an STM (current density $\sim 10^{11}$ electrons/Å^2).

The trapping of an electron by the resonator, i.e., localization of the electron at distances $l_z \sim d(eV-\phi)/eV \sim 2$ Å from the sample, changes the force field, $U(R)$, in which the surface atoms move. Let us estimate the electronic–vibrational coupling parameters

$$\alpha = \omega(\delta R)^2 \quad \text{and} \quad \beta = \delta\omega/\omega, \tag{4}$$

which determine the inelastic-transition probabilities and the accuracy of measurements of the vibrational spectra performed with an STM (δR is the displacement of the equilibrium position of a surface atom, and $\delta\omega$ is the change in the vibrational frequency in the presence of an electron). Let us take account of the Stark effect mechanism:

$$\delta U(R) = U_e(R) - U_0(R) \sim f_n D(R). \tag{5}$$

Here $U_e(R)$ is the potential determining the vibrational spectrum in the presence of an electron, $U_0(R)$ is the potential for the state of an empty resonator ($U_0(R) = M\omega^2 R^2/2$), and $D(R)$ is the dipole moment of a surface atom. Then for $V=8$ V, $d \approx 10$ Å, $D \sim 1$ a.u., $D'(D'') \sim 1$ a.u., for $\hbar\omega \sim 0.2$ eV we have

$$\alpha \sim 1, \quad \beta \sim 0.1. \tag{6}$$

Hence it follows that in the adiabatic approximation (when the vibrational frequency is less than the frequency of the electronic transitions) the spectra of the resonance values of the energies of electrons trapped by the resonator and interacting with the vibrational and spin degrees of freedom of a surface atom, have the form, to within $\sim 10\%$,

$$\epsilon_{j,m,v}(V,d) = -eV + \epsilon_n^0(V,d) + \hbar\omega(v+1/2) + \delta\epsilon_{j,n}(V,d), \tag{7}$$

where $j = s \pm 1/2$, $n = 1, 2, \ldots$, $v = 0,1,2,\ldots$, $\epsilon_n^0(V,d) \approx c(nV/d)^{2/3}$ is the energy of the nth electronic level in the resonator[14] and v is the vibrational quantum number ($\hbar\omega \ll \partial\epsilon_n^0/\partial n$). According to Eq. (7), the spectrum consists of electronic–vibrational–spin

series with electronic transition energies, $\partial\epsilon_n^0/\partial n \sim 1-2$ eV, with n-dependent exchange splitting, $\delta\epsilon_{j,n} \sim 0.1-0.2$ eV, and with j- and n-independent vibrational transition energies $\hbar\omega \sim 0.1-0.2$ eV.

In experiments with an STM operating in the field emission mode (i.e., with $eV > \phi \sim 5$ eV), the spectrum (7) of resonance states can be measured by scanning the current J as a function of V and (or) d. It is easy to show that in the case of clean ''blunt''[11–13] tips (with structureless electron densities, $\rho_t(\epsilon) \approx$ const) the field emission resonances (7) are manifested as maxima of the conductance, $\partial J/\partial V$, which appear at values of V and d which are roots of the equation

$$\epsilon_F = \epsilon_{j,n,v}(V,d). \tag{8}$$

Here ε_F is the Fermi level of electrons in the tip.

In experiments with pure ''single-atom'' tips or with tips containing adsorbed particles the field emission resonances (7) can be manifested as maxima of the total currents $J(V,d)$. Indeed, the electron densities of such tips have narrow peaks

$$\rho_t(\epsilon) = \rho_t(\epsilon_F) + \rho_0 \frac{\gamma^2}{(\epsilon-\epsilon_0)^2+\gamma^2}, \quad \epsilon_0 \leqslant \epsilon_F, \tag{9}$$

with half-widths $\gamma \leqslant 0.1$ eV,[21–26] which result in a growth of the currents for values of V and d which are roots of the equation

$$\epsilon_0 = \epsilon_{j,n,v}(V,d). \tag{10}$$

In the resonance approximation the functions $J(V,d)$ for such tips can be described by the expression

$$J(V,d) = J_0 \sum_{j,n,v} \frac{\Gamma^l_{j,n,v}\gamma^{\,r}_{j,n,}(V,d)}{(\epsilon_{j,n,v}(V,d)-\epsilon_0)^2+(\Gamma+\gamma)^2} \tag{11}$$

$(\epsilon_F - \epsilon_0) > (\Gamma+\gamma)$. Here

$$\Gamma^l_{j,n,v}(V,d) = \gamma^{\,l}_{j,n}(V,d) P_{0v}, \tag{12}$$

$$\gamma^{\,l}_{j,n}(V,d) = \gamma_0 \exp\left(-\frac{4}{3}\frac{\phi^{3/2}}{V}d\right) \tag{13}$$

are the probabilities of electron transitions from the tip into the resonator, P_{0v} are the Franck–Condon factors (the vibrational degrees of freedom of the PC are assumed not to be excited), $\gamma^{\,r}_{j,n}(V,d)$ are the probabilities of electron transitions from the resonator into the sample, and $\Gamma = \hbar/\tau_e$. (The derivation of expression (11) employed Eq. (20) of Ref. 27 and took account of the fact that for sufficiently high voltages, when $eV \gg \alpha\omega$, threshold effects can be neglected.)

According to expressions (11) and (7) the spectrum of resonance features of the IVC of an STM operating in the field emission mode can be described by the expression

$$eV_{j,n,v} = -\epsilon_0 + \epsilon_n^0(V_0,d) + \delta\epsilon_{j,n} + \hbar\omega(v+1/2), \tag{14}$$

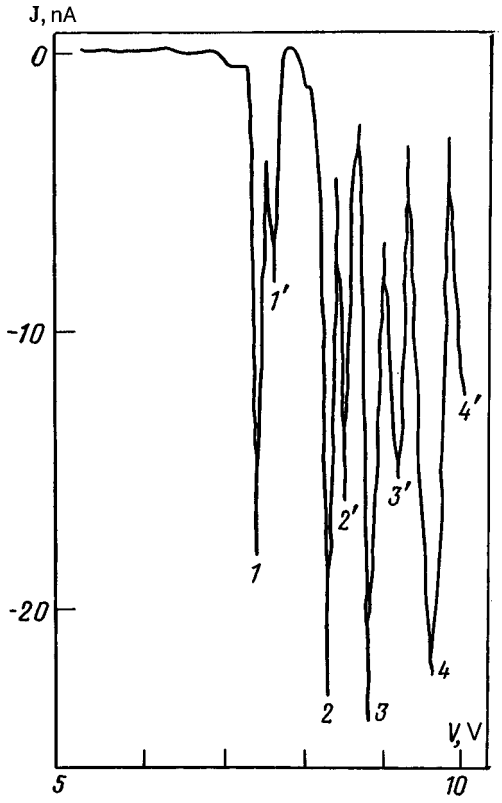

FIG. 1. Electronic–spin series of field emission STM resonances of oxidized titanium.

$\hbar\omega \ll eV_0$, $eV_0 = \epsilon_0$, $j = s \pm 1/2$, $n = 1,2,\ldots$, $v = 1,2,\ldots$, i.e., it has the form of an electronic–vibrational–spin series with envelopes determined by the Franck–Condon factors $P_{0v} \sim (\alpha^v/v!)\exp(-\alpha)$.

We shall employ the results obtained above to identify the surface complexes of oxidized titanium, whose field emission spectra have been measured in Ref. 17 with the aid of an STM. Fragments of two spectra (see Figs. 1 and 3 of Ref. 17) containing the effect of interest to us are presented on an enlarged scale in Figs. 1 and 2. In both cases the spectra contain split peaks; the magnitude of the splittings corresponds to the estimate (3). It is easy to see the general characteristics of the spectra being compared. The values of the threshold voltages, V_1, and the corresponding currents, $J(V_1)$, for these spectra are virtually identical (7.4 V and 7.3 V, 18 nA and 16 nA, respectively). The half-widths of the peaks are also close. These characteristics refer to electronic states and are determined by the resonator. Fundamental differences between two spectra measured at different points on the surface, i.e., referring to different surface complexes, can also be seen. If exchange splitting is neglected, then one can see that the first spectrum is represented by a sequence of nonequidistant peaks with nondecreasing heights:

$$J(V_n) \approx 20 \text{ nA}, \quad V_{n+1} - V_n \neq \text{const}, \quad n = 1,2,3,4. \tag{15}$$

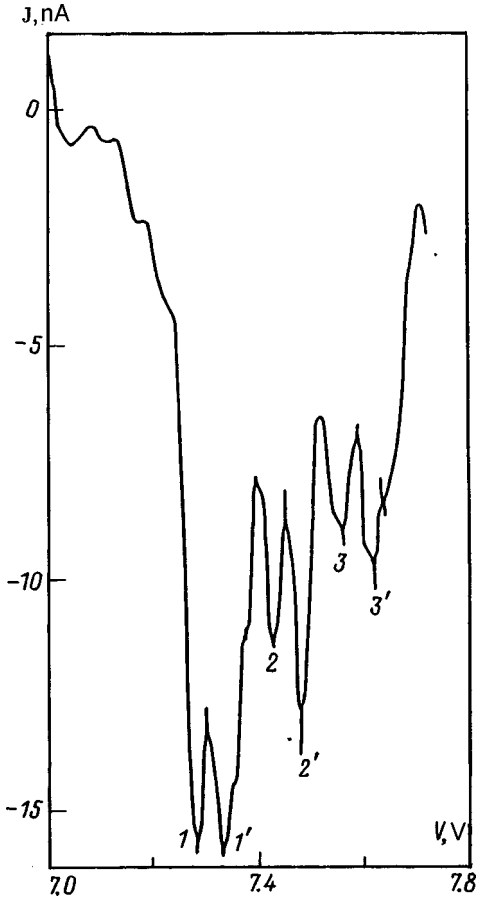

FIG. 2. Vibrational–spin series of field emission STM resonances of oxidized titanium.

The distances between the peaks correspond to the frequencies of electron transitions in the resonator ($e(V_{n+1}-V_n)\sim 1$ eV). In accordance with the estimate (1) the exchange splitting of different peaks is different ($\delta\epsilon_{I,4}\sim 0.4$ eV, $\delta\epsilon_{I,3}\sim 0.3$ eV, $\delta\epsilon_{I,2}\approx\delta\epsilon_{I,1}\sim 0.1$ eV). There are no vibrational lines in this spectrum, the parameter α is small, i.e., the dipole moment D is small. The smallness of the dipole moment is characteristic for point defects which are not associated with adsorption. Paramagnetic centers of titanium oxide which are not associated with adsorption are well known.[20] These are Ti^{3+} ions (O vacancies).

Let us now examine the spectrum presented in Fig. 2. Two series, shifted by

$$\delta V_I = V_{1'} - V_1 = V_{2'} - V_2 = V_{3'} - V_3 \approx 0.07 \text{ V}, \tag{16}$$

of equidistant and monotonically decreasing maxima, the distances between which

$$\delta V_v = V_{v+2} - V_{v+1} = V_{v'+2} - V_{v'+1} = 0.15 \text{ V} \quad (v, v' = 0,1,2\ldots) \tag{17}$$

correspond to a vibrational quantum of an adsorbed paramagnetic ion radical O_2^-, measured by the method of IR spectroscopy ($\hbar\omega = 1180\ \text{cm}^{-1} = 0.15\ \text{eV}$), (Ref. 19) can be distinguished in it.

Exchange splitting of the field emission resonances can be used as the basis of scanning tunneling spin spectroscopy, making it possible to observe single PCs of oxides and oxidized metals.

This work was supported by the Russian Fund for Fundamental Research (Project 96-03-34129).

[1] H.-J. Günterrodt and R. Wiesendanger, *Scanning Tunnelling Microscopy*, Springer Series in Surface Science, Vol. 20, Springer-Verlag, Berlin, 1992.
[2] Ph. Avouris (ed.), *Atomic and Nanometer Scale Modification of Materials: Fundamentals and Applications*, Klumer, Dordrecht, Netherland, 1993.
[3] I. Zambelli, J. V. Barth, J. Wintterlin, and G. Ertl, Nature **390**(4), 495 (1997).
[4] T.-C. Shen, C. Wang, G. C. Abeln *et al.*, Science **268**, 1590 (1995).
[5] B. C. Stipe, M. A. Rezaei, W. Ho *et al.*, Phys. Rev. Lett. **78**(23), 4410 (1997).
[6] Ph. Avouris, J. Phys. Chem. **94**, 2246 (1990).
[7] J. Lambe and R. C. Jaklevi, *Tunnelling Phenomena in Solids*, Plenum Press, New York, 1969, p. 243.
[8] Y. Manassen, E. Ter-Ovanesyan, and D. Shadal, Phys. Rev. Lett. **62**, 2531 (1989).
[9] D. Shadal and Y. Manassen, Phys. Rev. B **44**, 11528 (1991).
[10] Y. Manassen, E. Ter-Ovanesyan, and D. Shadal, in *Bioradicals Detected by ESR Spectroscopy*, edited by H. Ohya-Nishiguchi and L. Packer, Birkhäuser Verlag, Basel, Switzerland, 1995, p. 49.
[11] G. Binnig, K. H. Frank, and H. Fuchs, Phys. Rev. Lett. **55**, 991 (1985).
[12] R. S. Becker, J. A. Golovchenko, and B. S. Swartzentruber, Phys. Rev. Lett. **55**, 987 (1985).
[13] Y. Kuk in Ref. 1, p. 17.
[14] F. I. Dalidchik, M. V. Grishin, S. A. Kovalevskiĭ, and N. N. Kolchenko, JETP Lett. **65**, 325 (1997).
[15] F. I. Dalidchick, M. V. Grishin, N. N. Kolchencko, and S. A. Kovalevskii, Surf. Sci. **387**, 50 (1997).
[16] F. I. Dalidchik, M. V. Grishin, S. A. Kovalevski *et al.*, JETP Lett. **66**, 37 (1997).
[17] F. I. Dalidchick, M. V. Grishin, S. A. Kovalevskii *et al.*, Spectrosc. Lett. **30**(7), 1429 (1997).
[18] S. A. Kovalevskii, F. I. Dalidchick, M. V. Grishin *et al.*, Appl. Phys. A **66**, 51 (1998).
[19] O. V. Krylov and V. F. Kiselev, *Adsorption and Catalysis on Transition Metals and Their Oxides* [in Russian], Khimiya, Moscow, 1981.
[20] A. B. Roĭtsin and V. M. Maevskiĭ, Usp. Fiz. Nauk **159**, 297 (1989) [Sov. Phys. Usp. **32**, 891 (1989)].
[21] B. M. Smirnov, *Atomic Collisions and Elementary Processes in Plasma* [in Russian], Atomizdat, Moscow, 1968.
[22] F. J. da Paixao and M. A. P. Lima, Phys. Rev. Lett. **68**, 1698 (1992).
[23] M. B. Hugenschmidt, L. Gamble, and Ch. T. Campbell, Surf. Sci. **302**, 329 (1994).
[24] Jn. Whan Lyo and Ph. Avouris, Science **245**, 1369 (1989).
[25] A. Yazdani, D. M. Eigler, and N. D. Lang, Science **272**, 1921 (1996).
[26] N. D. Lang, Phys. Rev. B **55**(15), 9364 (1997).
[27] F. I. Dalidchik, Zh. Éksp. Teor. Fiz. **87**, 1384 (1984) [Sov. Phys. JETP **60**, 795 (1984)].

Translated by M. E. Alferieff

Quasielastic scattering of light by a photoexcited electron–hole plasma induced in a GaAs layer in the presence of InAs quantum dots

B. Kh. Baĭramov,[a] V. A. Voĭtenko, B. P. Zakharchenya, and V. V. Toporov
A. F. Ioffe Physicotechnical Institute, Russian Academy of Sciences, 194021 St. Petersburg, Russia

M. Henini and A. J. Kent
Department of Physics, University of Nottingham, Nottingham, NG7 2RD, UK

(Submitted 30 April 1998)
Pis'ma Zh. Éksp. Teor. Fiz. **67**, No. 11, 922–927 (10 June 1998)

The development of a method for registering quasielastic electronic light scattering spectra in the near-IR region, which makes it possible to detect light scattering by a photoexcited electron–hole plasma induced in a GaAs layer in the presence of a self-organized ensemble of InAs quantum dots, is reported. A substantial resonance intensification of such scattering, two orders of magnitude greater than the values established for the bulk material, is observed, and the main mechanism of such scattering is determined. © *1998 American Institute of Physics.* [S0021-3640(98)01611-9]

PACS numbers: 71.35.Ee, 73.61.Ey, 78.35.+c

Semiconductor quantum dots (QDs) in a wide-gap matrix are attracting increasing interest from investigators. In such structures size quantization in all three directions results in a substantial modification of the electronic density of states, with substantially greater charge-carrier localization, which, it seems, can substantially improve the main characteristics of a number of nanoelectronics devices. We report a further elaboration of the highly sensitive method presented in Ref. 1 for detecting inelastic electronic light scattering spectra in the near-IR region of the spectrum and for realizing the possibility of investigating light-scattering spectra in structures with QDs. As a result, we have been able to observe quasielastic electronic scattering of light by free charge carriers in an InAs QD system in a GaAs matrix. It was shown that such scattering is due to electron–hole plasma induced in the GaAs bulk in the presence of InAs QDs by the incident light. The ensemble of self-organized QDs was produced on the basis of spontaneous decomposition of a strongly strained InAs layer, grown on the GaAs surface, into coherent islands. The observed substantial intensification of the quasielastic electronic scattering of light is due to the resonance character of such scattering. It made it possible to detect spectra of quasielastic electron scattering of light in structures with QDs at an intensity level approximately two orders of magnitude greater than the values established for bulk material.

We investigated nominally undoped structures obtained by molecular-beam epitaxy

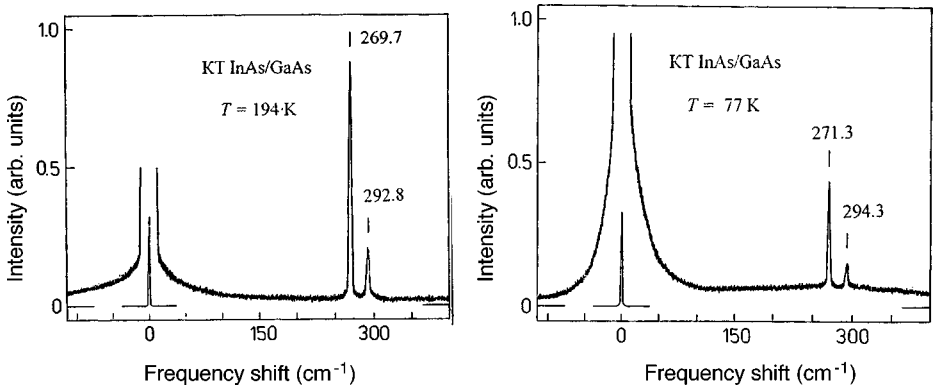

FIG. 1. Fragments of spectra obtained from a layer for a nominally undoped structure consisting of InAs QDs in a GaAs matrix grown on a semi-insulating *si*-GaAs substrate. The spectra were obtained at $T=194$ K (a) and $T=77$ K (b).

on semi-insulating *si*–GaAs substrates (with *n*-type conductivity) with a faceted (311)B surface. The islands were formed by the Stranskiĭ–Krastanov mechanism. The active region of the sample consisted of 10 rows of QDs, formed by successive deposition of InAs layers each with an effective thickness of 1.8 monolayers, separated by GaAs layers 5.1 nm thick. The transition from two-dimensional uniform to three-dimensional nonuniform growth of the InAs layers was monitored according to the change in the characteristic RHEED pattern from the surface of the growing layers. The effective dimensions of the InAs QDs were $\sim 12\times 6$ nm.

The spectra were excited by a highly stable solid-state cw neodymium-doped YAG laser with wavelength 1064.4 nm. Spectra obtained in the geometry of backscattering from the (311)B surface with parallel (yy) polarizations of the incident and scattered light were investigated. The y axis corresponds to the crystallographic direction $[-233]$. The spectral composition of the scattered light was analyzed with a high-transmission ($f=1-3$) double diffraction monochromator and detected with a cooled photomultiplier using two-channel photon counting. The spectral resolution was 2 cm^{-1}. The measurements were performed at exciting radiation densities in the range $P=0.2-1.0$ kW/cm^2, which do not give rise to local heating of the samples. The latter was monitored by registering the grating lines corresponding to scattering of light by transverse TO(Γ) and longitudinal LO(Γ) optical phonons from the *si*-GaAs substrate.

Figure 1 shows fragments of the inelastic light-scattering spectra obtained directly from a layer for a structure with InAs QDs in a GaAs matrix at $T=194$ K (a) and 77 K (b). These spectra, which lie in the not easily accessible low-frequency range adjacent to the exciting laser line, convincingly demonstrate observation of the Lorentzian wing of quasielastic electronic scattering of light. Figure 2 displays a similar spectrum obtained for a *si*-GaAs substrate at $T=300$ K under identical experimental conditions. The quite intense lines in these spectra at 271.3 and 294.3 cm^{-1}, 269.7 and 292.8 cm^{-1} are due to lattice scattering of light from the *si*-GaAs substrate by TO(Γ) and LO(Γ) phonons at $T=77$, 194, and 300 K, respectively. In the magnified ($20\times$) part of the spectrum of the *si*-GaAs substrate, the most intense and sharpest line at 159.7 cm^{-1} against the back-

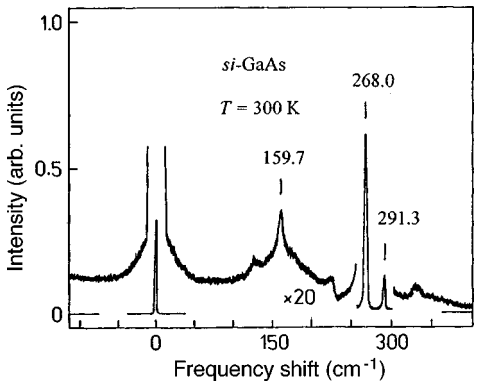

FIG. 2. Fragment of a spectrum obtained from a semi-insulating *si*-GaAs substrate on which nominally undoped structures consisting of InAs QDs in a GaAs matrix were grown. The spectrum was obtained at $T = 300$ K.

ground of comparatively weak lines corresponding to overtone scattering corresponds to overtone scattering with the participation of two acoustic 2TA(X, K) GaAs phonons. It is noteworthy that the intensity of the observed quasielastic electronic scattering of light in this spectrum is comparable to that of 2TA(X, K) phonons. This fact as well as the character and shape of the scattering line show that the *si*-GaAs substrate is of the *n* type with free charge-carrier density $n = 1.0 \times 10^{15}$ cm^{-3} (Ref. 2). The absolute intensity of such quasielastic electronic scattering of light drops sharply with decreasing temperature, and in agreement with the results of Ref. 3 it completely vanishes in the spectrum obtained at $T = 77$ K.

Investigation of the electronic light scattering process in the spectra of structures with InAs QDs in the GaAs matrix shows a completely different picture. Such scattering likewise differs strongly from the process of inelastic scattering of light by free holes in *p*-GaAs.[4] It is clearly seen from the spectra in Fig. 1 that at $T = 77$ K the contribution of lattice scattering is not dominant. Moreover, these spectra demonstrate an anomalous increase of the absolute intensity of quasielastic electronic light scattering with decreasing temperature. The observation of an intensification of the absolute intensity of quasielastic electronic light scattering in structures with InAs QDs in a GaAs matrix is also new. The intensification is approximately two orders of magnitude greater than the values established for bulk material. Moreover, an anti-Stokes component of such scattering appears at low temperatures.

It seems to us that such an intensification can arise as a result of the resonance character of the scattering, due to the selectively photoexcited electron–hole plasma induced in the GaAs layer in the presence of a self-organized ensemble of InAs QDs. Since the characteristic geometric sizes of the QDs are small compared to the wavelength of light ($d \ll \lambda$), in principle the electrostatic approximation can be used to find the characteristic modes of the electromagnetic field in them. The electric field inside QDs in an effective dielectric medium will be determined by the difference of the permittivities of InAs and GaAs at the frequency of the exciting light. The luminescence line with a maximum at 1031.4 nm indicates the presence of quantization of electrons in QDs. Since a periodic structure consisting of QD rows, whose characteristic geometric dimensions

are comparable to the periods of the structure in both directions — along and across the direction of growth, is formed, the electronic states of the discrete spectrum in such structures are collectivized. The degree of collectivization, i.e., the number of dots participating in it, depends on the dot-size variance and, specifically, it decreases sharply in the presence of coalescence, i.e., with the onset of the stage of large-dot formation as a result of a simultaneous decrease of the size of the other dots.[5] Collectivization of the quantum states is expressed on the energy scale as a fragmentation of the electronic bands, appearance of allowed minibands and minigaps in the band gap between $E_{g1}=0.424$ eV (InAs) and $E_{g2}=1.519$ eV (GaAs). For incident $\hbar\omega=1.165$ eV photons, a substantial portion of the volume of the system under study with effective band gap E_g can satisfy the resonance condition $\hbar\omega=E_g$.

The light scattering cross section Σ is determined by the ratio of the number of scattered photons emitted per unit volume to the photon flux density incident on the crystal surface. Let the incident radiation be characterized by the frequency ω_I and wave vector k_I and the secondary radiation by the quantities ω_S and k_S. The scattering cross section per unit solid angle and unit frequency can be written in the form

$$\frac{d^2\Sigma}{d\omega d\Omega}=\frac{\omega_I\omega_S^3}{2\pi c^4}\frac{1}{|A_0^I|^2|A_0^S|^2}\int d^3r\,d^3r'A_i^{*I}(r)A_k^S(r)$$
$$\times(\delta\chi_{ik}(r)\delta\chi_{mn}(r'))_\omega A_m^I(r')A_n^{*S}(r'). \quad (1)$$

Here $\omega=\omega_I-\omega_S$ is the shift of the frequency of the scattered light, $A^I(r)$ and $A^S(r)$ are the vector potentials of the field of the incident and scattered waves, A_0^I and A_0^S are the amplitudes of the electromagnetic waves outside the crystal, and $\delta\chi_{ik}(r)$ is the fluctuation part of the polarizability tensor of the crystal.

In accordance with the indicated resonance character of the scattering, photoionization of electron–hole pairs, which accumulate near the InAs QDs, occurs as a result of its excitation. From the classical standpoint, photoinduced excitonic liquid is injected from a region near dots, producing in the GaAs volume, which is transparent to the incident light, a nonequilibrium two-component plasma. For such a system, the sum of electron and hole contributions must be used for the permittivity fluctuations $\delta\chi$:[3]

$$\delta\chi_{ik}=-\delta_{ik}R_{eh}\frac{e^2}{m\omega_I^2}(\mu_e\delta n_e+\mu_h\delta n_h). \quad (2)$$

Here δn_e and δn_h are fluctuations of the electron and hole densities; μ_e and $\mu_h=\gamma_I$ are the reciprocals of the reduced masses of the electrons and holes, the latter being equal to the corresponding parameter γ_I in the Luttinger Hamiltonian; δ_{ik} is the Kronecker delta; and, R_{eh} is a resonance factor[6] determined by the band gap E_g and is given by $R_{eh}=E_g^2/[E_g^2-(\hbar\omega_i)^2]$. Our estimates show that the main contribution to the observed intensification of quasielastic light scattering is due to this factor, while the contribution associated with the decrease in A^I and A^S is only a factor of 2–3. Therefore the maximum resulting gain for the cross section is $R=3R_{eh}^2$.

To describe the Lorentzian wing of quasielastic electronic scattering of light we shall take account of the fact that the nonequilibrium carriers generated by the light have a zero macroscopic rate of spreading and a low mobility, limited by scattering by

phonons. For this reason, to describe the kinetics of the fluctuations $\delta\chi$ from Eq. (2) we shall employ, instead of the Navier–Stokes equation conventionally used in the hydrodynamic approximation, the continuity and diffusion equations

$$\frac{\partial \delta n_a}{\partial t}+\frac{1}{e}\nabla\cdot\delta j_a=0, \quad \delta j_a=(-1)^a\frac{\sigma_a E}{e}-D_a\nabla\delta n_a+g_a. \tag{3}$$

Here the index a enumerates the particles: $a=1$ for electrons and $a=2$ for holes; δj_a are the fluctuation currents; D_a and σ_a are the corresponding diffusion coefficients and conductivities; g_a are the random fluxes due to thermal motion and are the sources of the fluctuations; and, E is the intensity of the electric field, limiting the rate of motion during the diffusion of a charged particle in accordance with Poisson's equation. For the case of a GaAs matrix with periodically arranged QDs, the Fourier transforms in the coordinates r and time t can be used to solve the system of equations (3). Solving the algebraic system obtained we have

$$\delta n_{e,h}=-iq\frac{g_{e(h)}a_{h(e)}+g_{h(e)}b_{e(h)}}{a_e a_h-b_e b_h}, \tag{4}$$

where $a_a=-i\omega+q^2D_a+4\pi\sigma_a/\epsilon$, $b_a=4\pi\sigma_a/\epsilon$, and q is the Fourier-transform wave vector. According to Eq. (2), the spectral composition of the scattered light reflects the correlation of the electron and hole fluctuations. Such a correlation is always present. For this reason, on substituting expression (4) into Eqs. (2) and (1) it is necessary to examine all the correlation functions that arise, including those which are nondiagonal in the symbols e and h. Each correlation function can be expressed by means of Eq. (4) in terms of quadratic functionals of g_e and g_h, whose averages are determined by the universal correlation properties of the random currents. The latter are determined as follows:

$$(g_{ai}g_{\beta k})_{q\omega}=\delta_{\alpha\beta}\left(\frac{\partial n_\alpha}{\partial\zeta_\alpha}\right)_T F(\omega)\delta_{ik}\mathrm{Re}D_\alpha(\omega), \tag{5}$$

where $F(\omega)=\hbar\omega/[1-\exp(-\hbar\omega/T)]$ and n_a and ζ_a are, respectively, the stationary nonequilibrium density and Fermi quasilevels of particles of type a. Forming by means of Eq. (4) all possible spectral correlation functions of electrons and holes, from Eqs. (1)–(3) we can find the following expressions for the quasielastic scattering cross section:

$$\frac{\partial^2\Sigma}{\partial\omega\partial\Omega}=8\pi VR(\mathbf{e}_i\mathbf{e}_s)^2\frac{q^2F(\omega)}{\epsilon^2}\left(\frac{e^2}{mc^2}\right)^2(\mu_e+\mu_h)^2\tau_\mu^2\frac{D_e\left(\frac{\partial n_e}{\partial\zeta_e}\right)_T\sigma_h^2+D_h\left(\frac{\partial n_h}{\partial\zeta_h}\right)_T\sigma_e^2}{\omega^2+(q^2D_a-\omega^2\tau_M)^2}. \tag{6}$$

Here $\tau_M=\epsilon/[4\pi\sigma_e+\sigma_h)]$ is the Maxwell relaxation time and

$$D_a=\frac{\sigma_eD_h+\sigma_hD_e}{\sigma_e+\sigma_h} \tag{7}$$

is the ambipolar diffusion coefficient. According to Eq. (6), the relaxation observed in the quasielastic light-scattering spectra with a Lorentzian width $\Gamma=q^2D_a$ is due to the simultaneous diffusion of electrons and holes. It should be noted that the electron mobility $b_e=e\tau_e/m_e^*$ is greater than the heavy-hole mobility: $b_h/b_e=m_e^*\tau_h/m_h^*\tau_e\ll 1$. For this reason, Γ in Fig. 1b is determined by the smallest of the possible diffusion coefficients,

which belongs to the holes. A new fact is that the experimental values for Γ are found to be several times smaller than in bulk *n*-InP and *n*-GaAs crystals with comparable impurity density.[2–5,7,8] It is noteworthy that at lower temperatures a drift character of the charge-carrier motion develops in the space between quantum dots, which could increase their average population density compared with the case of ambipolar diffusion.

In conclusion, we note that the realization in practice of the possibility of measuring the near-IR quasielastic electronic resonance light scattering spectra in structures with QDs opens up new possibilities for studying the interaction of electromagnetic waves and diffusion of charge carriers in semiconductor nanostructures.

[a)]E-mail: bairamov@bahish.ioffe.rssi.ru

[1] B. Kh. Baĭramov, B. P. Zakharchenya, and V. V. Toporov, JETP Lett. **67**, 352 (1998).
[2] B. Kh. Baĭramov, V. A. Voĭtenko, and I. P. Ipatova, Usp. Fiz. Nauk **163,** 67 (1993) [Phys. Usp. **36**, 392 (1993)].
[3] B. H. Bairamov, V. A. Voitenko and I. P. Ipatova, Phys. Rep. **229**, 223 (1993).
[4] B. Kh. Baĭramov, V. A. Voĭtenko, I. P. Ipatova *et al.*, Fiz. Tekh. Poluprovodn. **28**, 913 (1994) [Semiconductors **28**, 531 (1994)].
[5] W. Ostwald, Z. Phys. Chem. **BdS**, 495 (1900).
[6] B. H. Bairamov, V. A. Voitenko, I. P. Ipativa *et al.*, Phys. Rev. B **50**, 14923 (1994).
[7] M. V. Klein, in *Light Scattering in Solids*, Vol. I, edited by M. Cardona, Springer-Verlag, Berlin, 1975 [Russian translation, Vol. I, Mir, Moscow, 1979, p. 174].
[8] B. H. Bairamov, G. Irmer, J. Monecke *et al.*, Phys. Status Solidi B **204**, 456 (1997).

Translated by M. E. Alferieff

Uniform rotation of smectic layers of a ferroelectric liquid crystal in an asymmetric electric field

S. V. Yablonskiĭ
Institute of Crystallography, Russian Academy of Sciences, 117333 Moscow, Russia

K. Nakayama, M. Ozaki, and K. Yoshino
Department of Electronic Engineering, Faculty of Engineering, Osaka University, 565 Osaka, Japan

(Submitted 30 April 1998)
Pis'ma Zh. Éksp. Teor. Fiz. **67**, No. 11, 928–933 (10 June 1998)

An asymmetric ac electric field with amplitude $E=10$ V/μm gives rise to a matched rotation of the normal to the smectic layers, while a sinusoidal field $E=1$ V/μm is used to study the rotation in the method of modulation total internal reflection ellipsometry, which makes it possible to probe the region of a ferroelectric liquid crystal (FLC) next to the electrode ($h\approx 0.7$ μm). It is shown that the angle of rotation of the normal to the smectic layers near the surface of the electrode varies reversibly as a function of the polarity and number of electric pulses applied, just as in the interior region. The characteristic dynamic properties of thin layers of nematic liquid crystals, such as an anomalously long relaxation time and a high-frequency relaxation process, are observed in thin FLC layers. © *1998 American Institute of Physics.* [S0021-3640(98)01711-3]

PACS numbers: 77.84.Nh, 07.60.Fs, 78.20.Jq

1. INTRODUCTION

Useful electrooptic effects in chiral ferroelectric liquid crystals (FLCs) are based on a change in the orientation of the director of the FLC with respect to rigid,[a)] stationary smectic planes. The static nature of the layered smectic structure was never questioned right up to the appearance of Ref. 2, where an irreversible rotation, bounded by the polar angle θ_0, of the normal to the smectic layers under the action of an electric field is observed in the C* phase. These investigations were further elaborated in Refs. 3–7. Their main result was the discovery of uniform and reversible rotation of smectic layers that is induced by an electric field with a special shape and a large amplitude. The rotation was monitored by observing in a polarizing microscope textured defects and the index ellipsoid averaged over the thickness of the sample. The rotation of the smectic layers was observed in C* and A phases of both ferroelectric and antiferroelectric LCs.[3,4] It has been shown that it is of a threshold character,[8] and it is critically dependent on the chemical composition of the orienting coatings and their mechanical treatment.

At present the physical mechanism of this phenomenon is not completely understood, but its dependence on the properties of the surface has stimulated the present work,

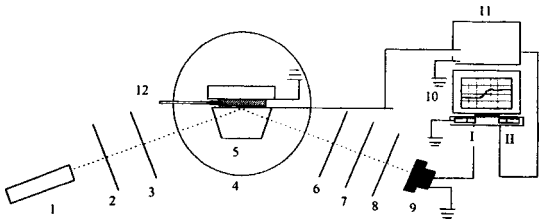

FIG. 1. Experimental apparatus: *1* — He–Ne laser; *2,6* — $\lambda/4$ plates, $\lambda = 632.8$ nm; *3* — polarizer; *4* — turntable; *5* — prism module with FLC; *7* — analyzer; *8* — filter; *9* — silicon photodiodes; *10* — personal computer; *11* — generator of special pulses; *12* — thermocouple, I and II — inputs of Sound Blaster 16 sound card.

where the method of modulation total internal reflection ellipsometry, which will be shown below to be sensitive to the orientation of the normal to the smectic layers, making it possible to probe thin layers of the LC near the surface and to investigate their dynamical properties,[9,10] is used to investigate the FLC next to the LC–electrode interface.

2. EXPERIMENTAL RESULTS AND DISCUSSION

In the case of a normal orientation of the smectic layers with respect to the bounding surfaces, under total internal reflection conditions the penetration depth L of the damped surface light wave equals[11] $L = \lambda(N^2 \sin \varphi^2 - n_{\text{eff}}^2)^{-1/2}$, where $\lambda = 0.6328$ μm, $N = 1.803$ is the index of refraction of a prism consisting of TF-10 heavy flint, $\varphi = 80°$ is the angle of incidence of the light wave, measured from the normal to the prism–electrode interface, $n_{\text{eff}} = (n_{\parallel}^2 \sin \theta_0^2 + n_{\perp}^2 \cos \theta_0^2)^{1/2}$, $\theta_0 = 25°$ is the tilt angle of the director with respect to the normal to the smectic layers, $n_{\parallel} = 1.66$, $n_{\perp} = 1.49$, and $n_{\text{eff}} = 1.52$. (The refractive indices $n_{\parallel}$ and $n_{\perp}$ used to estimate the penetration depth of the damped light wave were measured at the He–Ne laser wavelength $\lambda = 632.8$ nm in the smectic A phase at temperature
$T = 78$ °C). Therefore the maximum penetration depth of the light wave was equal to $h \approx 0.7$ μm, which was much smaller than the thickness of the sample $d = 10$ μm. The refractive-index modulation due to the motion of the LC director on a cone symmetric with respect to the normal to the smectic layers results in modulation of the phase of the reflected light waves polarized in and perpendicular to the plane of incidence. (Reflection occurs under total internal reflection conditions; the polarization vector of the light wave makes an angle of 45° with the plane of incidence.) After conversion by a Sernarmont compensator, the reflected light is detected with a photodetector connected to a computer (Fig. 1). A special program package called PhysLab, based on multimedia resources for a personal computer and implementing a number of virtual devices necessary for modulation ellipsometry, such as a synchronous detector, spectrum analyzer, and plotter, was used for the signal measurements.

In the general case the periodic ellipsometric signal has a complicated shape and contains both even and odd harmonics of the frequency ω of the exciting electric field, as shown in Fig. 2. The absence of odd harmonics in the optical response corresponds to, from symmetry considerations, the particular case when the normal to the smectic layers lies in the plane of incidence of the light wave.

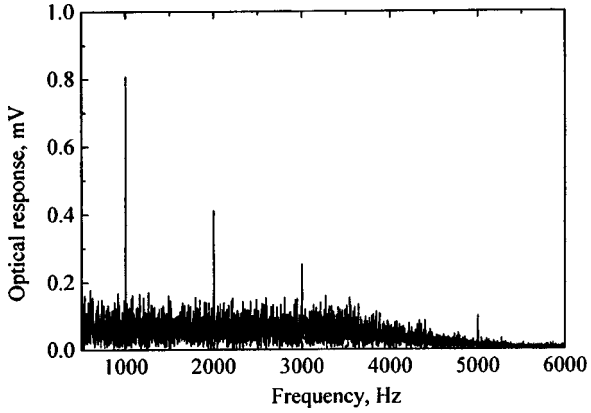

FIG. 2. Fourier spectrum of the electrooptic response obtained at temperature $T=45$ °C. A voltage with amplitude 10 V and frequency 1 Hz was applied to the sample.

Thus, in the present work special attention is devoted to synchronous detection of the X component of the optical response at the fundamental frequency of the exciting electric field, where $X=A(\omega)\cos\varphi$, $A(\omega)$ is the amplitude of the ellipsometric signal, and φ is the phase difference detected by the synchronous detector. The moment when the X component vanishes corresponds to the moment when the smectic layers pass through the plane of incidence of the light wave, and a change in sign of the X component corresponds to a change in sign of the angle between the normal to the smectic layers and the plane of incidence.

A chiral FLC (CS-1029 Chisso Co.), containing the following sequence of phases and phase transition temperatures in degrees celsius, was used: Cr–18–SmC*–73-SmA–85-N*–91-Iso. Orienting coatings based on polyvinyl alcohol (PVA) were deposited on half-transmitting electrodes (ITO), deposited on the surface of the prism and flat glass. After annealing at 120 °C for 1 h the initial orientation of the

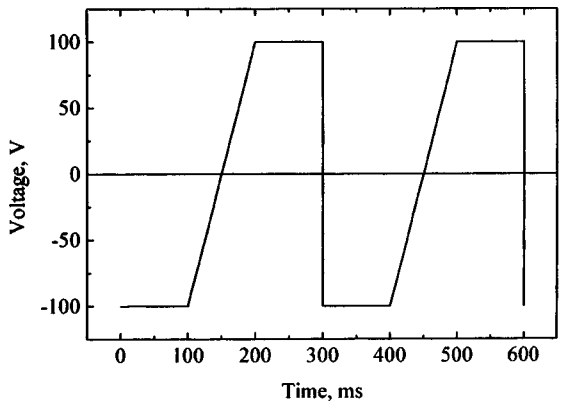

FIG. 3. Form and magnitude of the asymmetric voltage giving rise to rotation of the normal to the smectic layers.

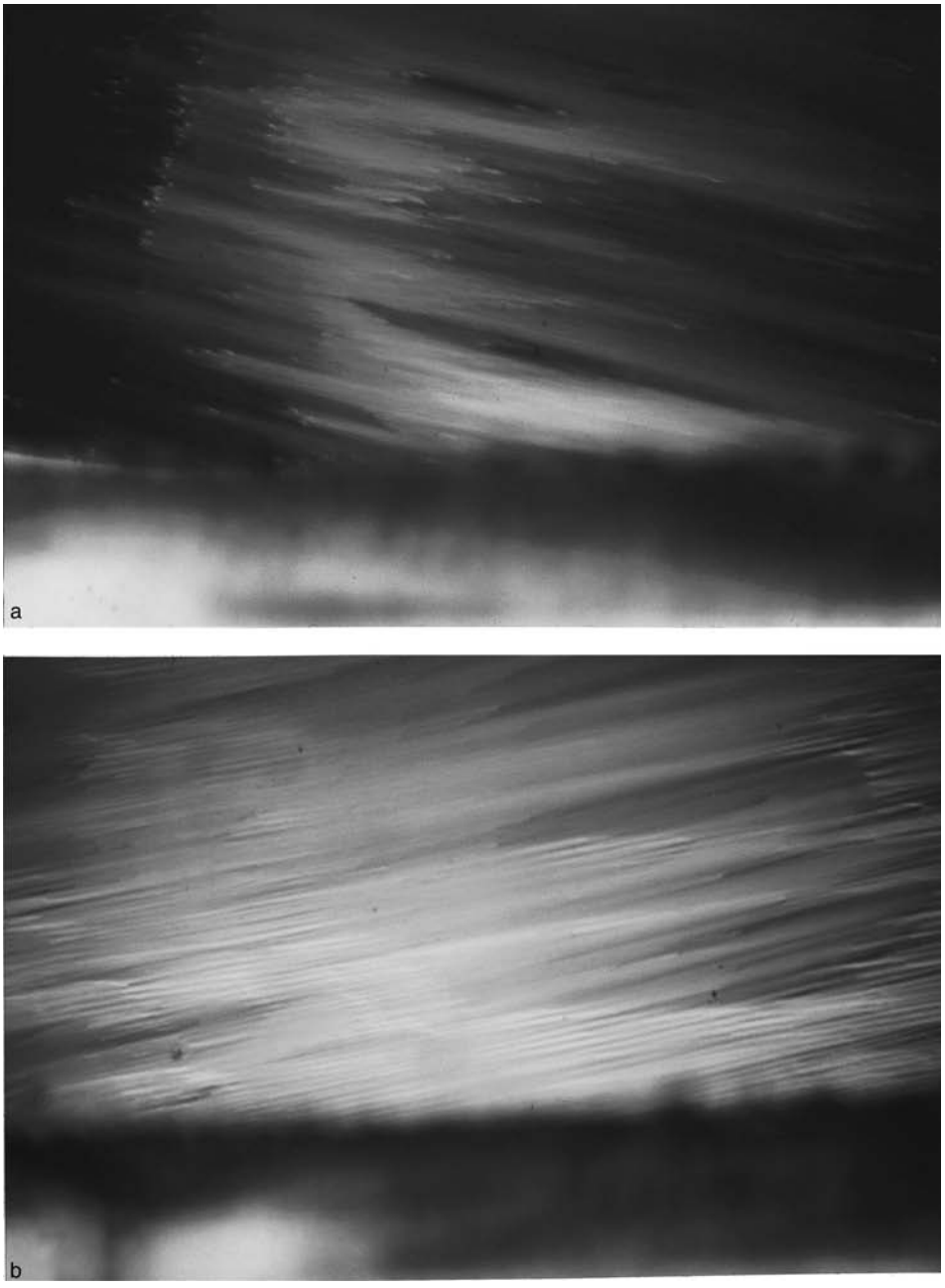

FIG. 4. Photographs obtained with a polarizing microscope: a — after 45-min action of an asymmetric voltage, b — after 90-min action on the texture shown in the preceding photograph.

FLC was formed by mechanical rubbing of the surface of the PVA with a nylon fabric. An important aspect was the procedure for obtaining weak azimuthal anchoring energy of the LC with the substrate. For this, the nylon fabric was put in contact with the substrate

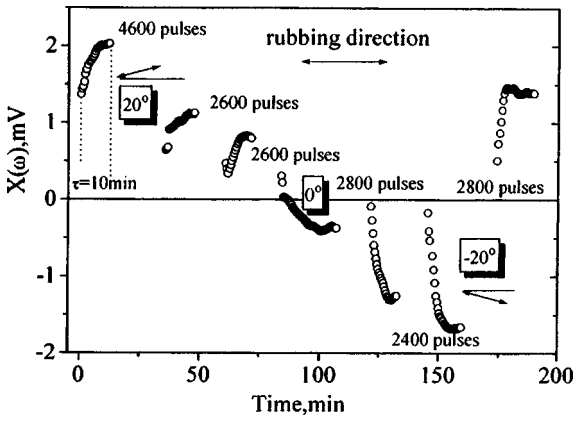

FIG. 5. Dependence of the $X(\omega)$ component of the optical response on the observation time. The amplitude and frequency of the sinusoidal voltage and the measurement temperature were equal to $U=10$ V, $\omega=2\pi\times1000$, and $T=45$ °C, respectively. An asymmetric voltage was applied during the pauses (the number of pulses is shown in the figure).

and then deformed to a depth of 0.5 mm. Next, the substrate was displaced with respect to the stationary fabric. Thirty cycles were sufficient to form a relief on the surface of the substrate and to induce a weak anisotropy of the anchoring energy with a low field threshold. The ferroelectric liquid crystal was placed in a prism module, shown in Fig. 1, at temperature $T=95$ °C and then cooled to room temperature $T=20$ °C. The initial arrangement of the smectic layers was perpendicular to the rubbing direction and the substrate surface. Next, an asymmetric electric field, whose form is shown in Fig. 3, was applied to the sample for 45 min. As a result, the optical texture rotated by an angle of 20° (Fig. 4a). After the inverted asymmetric voltage (mirror-symmetric with respect to the abscissa) was applied for 45 min the angle of inclination was equal to 0° and after 90 min the angle was equal to $-20°$ (Fig. 4b). The asymmetric voltage was switched off according to a definite protocol, as follows from Fig. 5, and the $X(\omega)$ component of the optical response to a sinusoidal voltage $U=10$ V with frequency $\omega=2\pi\times1000$, depending on the time, as shown in Fig. 5, was measured by modulation total internal reflection ellipsometry. The relaxation time of the FLC $\tau_p\approx10$ min was estimated from Fig. 5. This value is much greater than the response time of the crystal $\tau_\varphi\approx400$ μs. It is interesting to note that such behavior is not specific to FLCs, since, for example, the equilibration time in the surface layer of 5CB in the case of weak azimuthal anchoring energy with the substrate was also equal to $\tau_p\approx10$ min,[12] i.e., it was much greater than the relaxation time of the nematic liquid crystal $\tau_p\approx0.1$ s, calculated from the well-known expression $\tau_p=d^2\gamma/\pi^2K$, where $d=10$ μm, $\gamma=1$ poise, and $K=10^{-6}$ dyn. At the moment when the normal to the smectic layers coincided with the plane of incidence of the light wave the $X(\omega)$ component of the optical response vanished, while the predominant direction of the stripe defect structure coincided with the axis of easy orientation. Further action of the asymmetric voltage on the FLC resulted in a change in sign of the $X(\omega)$ component of optical response and, correspondingly, in a change in sign of the rotation angle of the normal to the smectic layers, as was confirmed by observation in a polarizing microscope.

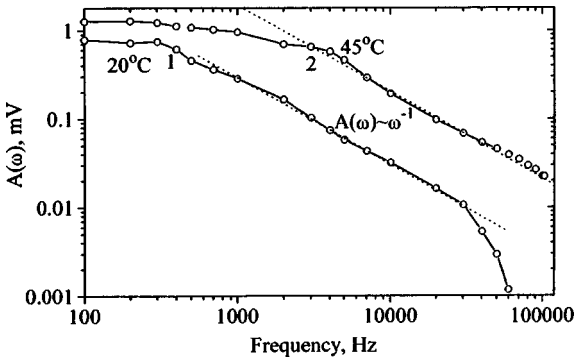

FIG. 6. Frequency dependence of the amplitude $A(\omega)$ of the optical response: *1* — at temperature $T=20$ °C, *2* — at temperature $T=45$ °C.

Since under total internal reflection conditions the change in the phase difference between the perpendicular and parallel components of the field of the light wave does not depend on the thickness of the LC layer for $d<h$,[11] for $\omega>1/\tau_p$ a situation when $\varphi(t) \sim A(\omega)e^{i\omega t}$, where $\varphi(t)$ is the azimuthal perturbation of the FLC director and $A(\omega)$ is the amplitude of the first harmonic of the optical response, is easily realized. Good agreement with the theoretical predictions of the frequency behavior of the azimuthal perturbation of the FLC[13] is shown in Fig. 6, where in the intermediate frequency range $A(\omega)\sim|\varphi(t)|\sim\omega^{-1}$. The curve *1*, obtained at room temperature $T=20$ °C, demonstrates additional damping at high frequencies $\nu>30$ kHz. (For the case $T=45$ °C, described by the curve *2*, this process is apparently shifted in the direction of high frequencies.) A similar high-frequency dissipative process, due to the effect of surface viscosity on the dynamics of a liquid crystal, has been observed in a compensated nematic liquid crystal MBBA.[14]

3. CONCLUSIONS

The dynamic behavior of a thin (thickness of the order of the wavelength of light) near-surface layer of a FLC in the uniform rotation, induced by an asymmetric electric field, of the normal to the smectic layers was investigated by modulation total internal reflection ellipsometry. It was shown that the rotation angle of the normal to the smectic layers near the surface of the electrode, just as in the bulk, varies reversibly as a function of the polarity and number of applied electric pulses. Measurements of the first harmonic of the optical response, characterizing the azimuthal disturbance of the FLC, as a function of the frequency of the sinusoidal voltage were also performed. It was found that the surface dynamics of the thin layers of the FLC is nonspecific and exhibits features which are characteristic of nematic liquid crystals.

This work was supported by the grants COPERNICUS (IC15-CT96-0744), INTAS 95-IN-RU-128, RFFI 98-02-17071 as well as a grant from the Japanese Ministry of Education, Science, Sports, and Culture. We thank S. P. Palto for the opportunity of using the PhysLab program package and S. A. Pikin for valuable remarks.

[a)]In principle, a wavelike instability of flat smectic layers is theoretically possible in smectics A.[1] But high field intensities are required in order to obtain an appreciable effect. Evidently, this is why it has not yet been observed.

---

[1] P. G. de Gennes, *The Physics of Liquid Crystals*, Clarendon Press, Oxford, 1975 [Russian translation, Mir, Moscow, 1977].
[2] J. S. Patel and J. W. Goodby, J. Appl. Phys. **59**, 2355 (1986).
[3] M. Ozaki, H. Moritake, K. Nakayama, and K. Yoshino, Jpn. J. Phys. **33**, L1620 (1994).
[4] K. Nakayama, H. Moritake, M. Ozaki, and K. Yoshino, Jpn. J. Phys. **34**, L1599 (1995).
[5] K. Nakayama, M. Ozaki, and K. Yoshino, Jpn. J. Phys. **35**, 6200 (1996).
[6] K. Nakayama, M. Ozaki, and K. Yoshino, Appl. Phys. Lett. **70**, 2117 (1997).
[7] K. Nakayama, M. Ozaki, and K. Yoshino, Jpn. J. Phys. **36**, 6122 (1997).
[8] K. Nakayama, M. Ozaki, and K. Yoshino, Mol. Cryst. Liq. Cryst. **304**, 339 (1997).
[9] L. M. Blinov, D. B. Subachius, and S. V. Yablonskii, J. Phys. II **1**, 459 (1991).
[10] L. M. Blinov, S. V. Yablonskii, and G. Durand, *Dynamic Properties of Surface Nematic Layers Studied by Modulation Ellipsometry*, British Liquid Crystal Society, Annual Conf. University of Bristol, 9–11 April 1990, p. IV.5.
[11] M. Born and E. Wolf, *Principles of Optics*, Pergamon Press, New York, 1969, 4th edition [Russian translation, Nauka, Moscow, 1973].
[12] V. P. Vorflusev, H.-S. Kitzerov, and V. G. Chigrinov, Appl. Phys. Lett. **70**, 3359 (1997).
[13] S. A. Pikin, *Structural Transformation in Liquid Crystals* [in Russian], Nauka, Moscow, 1981, p. 168.
[14] S. Yablonskii, M. Rajteri, C. Oldano, and G. Durand, Proc. Soc. Photo-Opt. Instrum. Eng. (SPIE) **2731**, 87 (1995).

Translated by M. E. Alferieff

Manganites at low temperatures and light doping: band approach and percolation

L. P. Gor'kov
National High Magnetic Field Laboratory, Florida State University, Tallahassee, FL 32310, USA; L. D. Landau Institute of Theoretical Physics, 117334 Moscow, Russia

V. Z. Kresin
Lawrence Berkeley Laboratory, University of California, Berkeley, CA 94720

(Submitted 30 April 1998)
Pis'ma Zh. Éksp. Teor. Fiz. **67**, No. 11, 934–939 (10 June 1998)

A tight-band model is employed for the e_{2g} orbitals in manganites. It is shown that a large intra-atomic Hund coupling J_H and the resulting double-exchange mechanism lead to antiferromagnetic ordering along one of the cubic axes, stabilized by the cooperative Jahn–Teller effect, which further decreases the band energy of the electrons. As a result, $LaMnO_3$ is a band insulator built of 2D ferromagnetic layers. The critical concentration ($x_c \simeq 0.16$) for the onset of ferromagnetic and metallic behavior at low temperatures in $La_{1-x}Sr_xMnO_3$ and the phase transition are treated in a percolation approach. © *1998 American Institute of Physics.* [S0021-3640(98)01811-8]

PACS numbers: 75.70.Pa, 71.30.+h, 75.30.Kz, 75.50.Dd

Current efforts in studies of the ''colossal magnetoresistance'' (CMR) in the manganites $R_{1-x}B_xMnO_3$ (usually R=La, B=Ca, Sr; see, e.g., Refs. 1–3 for a review and references) are naturally focused on phenomena occurring in the vicinity of the metal–insulator transition temperature T^*, which for $x=0.2-0.3$ reaches the room temperature range. There are no doubts that both the Jahn–Teller (JT) distortions and Zener double exchange (DE) mechanism[4,5] are two key ingredients of CMR.

The transition between the paramagnetic and conducting ferromagnetic phases is treated in Ref. 6 as a localization–delocalization ''crossover'' driven by thermal fluctuations of the local JT modes. In this paper we focus on the analysis of phenomena occurring at low T. In this region the approach should be different. Indeed, the two end members of the series, $LaMnO_3$ and $CaMnO_3$, are both antiferromagnetic (AF) insulators. ''Doping'' of $LaMnO_3$ by divalent atoms results in metallic conductivity only above a critical concentration $x_c \simeq 0.16$.

Low-temperature phases of manganites are usually interpreted in terms of localized orbitals,[7,8] more often than not in the modified Hubbard model (see, e.g., Ref. 9). Although it is widely accepted that electron–electron correlations play the key role in low-temperature behavior of manganites, we show that their major properties can be understood within the framework of the band approach as well, or in a percolation picture.

The following facts have to be explained: 1) The insulating state of the parent $LaMnO_3$; 2) the type-*A* antiferromagnetic ordering (alternating ferromagnetic planes); 3) the small value of the Néel temperature, $T_N \sim 150$ K, in the low-x range, while the structural changes occur at about 900 K; 4) the localization of ''holes'' introduced into the Mn^{3+} subsystem at $x < x_c$; 5) the threshold concentration, $x_c \simeq 0.16$, above which metallic conductivity sets in at low T.

In the band model properties 1) through 4) are brought about by the DE and JT mechanisms. We interpret the value $x_c \simeq 0.16$ in terms of percolation theory: both the cluster approach and the phase separation picture, which was first suggested for the cuprates,[10] seem to give the same criterion.[11]

Let us start from the fract that the ground state of $LaMnO_3$ is type-*A*. According to our picture, the appearance of such a magnetic state is *not* caused by any exchange interaction between localized spins on different sites. The mutual arrangement of the distorted octahedra and of the core ${}^3t_{2g}$ spins, $\mathbf{S}_i$ (S=3/2), is stabilized only by benefits in the kinetic *band* energy of the e_{2g} ''conduction'' electrons.

The single-electron Hamiltonian is then of the form Ref. 6

$$\hat{H} = \sum_{i,\delta} (\hat{t}_{i,i+\delta} - J_H \mathbf{S}_i \cdot \hat{\boldsymbol{\sigma}} + g \hat{\boldsymbol{\tau}}_i \cdot \mathbf{Q}_i + J_{el} \mathbf{Q}_i^2). \tag{1}$$

Here $\hat{t}_{i,i+\delta}$ is the nearest−neighbor tunneling matrix, defined on some basis of the two−dimensional cubic representation e_{2g}; $\mathbf{Q}_i$ are the active local JT modes with the matrix elements on that electronic basis expressed in terms of a ''pseudospin'' matrix $\hat{\boldsymbol{\tau}}$ (see, e.g., Ref. 7; the $\mathbf{Q}_i$ are defined as dimensionless parameters). The static JT deformations and the staggered magnetization, $\langle \mathbf{S}_i \rangle = (-1)^i \langle S \rangle$ of the *A*-type phase are treated below in the mean field approximation.

To avoid cumbersome expressions, we first discuss the competition between ferro− and antiferromagnetic order for the *one*−band model:

$$\varepsilon(\mathbf{p}) = t \cos(a p_z) + \overline{t}(\mathbf{p}_\perp). \tag{2}$$

We assume at first that the local (${}^3t_{2g}$) spins are ordered ferromagnetically. At large $J_H \gg t$ the low energy band is shifted down, by $-J_H \langle S \rangle$. The main contribution to the total energy is $E_H = -J_H \langle S \rangle n$ (n is the number of electrons per unit cell), while the kinetic energy contribution due to the polarized electrons is linear in $t, \overline{t}$.

Consider the same problem for AF ordering along the z axis (with a period of $2a$). It is convenient to discuss the more general case

$$\mathbf{S}_i = (\pm \langle S_z \rangle, M_x) \quad (S_z^2 + M_x^2 = S^2), \tag{3}$$

i.e., the canted AF structure[8] for the ${}^3t_{2g}$ spins. Solving the periodic electron spectrum problem in a manner similar to the solution for the two local sites,[5] one obtains the following four branches:

$$\varepsilon_l(\mathbf{p}) - \overline{t}(\mathbf{p}_\perp) = \pm \sqrt{J_H^2 S^2 + t^2(p_z) \pm 2 J_H |t(p_z)| |M_x|}. \tag{4}$$

At $J_H \gg t, \overline{t}$, the low energy spectrum reduces to

$$\varepsilon(\mathbf{p})_{1,2} - \overline{t}(\mathbf{p}_\perp) \simeq -J_H S \pm |t(\mathbf{p}_z)| (|M_x|/S). \tag{5}$$

The second term restores the familiar expression for transport:[5] $M_x = 2S|\cos\theta/2|$ (θ is the angle between the adjacent local spins).

For the AF case ($M_x \equiv 0$) the Brillouin zone is reduced by half, but there are now two branches in (5). As the result, the main term, $-J_H S$, does not change. For a single band, the antiferromagnetic order may even be energetically favorable, although the energy benefit would be small, of the order of (see (4))

$$t^2/J_H \ll t. \tag{6}$$

For two bands there are terms linear in t. The JT band splitting *is* necessary if we wish to decrease the ground state energy below the energy of the ferromagnetic state.

We have obtained the ''bare'' band spectrum of a cubic material with e_{2g} electrons. For calculating $\hat{t}_{ik}$, and hence, the electronic spectrum, $\varepsilon(\mathbf{p})$, use of the normalized basis functions of the form:

$$\psi_1 \propto z^2 + \epsilon x^2 + \epsilon^2 y^2, \quad \psi_2 \equiv \psi_1^* \tag{7}$$

($\epsilon = \exp(2\pi i/3)$), proves to be more convenient to account for the cubic symmetry of the initial lattice. The functions (7) are related to the real basis, $\varphi_1 \propto d_{z^2}$ and $\varphi_2 \propto d_{x^2-y^2}$:

$$\psi_1 = (\varphi_1 + i\varphi_2)/\sqrt{2}, \quad \psi_2 = (\varphi_1 - i\varphi_2)/\sqrt{2}. \tag{8}$$

The tight−binding spectrum of the e_{2g} electrons consists of two branches, which are discussed below.

Before proceeding further, we write down explicitly the local, JT part of the Hamiltonian (1) in the basis (7):

$$-\frac{g}{2}Q_0\begin{pmatrix} 0 & \exp(i\theta) \\ \exp(-i\theta) & 0 \end{pmatrix}. \tag{9}$$

In the standard notation:[7] $Q_2 = Q_0 \sin\theta$, $Q_3 = Q_0 \cos\theta$. Here Q_0 is the magnitude of the JT distortions, and the ''angles'' $\theta = 0, 2\pi/3, -2\pi/3$ correspond to elongations of the octahedron along the z, x, and y axes, respectively.

With the above in mind, consider the options for possible ground states in manganites. In the case of stoichiometric $LaMnO_3$ there is exactly one e_{2g} electron (Mn^{3+}) per unit cell. The ferromagnetic filling−up for two bands will produce a metallic spectrum. AF ordering along one axis results in the same leading contribution, $-J_H S$ (at large J_H), while the corresponding kinetic energy contribution becomes of the order of $t^2/J_H \ll t$. The terms of second order in t in Eq. (4) imply that the spectrum is much less dispersive along the z axis ($M_x \equiv 0$). Planes with antiparallel core spins become almost isolated.

AF ordering along any other direction would lack electronic transport along this direction, again shrinking the bands. Thus it is enough to have AF order along one axis to achieve the major energy benefit $-J_H S$. However, to stabilize the AF order along *one* axis, one needs to further reduce the total energy by antiferroelastic JT distortions along the remaining directions.

Note again that after the AF ordering sets in, say, along the z axis, the communication between adjacent layers in real space becomes very weak. Therefore, at large J_H it is possible to reduce the problem in leading order to a problem of two−dimensional (2D)

electrons. For decoupled layers, electrons inside the layer are ferromagnetically polarized along the $^3t_{2g}$ (core) spins. Again, in this 2D problem there is one electron per (2D) cell. The metallic spectrum simplifies to the form:

$$\varepsilon_{1,2}^{2D}(\mathbf{p}) = (A+B)(\cos ap_x + \cos ap_y) \pm (A-B) \times \{(\cos ap_x + \cos ap_y)^2 + 3(\cos ap_x - \cos ap_y)^2\}^{1/2}, \quad (10)$$

where $i,k=(x,y,z)$;

$$A \propto \overline{\varphi_1(z;x,y)\varphi_1(z+a;x,y)}, \quad B \propto \overline{\varphi_2(z;x,y)\varphi_2(z+a;x,y)}$$

are the two overlap integrals between two sites separated by the lattice constant a. We now introduce JT distortions in a layer with the structure vector (π,π) in a plane. If the JT splitting is strong enough, then instead of (9), the new spectrum will consist of two pairs of bands separated by energy gaps over the entire (new) Brillouin zone, with the low-energy bands fully occupied. This completes the band picture for the insulating A-type ground state in $LaMnO_3$.

For this interpretation one needs:

$$J_H \gg t,\ gQ_0; \quad gQ_0 \gtrsim t. \quad (11)$$

Equation (10) does not impose any severe limitations on the model parameters. The above physics should be present in any realistic band structure. Usually band calculations use the experimental lattice parameters, and it is not straightforward to single out (e.g., in Ref. 3) the competition of the effects considered above.

Finding the single-electron spectrum in the presence of the JT distortions from (8), (9), writing the total energy of the filled-up bands, and then minimizing the total energy is a straightforward but rather tedious task. In the general case, there is no small parameter. We will consider numerical aspects elsewhere.

Below we take advantage of the transparent physics of the independent 2D-layer approximation. First of all, the 2D ferromagnetic ground state in each layer which was obtained in the mean field approximation will be smeared out by fluctuations: ferromagnetism does not exist as a stable thermodynamic phase in 2D, unless there is a weak interlayer coupling t^2/J_H (Eq. (6)). This results in a rather low Néel temperature in $LaMnO_3$, $T_N \simeq 150$ K at $t \sim 0.1$ eV, $J_H \sim 1$ eV.

To illustrate the above, let us consider the ''symmetric'' model,[9] $A=B=t/2$ in (9):

$$\varepsilon(\mathbf{p}) = t(\cos\, ap_x + \cos\, ap_y) \equiv \tilde{t}(\mathbf{p}). \quad (12)$$

Equation (11) gives two degenerate bands. For one polarized 2D electron per unit cell, the two Fermi surfaces run along the lines $p_x \pm p_y = (\pm \pi/a)$. In the presence of JT distortion (8) the new spectrum (in the reduced Brillouin zone, with the structural vector $(\pi/a,\pi/a)$) consists of the four branches $\varepsilon_l(\mathbf{p}) = \pm||t(\mathbf{p})| \pm \Delta|$, where $\Delta = |gQ_0/2|$. At $\Delta > 2t$ there are two pairs of energy bands, and the insulating gap, equal to $\Delta - 2t$, sets in at $p_x = p_y = 0$. The distortion $gQ_0 = g^2/J_{el}$ is defined from the on-site problem.

Turning back to the parameters (J_H, J_{el}, g, A, B) of our general model, connections between gQ_0, J_{el} and A and B are established by minimization of the total (electronic and elastic) energies with respect to Q and M_x (see Eq. (5)). The deformations (Q_0) of the octahedra are known from the structural data (see, e.g., Ref. 3). One may also expect

that $B \ll A$: tunneling between Mn sites takes places through the shared oxygen ions, and the notion that the size d of the d shell is small compared to the lattice constant a ($d \ll a$), is quite helpful in respect to oxides of transition metals.[7,12,13] The spin wave spectrum in $LaMnO_3$ is now available.[14] Although we postpone the study of the spin wave spectrum for the future, it is worth mentioning that coexistence of the localized $^3t_{2g}$ spins and itinerant e_{2g} electronic states (which in the AF environment are not characterized by the spin-projection quantum number), may result in deviations from an anisotropic Heisenberg model.

Finally, let us briefly discuss the concentration dependence. At small x there are two mechanisms that lead to localization of a doped hole. The first one is directly related to the 2D physics. According to Eq. (1), interaction of a hole with the JT modes may decrease the energy of the hole by an amount of the order of g^2/J_{el}. If its energy is now below the band bottom, the hole becomes self-trapped. Two-dimensionality plays a crucial role in that there are no energy barriers for the process.[15] If the dimensionless parameter $C \sim g^2/J_{el}W$ (W is a bandwidth) exceeds a critical value of the order of unity, no itinerant states are possible in the 2D system. The second mechanism is the Coulomb binding of holes near dopants.[8]

At larger x the band approach becomes useless. Instead, we adopt the point of view of percolation theory. Let us start first with the *cluster* description.[11] In the so-called site problem, consider the formation of an infinite cluster of neighboring divalent ions. For the simple cubic lattice the critical concentration is $x_{\rm cr}(s) = 0.31$. This value is not universal.

It is well known[11] that correlations between sites rapidly reduce $x_c(s)$ to the value $x_c \simeq 0.16$, which is also a threshold concentration for a continuous percolation problem. Although holes are located near divalent ions (forming the skeleton of the cluster), the hopping of holes takes place along adjacent Mn sites, correlated by the fact that the wave function of a single hole is spread over a few interatomic distances, tending to suppress the JT distortions and to align spins ferromagnetically in the vicinity of a hole. Although the structure of a cluster is complicated, at $x > x_c$ one may expect that locally its properties are close to those of the homogeneous metallic ferromagnetic state. The rest of the sample does not conduct.

Another plausible view is that the material may separate into coexisting insulator and metallic phases.[10] In the cluster approach the Coulomb energy plays a crucial role, confining holes in the vicinity of the skeleton. In the continuous description the Coulomb energy would limit the sizes of the domains of the phases. In both approaches the Coulomb energy may be strongly reduced by a sufficiently large dielectric constant of the insulating phase and due to metallic screening in the ferromagnetic phase.

With increasing temperature the concentration of the metallic phase decreases: temperature-induced JT distortions[6] provide stronger localization of ''doped'' holes. From this point of view the metal–insulator transition temperature T^* may also be interpreted as a percolation point (at fixed x), and this agrees well with the extreme sensitivity of the CMR to an applied magnetic field.

To summarize, the interpretation of $LaMnO_3$ as a band insulator is consistent with the main experimental facts. The large intra-atomic Hund exchange J_H forces the cubic system to order antiferromagnetically along one direction because the band energy of the

electrons can then be effectively reduced by the JT instability, resulting in a new (tetragonal) lattice ($\sqrt{2}a\times\sqrt{2}a\times 2a$). At $J_H \gg t, gQ_0$, the e_{2g} electrons form almost disconnected 2D layers. This manifests itself in a low Néel temperature. A percolation analysis can explain the value of the critical concentration $x_c \simeq 0.16$ and the CMR itself, suggesting some interesting new physics.

The work was supported (L. P. G.) by the National High Magnetic Field Laboratory through NSF Cooperative Agreement # DMR-9016241 and the State of Florida, and (V. Z. K.) by the U. S. Office of Naval research under Contract # N00014-97-F0006.

[1] H. Kawano, R. Kajimoto, M. Kubota, and H. Yoshizawa, Phys. Rev. B **53**, 14709 (1996).
[2] J. Coey, M. Vivet, and S. von Molnar, unpublished (1997).
[3] W. Pickett and S. Singh, Phys. Rev. B **53**, 1146 (1996).
[4] G. Zener, Phys. Rev. **82**, 403 (1951).
[5] P. W. Anderson and H. Hasegawa, Phys. Rev. **100**, 675 (1955).
[6] A. Millis, B. Shraiman, and R. Mueller, Phys. Rev. Lett. **77**, 175 (1996).
[7] J. Kanamori, J. Appl. Phys. (Suppl.) **31**, 145 (1960).
[8] P. G. de Gennes, Phys. Rev. **118**, 141 (1960).
[9] For review, see K. Kugel' and D. Khomskiĭ, Usp. Fiz. Nauk **136**(4), 231 (1982) [Sov. Phys. Usp. **25**, 231 (1982)].
[10] L. P. Gor'kov and A. Sokol, JETP Lett. **46**, 420 (1987).
[11] H. Scher and R. Zallen, J. Chem. Phys. **53**, 3759 (1970); for review see B. Shklovskii and A. Efros, *Electronic Properties of Doped Semiconductors*, Springer-Verlag, Berlin, 1984; G. Deutcher, in *Chance and Matter*, Part 1, edited by J. Souletie, J. Vannimenus, and R. Stora, Elsevier, Amsterdam, 1987.
[12] J. Coodenough, in *Progress in Solid State Chemistry*, Vol. 5, edited by H. Reiss, Pergamon Press, New York, 1971, p. 145.
[13] P. W. Anderson, in *Magnetism*, Vol. 1, edited by G. Rado and H. Suhl, Academic Press, New York, 1963, p. 75.
[14] K. Hirota, N. Kaneko, A. Nishizwa, and Y. Endoh, J. Phys. Soc. Jpn. **65**, 3763 (1996).
[15] E. Rashba, in *Excitons*, edited by. E. Rashba and M. Sturge, North-Holland, Amsterdam, 1982, p.473; Y. Toyozawa and Y. Shinozuka, J. Phys. Soc. Jpn. **52**, 1446 (1983).

Published in English in the original Russian journal. Edited by Steve Torstveit.

Mössbauer investigations of the surface state of hexagonal ferrites Sr-*M* near the Curie point

A. S. Kamzin[a)] and V. L. Rozenbaum
A. F. Ioffe Physicotechnical Institute, Russian Academy of Sciences, 194021 St. Petersburg, Russia

(Submitted 6 May 1998)
Pis'ma Zh. Éksp. Teor. Fiz. **67**, No. 11, 940–944 (10 June 1998)

The temperature dependence of the parameters of the hyperfine interaction in the surface layers and in the bulk of macroscopic crystals of hexagonal ferrites of the type Sr-*M* ($SrFe_{12}O_{19}$) is investigated by the method of simultaneous gamma-, x-ray, and electron Mössbauer spectroscopy. It is shown experimentally that the transition of an ~ 200 nm thick surface layer of macroscopic ferromagnets to the paramagnetic state occurs at a temperature 3° below the Curie point (T_C) for the bulk of the crystal. It was established that the transition temperature $T_C(L)$ of a thin layer localized at a depth L from the surface of the crystal increases away from the surface and reaches the value T_C at the lower (away from the surface) boundary of the so-called ''critical'' surface layer. A nonuniform state in which the bulk region of the crystal is magnetically ordered while the surface region is disordered is observed near T_N. © *1998 American Institute of Physics.*
[S0021-3640(98)01911-2]

PACS numbers: 76.80.+y, 71.70.Jp, 75.70.Cn

Investigations of the magnetic properties of surfaces are now attracting a great deal of attention from experimenters. This is due to both the importance of understanding the properties of surfaces as well as the need to study experimentally the effect of a ''defect'' such as the surface on the magnetic properties of surface and subsurface layers of a crystal, as described in numerous investigations (see, for example, Ref. 1). Of special interest are surface processes which accompany fundamental phenomena, such as phase transitions, occurring in the bulk of a crystal. Investigations of the properties of surfaces are now important from the applied standpoint because an understanding of the nature of surface anisotropy, for example, will make it possible to produce magnetic data-storage media with ultrahigh storage density.

The concept of surface magnetic energy[2] was introduced in the first theoretical investigations of the properties of surfaces in order to describe phenomena on the surfaces of massive crystals. It was shown that for negative values of this energy the surface of a crystal can possess magnetization at temperatures above the Curie point of the bulk of the sample. The surface magnetization should decrease exponentially in a direction into the sample. Theoretical investigations of the surfaces of antiferromagnetic crystals[3]

also showed that there is a possibility of surface magnetism at temperatures above the Néel point. In the works following after Refs. 2 and 3, virtually all of the methods developed for studying the properties of bulk crystals were used to describe the properties of surfaces. As a result of theoretical investigations, a phase diagram of the states of the surface and the bulk of a semibounded magnet near the Curie point was constructed (see, for example, Ref. 1).

Although a large number of theoretical works on surface properties are now available, the volume of experimental data is much smaller. This is due to the lack of experimental methods making it possible to investigate and compare the properties of a thin surface layer and the bulk of a bulk crystal. For this reason, most experimental studies of surface properties have been performed either using fine powders (in which the ratio of the number of ions located at the surface to the number of ions occupying positions in the interior volume of the crystallites increases substantially) or for the example of ultrathin films. Experimental investigations of such objects have confirmed the results of theoretical works on the existence of surface magnetism. For example, it has been shown that magnetization exists on Cr, Co, Ni, Tb, and Gd surfaces at temperatures above the point of magnetic ordering in the bulk of these substances (see the review in Ref. 4 and the references cited therein).

However, to understand surface phenomena and to establish the connections between effects occurring at the surface and in the bulk of a crystal it is necessary to have methods that make it possible to investigate the surface of macroscopic crystals and the profiles of the variation of the properties (layerwise analysis) of a surface layer in direct comparison with the bulk of the sample. The method of simultaneous gamma-, x-ray, and electron Mössbauer spectroscopy (SGXEMS), proposed in Ref. 5 and developed in Ref. 6, satisfies these conditions. The main advantage of the SGXEMS method is that information about the bulk properties of the crystal and a surface layer ranging in thickness from 0 to 300 nm is extracted simultaneously under the same conditions as the experimental object.

It has been established by SGXMES[7–9] that in antiferromagnets with weak ferromagnetism the paramagnetic transition temperature of the surface of a macroscopic crystal is lower than the Néel point at which the bulk of the sample passes into the paramagnetic state. The order–disorder transition temperature decreases continuously within a surface layer with a ''critical'' thickness.[7–9]

In summary, the results of experimental works on the existence of surface magnetism at temperatures above the Curie point are in agreement with the results of theoretical investigations.[1–4] At the same time, the experimental fact[7–9] that there exists on the surface of macroscopic weakly ferromagnetic crystals a thin layer in a paramagnetic state at temperatures below the Néel point does not agree with theoretical descriptions of surface magnetism. This discrepancy could be due to the fact that the ferromagnets were investigated theoretically, while experiments were performed on antiferromagnets with weak ferromagnetism.

In the present work we posed the problem of studying experimentally processes occurring on the surface of macroscopic ferromagnetic crystals near the Curie temperature.

The investigations were performed on hexagonal ferrites $SrFe_{12}O_{19}$ (of the type Sr-

M). The compound $SrFe_{12}O_{19}$ has the hexagonal crystal structure of magnetoplumbite. At temperatures below the Curie point, $T_C = 730$ K, the magnetic structure of a $SrFe_{12}O_{19}$ crystal is that of a collinear ferromagnet which has a high anisotropy field and whose easy axis is the hexagonal axis or the crystallographic C axis.

Wafers ranging in thickness from 80 to 100 μm, cut from $SrFe_{12}O_{19}$ single crystals synthesized in a fluxed solution, were used for the measurements. The crystallographic C axis was directed perpendicular to the plane of the wafers. For the surface investigations the crystals were subjected to chemical polishing by boiling in orthophosphoric acid at ~ 90 °C. Previous experiments[5–7] and the experiments performed in the present work showed that the use of the surface preparation method ensures reproducibility of the results.

The experimental Mössbauer spectra were obtained by the SGXEMS method in the temperature range from 300 to 750 K. The temperature was maintained to within $\pm 0.1°$. Gamma-ray source was Co^{57} in a Rh matrix. The law of motion of the gamma-ray source had a triangular form. The linearity of the motion was corrected in two channels: the first channel consisted of the standard negative feedback scheme and the second channel consisted of computer correction.[10]

The iron ions in $SrFe_{12}O_{19}$ occupy five nonequivalent positions. For this reason the Mössbauer spectrum of this compound in the magnetically ordered region consists of five Zeeman sextuplets. Such a large number of spectral lines substantially degrades their resolution and therefore the accuracy with which the hyperfine interaction parameters are determined. The following circumstance was used to improve the resolution of the lines: A cut of the crystal such that the wave vector of the gamma radiation from the Mössbauer source was oriented in the direction of the effective magnetic fields in the crystal was chosen, and the number of lines in the experimental spectrum was decreased, since the second and fifth lines of the Zeeman sextuplets are absent in this case.

The hyperfine interaction parameters and the intensities and widths of the lines in the Zeeman sextuplets were calculated from the experimental spectra with the aid of a computer. The following circumstances were used to increase the accuracy of the mathematical processing of the spectra (aside from the above-noted absence of the second and fifth lines of the Zeeman sextuplets in the spectra: 1) The numbers of iron ions in the nonequivalent positions are in the ratio 12:4:4:2:2, and therefore the intensities of the lines in different sextuplets are in the ratio 12:4:4:2:2, and 2) the fact that the number of magnetic bonds of iron ions occupying nonequivalent positions is different has the effect that the effective magnetic fields at the nuclei of the iron ions are different from one another, and on account of the quadrupole splittings the lines of the sextuplets are substantially shifted relative to one another.

The temperature dependences of the effective magnetic fields at the iron nuclei are shown in Fig. 1, which shows the temperature dependences of the fields at the iron nuclei occupying nonequivalent $12k$ and $4f$ positions because of the fact that the resolution of the spectral lines corresponding to these positions is better. The magnitudes of the effective magnetic fields at the iron nuclei in the $2a$ and ab nonequivalent positions are not shown so as not to complicate the figure. As one can see from Fig. 1, the effective fields at the iron nuclei located in a 200 nm thick surface layer of $SrFe_{12}O_{19}$ decrease with increasing temperature more rapidly than the fields at the iron nuclei located in the bulk

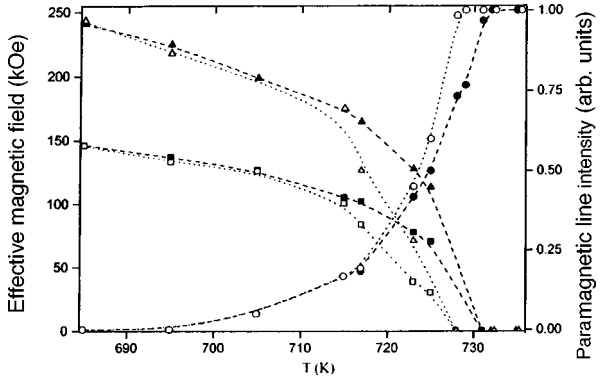

FIG. 1. Temperature dependences of the effective magnetic fields in $SrFe_{12}O_{19}$ on iron nuclei occupying nonequivalent $12k$ and $4f$ positions in the bulk of the crystal (■,▲) and in a 200 nm thick surface layer (□, △) as well as the intensity of the paramagnetic line of iron ions located in the bulk (●) and in the surface layer (○).

of this crystal. The effective magnetic fields obtained from the gamma-ray spectra, i.e., the fields at the iron nuclei located in the bulk of the crystal, vanish at the Curie temperature, equal to 731 K, while the effective magnetic fields calculated from the conversion and Auger electron spectra, i.e., at the iron nuclei located in a ~200 nm thick surface layer, decrease to zero, as one can see from Fig. 1, at temperature 728 K, which is three degrees below the Curie temperature. The spectra were obtained in different sequences on the temperature scale. Analysis of the data showed that the results obtained are reproducible.

The experimental Mössbauer spectra obtained at temperature 723 K and presented in Fig. 2 provide direct confirmation of the fact that the paramagnetic transition in the

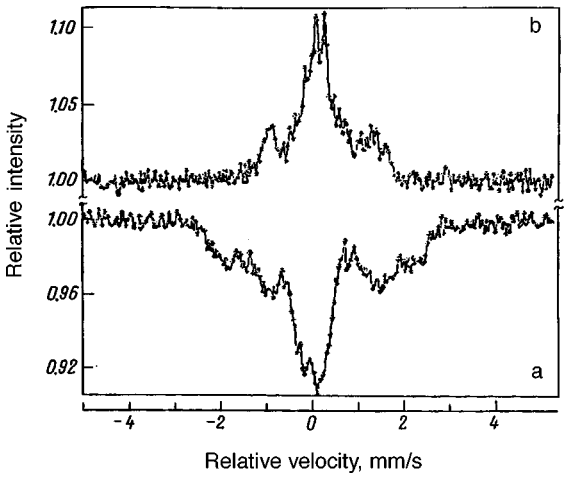

FIG. 2. Mössbauer spectra obtained for $SrFe_{12}O_{19}$ at a temperature of 723 K by detecting gamma rays, i.e., from the bulk of the crystal (a), and by detecting conversion and Auger electrons from a ~200 nm thick surface layer (b).

surface layer occurs at a temperature below the Curie point for the bulk of the crystal. It should be noted that the spectrum obtained by detecting gamma rays (Fig. 2a) is similar to the Mössbauer spectra recorded near the Curie point by other authors.[11] Comparing the spectra obtained near the Curie point (Fig. 2a) shows that the Zeeman lines in the Mössbauer spectrum have a much larger splitting than the Zeeman lines in the spectrum measured by detecting conversion and Auger electrons (Fig. 2b). Therefore the effective magnetic fields at the iron nuclei occupying positions in the bulk of the sample are larger than the effective fields at the iron nuclei located in the surface layer.

The paramagnetic transition temperature was determined by all methods employed in Mössbauer spectroscopy: 1) the spectrum in which there is no Zeeman splitting and only quadrupole lines of the paramagnetic phase are observed was determined from the experimental spectra obtained near a phase transition. The value of the temperature at which the Zeeman lines vanish was taken as the Néel point. 2) The temperature scanning method was also used. In this method the transition point is determined from the temperature dependence of the number of detected photons with a stationary gamma-ray source (Fig. 1). As the transition point is approached from the side of lower temperatures, as one can see from Fig. 1, the number of detected photons increases. At the transition point the curve saturates, and the number of detected photons remains unchanged as the temperature increases further. The values of the paramagnetic transition temperatures determined by the methods described above were identical.

Analysis of the experimental spectra showed that the paramagnetic transition in the bulk of the ferromagnet occurs as follows. When the crystal is heated, a paramagnetic phases arises on the surface of the crystal; this occurs at temperatures below the Curie point. The transition temperature in a thin layer localized at a depth L from the surface $[T_C(L)]$ increases away from the surface, reaching the value T_C for the bulk of the crystal when $L \gtrsim 300$ nm. As the temperature increases further, apparently, increasingly deeper-lying layers pass into the paramagnetic phase. At the Curie point the thermal energy destroys the magnetic ordering in the entire remaining volume of the crystal.

In summary, we have presented the first experimental data indicating the fact that a thin surface layer of a macroscopic ferromagnet passes into a paramagnetic state at a temperature below the Curie point for the bulk of the crystal. At temperatures below the Curie point a nonuniform state is observed at the surface of the sample: a magnetically disordered surface layer alongside a magnetically ordered bulk region of the crystal.

This work was supported by the Russian Fund for Fundamental Research under Grant 98-02-18279.

[a)]e-mail: kamzin@kas.ioffe.rssi.ru

[1] M. P. Kagan and A. V. Chubukov in *Magnetic Properties of Crystalline and Amorphous Media* [in Russian], Nauka, Novosibirsk, 1989, p. 148.
[2] M. I. Kaganov and A. N. Omel'yanchuk, Zh. Éksp. Teor. Fiz. **61,** 1679 (1971) [Sov. Phys. JETP **34**, 895 (1971)].
[3] D. L. Mills, Phys. Rev. B **3**, 3887 (1971).
[4] T. Kaneyoshi, J. Phys.: Condens. Matter **3**, 4497 (1991).
[5] A. S. Kamzin, V. P. Rusakov, and L. A. Grigor'ev, in *Physics of Transition Metals*, Proceedings of an International Conference, Kiev, USSR (1988), Pt. 2, p. 271.

[6] A. S. Kamzin and L. A. Grigor'ev, Pis'ma Zh. Tekh. Fiz. **16**, 38 (1990) [Sov. Phys. Tech. Phys. **16**, 616 (1990)].
[7] A. S. Kamzin and L. A. Grigor'ev, JETP Lett. **57**, 552 (1993); Zh. Éksp. Teor. Fiz. **105,** 377 (1994) [JETP **78**, 377 (1994)].
[8] A. S. Kamzin, L. A. Grigor'ev, and S. A. Kamzin, Fiz. Tverd. Tela (St. Petersburg) **36**, 1371 (1994) [Phys. Solid State **36**, 765 (1994)].
[9] A. S. Kamzin and L. A. Grigor'ev, Fiz. Tverd. Tela (St. Petersburg) **37**, 67 (1995) [Phys. Solid State **37**, 33 (1995)].
[10] A. S. Kamzin and L. A. Grigor'ev, Prib. Tekh. Eksp. No. **1**, 80 (1993); A. S. Kamzin and L. A. Grigor'ev, Pis'ma Zh. Tekh. Fiz. **19**(8), 50 (1993) [Tech. Phys. Lett. **19**, 245 (1993)].
[11] Sh. Sh. Bashkirov, A. B. Liberman, and V. I. Sinyavskiĭ, *Magnetic Microstructure of Ferrites* [in Russian], Kazan State University Press, 1978.

Translated by M. E. Alferieff

Multiplicative-noise-induced amplification of weak signals in a system with on–off intermittency

O. V. Gerashchenko,[a] S. L. Ginzburg, and M. A. Pustovoĭt
B. P. Konstantinov St. Petersburg Institute of Nuclear Physics, 188350 Gatchina, Leningrad Region, Russia

(Submitted 19 March 1998; resubmitted 27 April 1998)
Pis'ma Zh. Éksp. Teor. Fiz. **67**, No. 11, 945–950 (10 June 1998)

A model of an overdamped Kramers oscillator perturbed by strong multiplicative Gaussian noise and a weak periodic signal is studied theoretically and experimentally. It is shown that under certain conditions such a system demonstrates on–off intermittency and sensitivity to very weak periodic signals, making possible many-fold (experimentally, by two orders of magnitude) amplification of the signal amplitude. © *1998 American Institute of Physics.*
[S0021-3640(98)02011-8]

PACS numbers: 05.40.+j

After the discovery of the phenomenon of stochastic resonance, where external additive noise plays a constructive role by increasing the signal/noise ratio, the study of the effect of noise on the behavior of different dynamical systems has been attracting a great deal of interest. We have shown theoretically and experimentally that amplification of weak signals is possible in a nonlinear dynamical system with multiplicative noise.

In the present letter we shall consider the effect of a weak periodic signal on an overdamped Kramers oscillator[1,2] with multiplicative noise. Following Stratonovich, we write the stochastic equation for such a system as

$$\frac{dx}{dt}=\lambda x-Ux^3+\beta\xi(t)x+AR(t)+\sigma\phi(t), \tag{1}$$

where $\xi(t)$ and $\phi(t)$ are δ-correlated statistically independent random processes and $R(t)$ is a periodic square signal with zero mean and unit amplitude.

An analytical investigation and numerical modeling of Eq. (1) were performed in Ref. 3, where it was shown that for small values of the parameter $\alpha=2\lambda/\beta^2$ the system exhibits hypersensitivity to weak alternating signals — an extremely weak action of the order of $\exp(-1/|\alpha|)$ gives rise to a response of the order of unity.

The Fokker–Planck equation for the stochastic equation (1) is written

$$\frac{\partial F}{\partial t}=-\frac{\partial}{\partial x}\left\{\left(\left(\lambda+\frac{\beta^2}{2}\right)x-Ux^3+AR(t)\right)F\right\}+\frac{1}{2}\frac{\partial^2}{\partial x^2}\{(\beta^2x^2+\sigma^2)F\}. \tag{2}$$

In the adiabatic approximation, when the period of the signal $R(t)$ is much greater than the time to establish a stationary probability density $F(x)$, the solution of Eq. (2) in the case $(A,\sigma)\ll(\lambda,\beta,U)$ is

$$F(x)=C\left(x^2+\frac{\sigma^2}{\beta^2}\right)^{(\alpha-1)/2}\exp\left\{\frac{2AR(t)}{\beta\sigma}\tan^{-1}\frac{\beta x}{\sigma}-\frac{Ux^2}{\beta^2}\right\},\quad \alpha=\frac{2\lambda}{\beta^2},\tag{3}$$

where C is a normalization constant. Therefore α is the main parameter determining the behavior of the system.

In the case that the weak signal is much stronger than additive noise ($\sigma\to 0$), we obtain from Eq. (3)

$$F(x)=C|x|^{\alpha-1}\theta(\mathrm{sign}(AR(t)x))\exp\left\{-\frac{2AR(t)}{\beta^2 x}-\frac{Ux^2}{\beta^2}\right\},\tag{4}$$

where θ is the Heaviside unit step function. The normalization factor C cannot be calculated exactly, and its asymptotic representations for $|\alpha|\ll 1$ and $U/\beta^2\sim 1$ are

$$C=\begin{cases}\alpha & \alpha>0,\ z\gg 1\\ 1/\ln\dfrac{1}{A} & z\ll 1\\ |\alpha|A^{|\alpha|} & \alpha<0,\ z\gg 1\end{cases},\quad z=|\alpha|\ln\frac{1}{A}.$$

A change in the asymptotic behavior (crossover) occurs here when the parameter $z\sim 1$, i.e., for signal amplitude $A_0=\exp(-1/|\alpha|)$. Therefore for small values of α a very weak signal is capable of radically changing the distribution density.

Let us point out the characteristic features of the solution (4) in the case $|\alpha|\ll 1$ which is of practical importance: first, the power-law dependence of the probability density in a wide range of values of x, as is characteristic for on–off intermittency phenomena;[2,4,5] second, ''sensitivity'' to the sign of the signal $R(t)$ for signal amplitude $A>A_0$. To estimate the amplitude of the output signal we shall calculate the first moment of $F(x)$:

$$\langle x(t)\rangle=\begin{cases}R(t)\dfrac{\beta}{2}\sqrt{\dfrac{\pi}{U}}/\ln\dfrac{1}{A}, & z\ll 1,\ |\alpha|\ll 1\\ R(t)\dfrac{\beta}{2}\sqrt{\dfrac{\pi}{U}}|\alpha|A^{|\alpha|}, & z\gg 1,\ \alpha<0,\ |\alpha|\ll 1\end{cases}.\tag{5}$$

The expression for the gain in the case $|\alpha|\ll 1$ is

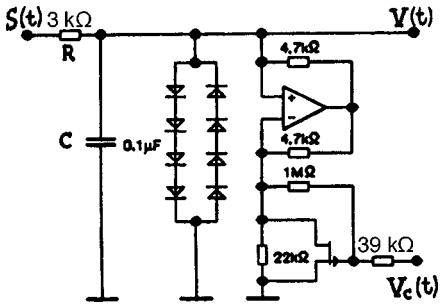

FIG. 1. Analog electronic circuit modeling Eq. (1). Diodes — D107 silicon type. Operational amplifier — KR544UD1, field-effect transistor — KP103K.

$$K=\frac{\langle x(t)\rangle}{AR(t)}=\begin{cases}\sqrt{\dfrac{\pi}{4U}}\beta/A\ln\dfrac{1}{A}, & z\ll 1\\ \sqrt{\dfrac{\pi}{4U}}\beta|\alpha|/A^{1-|\alpha|}, & z\gg 1,\ \alpha<0\end{cases}. \tag{6}$$

Moreover, it can be shown that qualitatively the behavior of the system does not depend on the type of nonlinearity in Eq. (1) (quadratic, cubic, exponential, and so on).

Figure 1 shows an analog circuit which simulates Eq. (1). It consists of parallel-connected capacitor, a nonlinear component consisting of back-to-back semiconductor diodes, and a component, consisting of an operational amplifier and a field-effect transistor, with negative conductance $G(t)$ controlled by a voltage $V_c(t)$. The control voltage $V_c(t)=V_{c0}+v_n(t)$ is applied to the gate of the field-effect transistor and is the sum of constant and noise voltages. The noise voltage in $V_c(t)$ was set by a white-noise generator with a cutoff frequency of about 30 kHz and $\langle v_n(0)v_n(t)\rangle=V_n^2\exp(-\Gamma|t|)$, $V_n\approx 1.5$ V. Here $\Gamma\approx 2\times 10^{-5}$ s^{-1}. A square input signal $S(t)$ with zero mean, amplitude A, and period $T=2$ s was applied through a resistor R. The static current–voltage characteristic (IVC) of the entire circuit as a whole is shown in Fig. 2. One can see that for $|V|<1$ V the slope of the IVC is close to zero. The IVC contains a slight asymmetry for $V<0$ and $V>0$. This asymmetry is due to the technological variance in the parameters of the semiconductor diodes. From the IVC the cutoff voltage can be determined as $|V_0|\approx 2$ V. For $|V|>V_0$ the nonlinearity of the IVC $I_1(V)$ leads to a cutoff $V(t)$ at about 2.5 V.

The equation for this circuit is

$$\frac{S(t)-V(t)}{R}=C\frac{dV}{dt}+I_1(V)+I_2(V), \tag{7}$$

where $V(t)$ is the output voltage, CdV/dt is the current through the capacitor, and $I_1(V)$ is the current through the nonlinear component consisting of back-to-back semiconductor diodes and has the form

$$I_1(V)=I_0(\exp(bV)-\exp(-bV)),\quad b\sim 1/V_0.$$

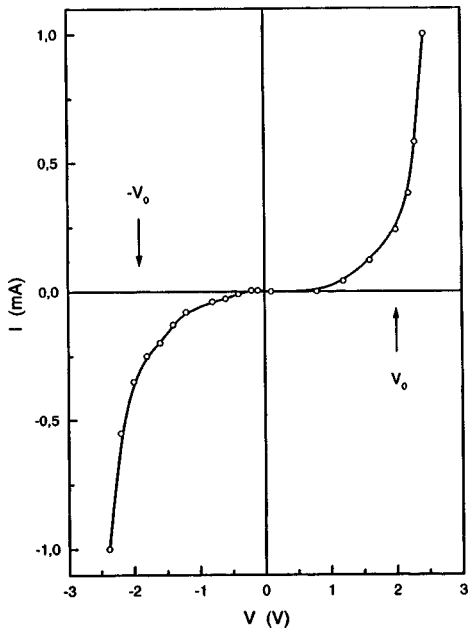

FIG. 2. Static IVC of the electronic circuit shown in Fig. 1. Cutoff voltage $|V_0| \approx 2$ V.

The current through the component with negative conductance in our voltage range can be written in the form

$$I_2(V) = G(t)V, \quad G(t) = -|G_0| - g(t),$$

where $g(t) = \gamma v_n(t)$ is a fluctuating conductance, and $\gamma \approx 10^{-3}/(\Omega \cdot \mathrm{V})^{-1}$. Then

$$RC\frac{dV}{dt} = \lambda V - f(V) + g(t)V + S(t), \tag{8}$$

$$\lambda = R(|G_0| - R^{-1} - G_L), \quad f(V) = R(I_1(V) - G_L V).$$

G_L is determined so that $f(V)$ would not contain a term linear in V. One can see that the noise enters Eq. (8) multiplicatively, i.e., it is multiplied by V. Since $G(t)$ depends on the control voltage $V_c(t)$, by adjusting the value of G_0 with the aid of the dc component of $V_c(t)$, the coefficient λ in Eq. (8) can be made to be close to zero. From the slope of the IVC in Fig. 2 it is possible to determine $\lambda \approx -0.1$ for $|V| \leqslant 1$ V, $RC = 3 \times 10^{-4}$ s.

Let us now switch in Eq. (8) to the dimensionless time $\tau = t/RC$:

$$\frac{dV}{d\tau} = \lambda V - f(V) + \beta\xi(\tau)V + S(\tau), \tag{9}$$

$$\beta = \sqrt{\frac{2}{\Gamma RC}}\, R\gamma V_n \approx 0.8, \quad \alpha = \frac{2\lambda}{\beta^2} \approx -0.3.$$

Thus, one can see that Eq. (9) is identical to Eq. (1), differing from it only by the form of the nonlinearity, which is not important for our phenomena.

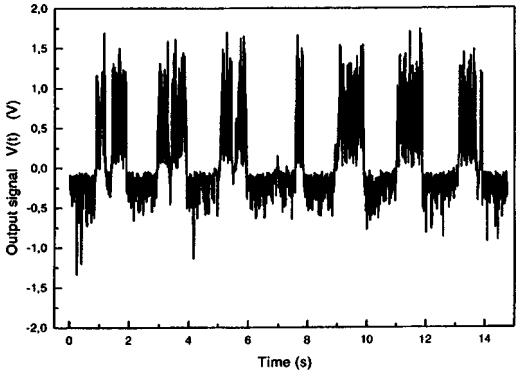

FIG. 3. Output voltage $V(t)$ for the case when a square signal with amplitude $A=3$ mV and period 2 s is fed into the input of the circuit. The gain $K\approx 90$.

Let us underscore the main features of our model: First, the equation is fundamentally nonlinear, since the coefficient of the linear term approaches zero; second, noise is multiplied by the dynamical variable V, i.e., it is multiplicative.

Figure 3 shows the output voltage $V(t)$ when a square signal with amplitude $A=3$ mV is fed into the input of the circuit. We note that the asymmetry of the spikes on

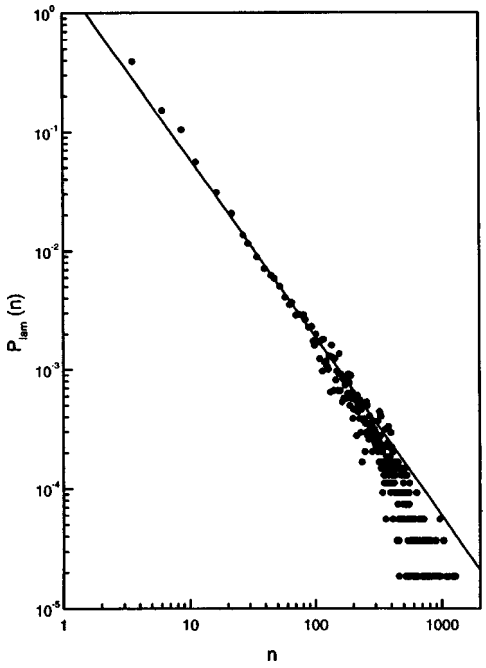

FIG. 4. Probability density distribution of the length of the laminar phase for a constant input signal $E=-14$ mV and laminarity threshold $p=0.1$. The slope of the straight line equals $-3/2$.

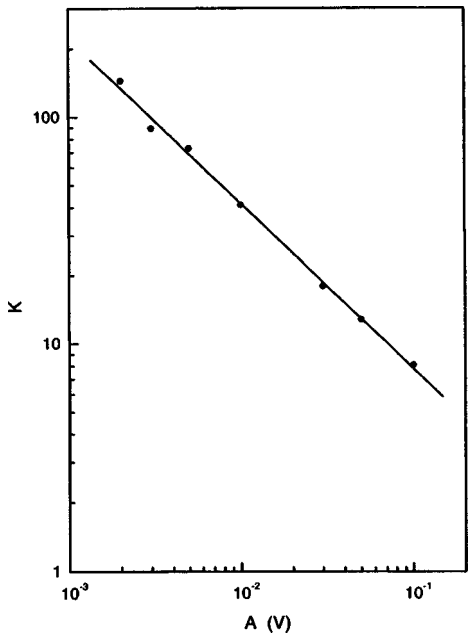

FIG. 5. Gain versus the amplitude of a square input signal with period 2 s. The slope of the straight line equals approximately -0.8.

the positive and negative sides is due to the asymmetry of the IVC of the circuit in the voltage range $V<0$ (see Fig. 2).

One can see that the system responds to a weak input signal by producing ''spikes'' up to the cutoff $|V_0|\approx 2$ V, thereby amplifying the signal. Such behavior is characteristic for on–off intermittency phenomena, when a system in a laminar phase is suddenly excited to cutoff and returns to the laminar phase. A characteristic indicator of on–off intermittency is a power-law behavior of the probability density for the length of the laminar phase:[6–8]

$$P_{\mathrm{lam}}(n)\sim n^{-3/2}, \tag{10}$$

where n is the length of the laminar section.

The laminar phase was determined experimentally as follows: The realization of $V(t)$ contained a maximum spike $V_{\max}\approx 2.5$ V, the laminarity threshold p was given as a fraction of $V_{\max}$, and the laminar phase of $V(t)$ was determined by the condition $V(t)<pV_{\max}$. Figure 4 shows the function $P_{\mathrm{lam}}(n)$ for a constant input signal $S(t)=E=-14$ mV and laminarity threshold $p=0.1$, in good agreement with the theoretical dependence (10). We note that the dependence (10) was also observed for $E>0$ and for other laminarity thresholds ($p=0.05$, 0.2, and 0.5).

Figure 5 shows the gain as a function of the amplitude of the input signal $K(A)=\sqrt{S_V(f_0)\Delta f}/A$, where $S_V(f_0)$ is the spectral intensity of the first harmonic of the output signal and $\Delta f=0.1$ Hz is the frequency step used in measuring $S_V(f)$. From the slope of the straight line we obtain $\alpha\approx -0.2$ in Eq. (3), in good agreement with the estimate in

Eq. (9). The fact that α is different from zero is due to the asymmetry of the IVC in the region of negative values of V (see Fig. 2), which leads to a smaller gain for $V<0$.

Thus, it has been shown experimentally that a weak periodic signal in the analog model (8) of Eq. (1) can be amplified by strong multiplicative noise.

In conclusion, it should be noted that when the signal $S(t)$ is fed into the analog model (8) of Eq. (1) together with external additive white noise $\sigma\phi(t)$ that does not depend on $\xi(t)$ and is such that the noise voltage is of the order of the signal amplitude A in a frequency band of the order of 1 MHz, the circuit operates as a low-pass filter, cutting off frequencies $f>f_c$ in the spectrum of the input signal. For this reason, the high-frequency spectral components of the input noise do not influence the output signal $V(t)$. Measurements of the spectrum $S_V(f)$ of the output signal yieled a value of the cutoff frequency $f_c\approx 20$ Hz.

In summary, we have demonstrated experimentally that the simple stochastic system (8) with on–off intermittency, similar to the system (1), exhibits for small absolute values of the parameter α a noise-induced sensitivity to weak alternating signals, making possible amplification of the signals and thereby being an example of the constructive role of noise in nature.

This work is supported by the Government program ''Physics of Quantum and Wave Processes,'' subprogram ''Statistical Physics,'' Project VIII-3, and by the Government program ''Neutron Studies of Matter.''

[a)]e-mail: gerashch@hep486.pnpi.spb.ru

---

[1] W. Horsthemke and R. Lefever, *Noise-Induced Phase Transitions*, Springer, New York, 1984.
[2] H. L. Yang and E. J. Ding, Phys. Rev. E **54**, 1361 (1996).
[3] S. L. Ginzburg and M. A. Pustovoit, submitted to Phys. Rev. Lett.
[4] A. S. Pikovsky, Phys. Lett. A **165**, 33 (1992).
[5] A. S. Pikovsky and P. Grassberger, J. Phys. A **24**, 4567 (1991).
[6] N. Platt, E. A. Spiegel, and C. Tresser, Phys. Rev. Lett. **70**, 279 (1993).
[7] J. F. Heagy, N. Platt, and S. M. Hammel, Phys. Rev. E **49**, 1140 (1994).
[8] N. Platt, S. M. Hammel, and J. F. Heagy, Phys. Rev. Lett. **72**, 3498 (1994).

Translated by M. E. Alferieff